ABSTRACT

ANXI JIA. Stochastic Capacity at Freeway Bottlenecks with Application to Travel Time Prediction. (Under the direction of Dr. Nagui M. Rouphail and Dr. Billy M. Williams.)

The stochastic nature of freeway bottleneck breakdown and queue discharge are investigated in this study through a comprehensive analysis of sensor data collected at bottleneck sites in the San Francisco Bay Area, California and San Antonio, Texas. A new procedure is proposed to define the stochastic variation of the onset of freeway breakdown and of queue discharge capacity based on time indexed field data of speed-flow profiles. The former is developed as a function of average vehicle time headways preceding observed conditions where both speed is below and density is above locally defined congested flow thresholds. Full year 15-minute data series were used in the demonstration and testing of the procedure, yielding a high degree of statistical confidence in the resulting headway distribution parameter estimates. The statistical analysis indicated that the probability function of freeway bottleneck pre-breakdown flow rates follows a generalized logistic distribution. In addition, a recursive queue discharge model is proposed for bottleneck flows under congested (queued) conditions. The proposed queue discharge model is a simple autocorrelated time series recursion that is seeded with the corresponding pre-breakdown flow and dampens to the mean queue discharge rate. The proposed stochastic models are robust and accurate and represent a significant improvement in the understanding and modeling of freeway bottleneck flow.

Focusing on investigating underlying reason of stochastic capacity and queue discharge at macro-level analysis, this study subsequently analyzes the individual vehicle

trajectory data by using the simplified car following model and demonstrates experimental distributions of stochastic wave speed and jam density. Despite the limitations due to some simplified assumptions, it is reasonable to conclude that the heterogeneity of k_{jam} and w at the micro-level results from individual driving behavior, and the corresponding stochastic capacity and queue discharge rate observed in the field data (marco-level) are also generated by the heterogeneity between individual driving behaviors.

Furthermore, in order to recognize and capture the stochastic day-to-day travel time evolution process, this study tries to apply several theoretical approaches to explicitly account for the travel time variability caused by stochastic capacity and demonstrate the travel time variability in an empirical study. Comparisons are made between the travel time predictions from stochastic and deterministic (HCM level) capacity under the same demand level. The results show to what extent the stochastic capacity contributes to the observed travel time variability.

Stochastic Capacity at Freeway Bottlenecks with Application to Travel Time Prediction

by
Anxi Jia

A dissertation submitted to the Graduate Faculty of
North Carolina State University
in partial fulfillment of the
requirements for the Degree of
Doctor of Philosophy

Civil Engineering

Raleigh, North Carolina

2013

APPROVED BY:

Chair of Advisory Committee
Dr. Nagui M. Rouphail

Co-Chair Dr. Billy M. Williams

Dr. Joseph Hummer

Dr. Peter Bloomfield

Dr. Xuesong Zhou

DEDICATION

This dissertation is dedicated to my ever-supportive parents, Feinan Zhao and Jianping Jia, my loving wife, Fang Li and my amazing son, Ivan Jia.

BIOGRAPHY

Anxi Jia was born on November 16th 1982 in the city of Taiyuan, China. He earned a Bachelor of Science degree in Computer Science and Technology in July, 2004, from Xidian University, Xi'an, China. He obtained the Master of Science degree in Transportation Engineering in August, 2008, from Texas A&M University-Kingsville. He entered the Civil Engineering program at North Carolina State University in 2008 and expects to graduate with a PH.D in May, 2013.

During his time at N.C. State, Anxi served as a graduate research assistant on several research projects under advisor Dr. Nagui M. Rouphail and Dr. Billy M. Williams. After graduation, he wishes to pursue a career in traffic modeling and dynamic traffic assignment.

ACKNOWLEDGMENTS

First and foremost, I would like to express my deepest gratitude to my advisor, Dr. Nagui M. Rouphail, and my co-advisor, Dr. Billy M. Williams. Their guidance, passion for the sharing of knowledge, and tireless dedication has been inspirational over the past four years. Their advice, support and ideas make this research possible. It was personally a rewarding experience to work with them.

I would also like to extend a special thank you to the committee members Dr. Joseph Hummer, Dr. Xuesong Zhou and Dr. Peter Bloomfield. Dr. Hummer's vision and broad outlook helped this study throughout the process and his questions made it stronger. Dr. Zhou's ability to immediately absorb new ideas and share insight provides invaluable resource to achieve my goals. Dr. Bloomfield's expertise in the field of Statistics provides invaluable guidance and technical support through this study.

I would also like to thank the entire C-05 research team, including Wayne Kittelson, Brandon Nevers, William Reynolds, Hyejung Hu, and Li Jin. Their time and contributions set the foundation for this study, and their ideas and feedback were invaluable.

Special thanks to Thomas Chase, Zachary Bugg, Sangkey Kim and Soheil Sajjadi for the technique help.

Finally, I would like to thank my family for the love and support.

TABLE OF CONTENTS

LIST OF TABLES viii

LIST OF FIGURES ix

1. INTRODUCTION 1

1.1 Background 1

1.2 Problem Statement 3

1.3 Research Objectives 7

1.4 Dissertation Organization 8

2. LITERATURE REVIEW 10

2.1 Stochastic Capacity Concept 10

2.2 State of the Practice of Breakdown Identification 11

2.3 Stochastic Capacity Models 13

2.4 Effects of Stochastic Capacity on Dynamic Traffic Assignment Models 15

2.4.1 Conceptual Framework 17

2.4.2 Route Choice Utility Function and Route Switching Rule 18

2.5 Impacts of Stochastic Capacity on Travel Time Prediction 22

3. STOCHASTIC CAPACITY MODELS AT MACRO-LEVEL 25

3.1 Data and Study Site Description 25

3.2 Breakdown Determination 31

3.3 Models for Stochastic Capacity and Queue Discharge 36

3.3.1 Stochastic Capacity Model for Freeway On-ramp Bottlenecks 40

3.3.2 Stochastic Queue Discharge Model 45
3.4 Implementation of Stochastic Capacity Model into DTA Simulation Tool 52
3.5 Summary 63
4. INVESTIGATING STOCHASTIC CAPACITY AT MICRO-LEVEL 65
4.1 Data Description 65
4.2 Methodology 68
4.3 Stochastic Wave Speed and Jam Density 72
4.4 Correlation with the Deterministic Capacity at Marco-Level 81
4.5 Summary 83
5. INVESTIGATING TRAVEL TIME VARIABILITY WITH EMPRIRICAL STUDY 85
5.1 Study Site 86
5.2 Formulate Demand and Capacity distribution 89
5.2.1 Stochastic Capacity Distribution 89
5.2.2 Demand Distribution 90
5.3 Formulate travel time prediction function 98
5.3.1 BPR Function 99
5.3.2 Queuing Theory Approach 104
5.3.3 Shock Wave Theory 110
5.4 Summary 125
6. SUMMARY, CONCLUSIONNS AND RECOMMENDATIONS 127
6.1 Summary 127

6.2 Conclusion 129
6.3 Recommendations 130
7. REFERENCES 132
APPENDICES 140
APPENDIX A: CANDIDATE STUDY SITES 141
APPENDIX B: FLOW-SPEED CURVES OF STUDY SITES 145
APPENDIX C: GOODNESS OF FIT OF THE CAPACITIES 148
APPENDIX D: THE DISTRIBUTIONS OF CAPACITIES 162
APPENDIX E: THE DISTRIBUTIONS OF DEMAND 166
APPENDIX F: SIMULATION FRAMEWORK AND SYSTEM IMPLEMENTATION ... 170

LIST OF TABLES

Table 3.1 Information provided in Transguide database 26

Table 3.2 Information provided in Bay Area database 27

Table 3.3 Basic Information for the Study Sites 30

Table 3.4 Calibrated Traffic Parameters for Each Study Site 35

Table 3.5 Summary of Pre-breakdown Observations Screening Results 38

Table 3.6 Summary of Pre-breakdown Flow Rate Distribution Parameters 43

Table 3.7 Summary of Fitted Queue Discharge Model 48

Table 3.8 Statistics of the Duration of Breakdown 50

Table 3.9 Parameter Estimation of the Cumulative Logistic Regression 51

Table 3.10 Network-wide Travel Time Characteristics of Alternative Improvement Strategies 62

Table 5.1 Parameters of Demand Distribution for Different time Periods 93

Table 5.2 The RMSD of Average Travel Time 124

Table 5.3 The RMSD of Travel Time Standard Deviation 125

LIST OF FIGURES

Figure 1.1 Weekday Travel Times on SH-520 2

Figure 2.1 I-880 Speed Flow Data 13

Figure 2.2 Estimated Capacity Distribution for Freeway A1 14

Figure 3.1 Location of bottlenecks and Detectors in San Antonio Area 29

Figure 3.2 I-880 Speed Flow Data 32

Figure 3.3 Illustrations of the Identification of Pre-breakdown and Breakdown 36

Figure 3.4 Pre-breakdown Flows and Outliers for I-880 40

Figure 3.5 Probability Density and Cumulative Distribution of Pre-Breakdown Flow Rate for I-880 44

Figure 3.6 Simplified Recursive Queue Discharge Model 47

Figure 3.7 Portland Network Study Area 52

Figure 3.8 Network-Wide Simulation Results 59

Figure 3.9 Locations of OR-217 and TV Highway in the Network 60

Figure 4.1 Study Area for NGSIM US 101 Data (Source: (*42*)) 66

Figure 4.2 Study Area for NGSIM I-80 data (Source: (*42*)) 67

Figure 4.3 Vehicles' Trajectories according to Newell's Car Following Model 69

Figure 4.4 An Example of Stop-and-go Condition from NGSIM Data 70

Figure 4.5 Typical Triangular Flow-Density Diagram 71

Figure 4.6 Distribution of w 72

Figure 4.7 Distribution of k_{jam} 73

Figure 4.8 Scatter Plot of Jam Density and Wave Speed 76

Figure 4.9 The Distribution of Stochastic Capacity in Respond to the Distribution of k_{jam} and w 78

Figure 4.10 The Distribution of Stochastic Capacity at Macro-level 79

Figure 4.11 The Distribution of Speed Observed at Capacities 80

Figure 4.12 Wave Propagation along a Platoon 81

Figure 5.1 Study Site 86

Figure 5.2 Average Travel Time of the Target Link from Inrix 88

Figure 5.3 Travel Time Standard Deviation of the Target Link from Inrix 88

Figure 5.4 Stochastic Capacity Distribution of Target Link 89

Figure 5.5 Example of Traffic Demand Estimation 92

Figure 5.6 Demand Distribution for Time Period 6:00 – 6:15 94

Figure 5.7 Correlation between Demands at Two Consecutive Time Intervals 94

Figure 5.8 Implementation Framework of Stochastic Capacity Generation 97

Figure 5.9 Average Travel Time: BPR Simulation vs. Inrix (Deterministic Capacity) 100

Figure 5.10 Travel Time Standard Deviation: BPR Simulation vs. Inrix (Deterministic Capacity) 101

Figure 5.11 Average Travel Time: BPR Simulation vs. Inrix (Stochastic Capacity) 102

Figure 5.12 Travel Time Standard Deviation: BPR Simulation vs. Inrix (Stochastic Capacity) 102

Figure 5.13 Average Travel Time: Queuing Simulation vs. Inrix (Deterministic Capacity) 106
Figure 5.14 Travel Time Standard Deviation: Queuing Simulation vs. Inrix (Deterministic Capacity) 107
Figure 5.15 Average Travel Time: Queuing Simulation vs. Inrix (Stochastic Capacity).... 109
Figure 5.16 Travel Time Standard Deviation: Queuing Simulation vs. Inrix (Stochastic Capacity) 110
Figure 5.17 Illustrative Example of Wave Propagation with Stochastic Demand and Capacity 111
Figure 5.18 Demonstration of Wave Propagation for the Illustrative Example 113
Figure 5.19 Summary of Shock Wave Propagation..... 114
Figure 5.20 Illustrative Example of Vehicle Delay Calculation..... 117
Figure 5.21 Average Travel Time: Shockwave Simulation vs. Inrix (Deterministic Capacity) 120
Figure 5.22 Travel Time Standard Deviation: Shockwave Simulation vs. Inrix (Deterministic Capacity)..... 121
Figure 5.23 Average Travel Time: Shockwave Simulation vs. Inrix (Stochastic Capacity)122
Figure 5.24 Travel Time Standard Deviation: Shockwave Simulation vs. Inrix (Stochastic Capacity)..... 123
Figure F-1 Comprehensive Conceptual Simulation Framework 170
Figure F-2 Implementation Framework of Stochastic Capacity Generation..... 172

Figure F-3 Implementation Framework of Route Choice Mechanism 173

1. INTRODUCTION

1.1 Background

Traffic congestion problems lead to a wide range of adverse consequences such as traffic delays, travel time unreliability, increased noise pollution, as well as air quality deterioration. Broadly speaking, traffic congestion occurs because the available capacity cannot serve the desired demand on a portion of roadway at a particular time. Major sources of congestion include physical bottlenecks, incidents, work zones, bad weather, poor signal timing, special events and day-to-day fluctuations in normal traffic *(1).* Among the seven major congestion sources, physical system bottlenecks, the primary source of recurring congestion, contribute 40% of the travel delay on roadway networks *(1),* which is much greater than the others. Therefore, considerable research efforts have been devoted to understanding the impacts of these physical bottlenecks and analyzing the effectiveness of different traffic mitigation strategies.

To address the impacts of physical bottlenecks, capacity enhancement strategies, including both construction and operational strategies, were widely studied by transportation agencies. A challenge to both transportation practitioners and decision makers is quantifying the effects of these capacity enhancement strategies for the purposes of making investment decisions. Data from field measurement are costly and not readily available to support decision-making. Moreover, their benefits may vary by local conditions, such as transportation network complexity, traffic demand, driver behavior, etc. Therefore, traffic simulation has become an important tool for transportation planners and traffic engineers to

study congestion caused by physical bottlenecks and analyze the effectiveness of various capacity enhancement strategies.

Day-to-day/within-day variations in travel conditions pose a big challenge in a simulation study. For example, Figure 1.1 shows the weekday travel time patterns from 5:00 PM to 6:00 PM on State Highway (SH) 520 Eastbound, Seattle, WA *(1)*.

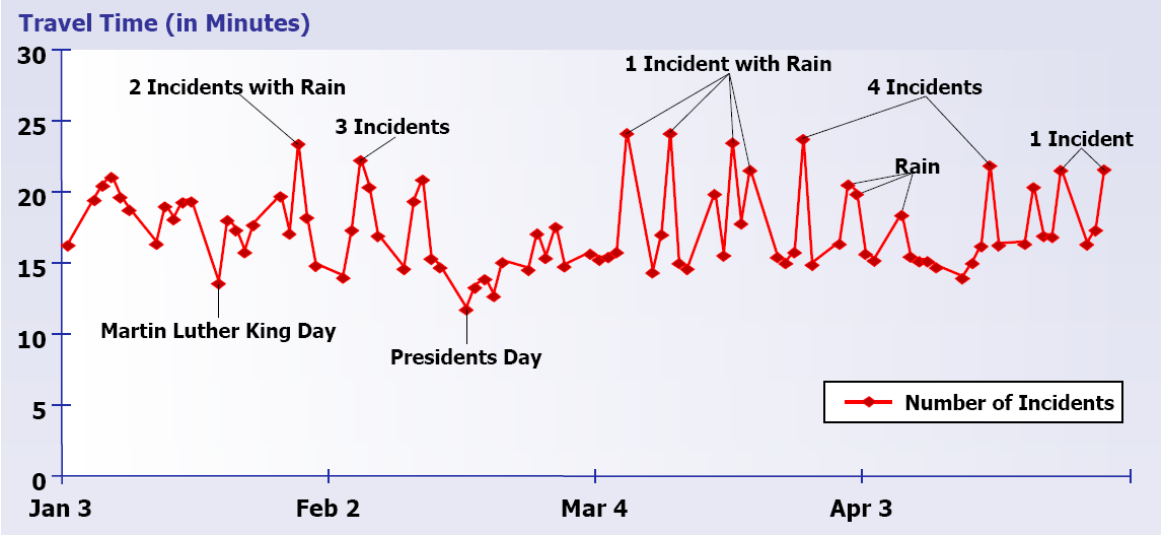

(Source: http://onlinepubs.trb.org/onlinepubs/webinars/PredictingTravelTimeReliabilityPresentations.pdf)

Figure 1.1 Weekday Travel Times on SH-520

Based on the travel time pattern, there are obvious travel time variations on this route even on normal weekdays (i.e., no incidents and good weather). Conventionally, it is widely believed that the day-to-day demand variations result in a fluctuation of the travel time pattern. This conclusion is made based on the assumption that the road capacity is always constant, but this assumption may not be valid. Recently, a research project sponsored by the

Strategic Highway Research Program (SHRP2), titled "Understanding the Contribution of Operations, Technology, and Design to Meeting Highway Capacity Needs," was carried out to investigate this issue. One primary finding from this project is the existence of variations in roadway capacity at the physical bottlenecks in the transportation network. Therefore, besides demand variability, it is quite possible that the capacity variance may also contribute to the observed travel time fluctuation, because the travel time is the function of both demand and capacity.

1.2 Problem Statement

There have been multiple studies aimed at understanding the impacts of physical bottlenecks and analyzing the effectiveness of different traffic mitigation strategies (e.g., road capacity enhancement). Both macroscopic and microscopic models have limitations when it comes to evaluating capacity enhancement strategies in large-scale transportation networks. For example, macroscopic models represent traffic flow in terms of aggregate measures such as flow rate, density, and speed over the modeled time period. Consequently, they are not sensitive to some operational effects of strategies, such as Advanced Traveler Information Systems (ATIS), because they do not consider the constituent individual vehicles and cannot identify more severe traffic problems presented during smaller time intervals. Although they can still handle such operational effects as percent of traffic diverting, they cannot do it in the adaptive and dynamic way since it is assumed that in macroscopic models, all vehicles in the network have the same characteristics. Microscopic models represent individual vehicles' movement and their interaction in detail by implementing car-following models, lane

changing models, etc. Although micro models can provide a more realistic representation of traffic conditions and examine certain complex traffic scenarios, when handling relatively large real-world transportation network the calibration and validation of micro model can be exceedingly time consuming, and the simulation may require an inordinate amount of computational resources compared to their macro counterpart.

Mesoscopic models are at the intermediate level between micro and macro models. Mesoscopic models represent individual vehicle motion based on macroscopic traffic relationships (ex., speed-density function), but not their interactions (*2*). Since mesoscopic models keep recording the travel experience of each individual vehicle, they are normally used as an evaluation tool for traveler information systems. Mesoscopic models integrated with Dynamic Traffic Assignment (DTA) (*3, 4*) have become popular tools for traffic analysts to perform such applications (i.e., capacity enhancement strategy assessment) on large-scale transportation networks because of thier ability to allocate individual vehicle within the network to their destination based on factors that affect their route choice. Over the last three decades, the focus of DTA research has been on the demand characterization side, such as incorporating dynamic time-dependent demand, stochastic departure times, and multiple user classes.

By contrast, the supply side, in which link capacity is a critical factor that may determine the impacts of physical bottlenecks and then the route choice, was mostly overlooked by researchers in the field of DTA. Conventional static and dynamic traffic assignment methods typically assume deterministic (i.e., fixed) road capacity. However,

examination of freeway detector data reveals that breakdowns occur across a wide range of volumes. Even under constant geometric and operational conditions, road capacities vary with time over a certain range around a mean value. Based on the capacity distribution function derived from field data (refer to the data discussed in Chapter 3), the mean value of capacity is about 1900 pc/h/ln, and the maximum capacity is about 2,370 pc/h/ln, which is very close to the value predicted by Highway Capacity Manual (HCM) 2000.

Only recently has the research community begun to accept and study the stochastic capacity concept. Similar to the traditional definition of capacity in the HCM, the queue discharge flow rate is also typically characterized in a deterministic manner. In other words, after a breakdown occurs, the queue will discharge at a constant flow rate. If the capacity were stochastic, it also quite possible that after a breakdown occurs, the queue discharge rate would be stochastic as well. However, few studies have investigated the characteristics of the queue discharge at freeway bottlenecks. Therefore, the characteristics of the queue discharge are also of interest in this study. It is expected that stochastic capacity/queue discharge variability will significantly alter our traditional understanding of the physical bottlenecks under breakdown and queue discharge conditions. Based on the discussion above, HCM capacity levels are more representative of the upper tail of capacity distribution function derived from the field data, and the expected or mean value of capacity appears to be approximately 500 pc/h/ln lower than the HCM-based values. Correspondingly, conventional network modeling tools, which rely on the HCM capacity levels, need to be improved by incorporating stochastic link capacities because they are likely to under-represent the

frequency, duration, and, consequently, the traffic operational impact of network bottlenecks as well as the impact of operational enhancements.

Roadway capacity has conventionally been a constant value. The implication of this definition is that traffic breakdown will occur only if the traffic demand is greater than the constant capacity, which is widely used in traffic condition analysis. However, this is not consistent with field observations: examination of freeway detector data reveals that breakdowns occur across a wide range of traffic volumes. As suggested by field data, capacity could be better represented as a stochastic variable rather than a constant. As a consequence, the stochastic capacity concept will significantly change the way that we analyze traffic networks. For example, considering a single freeway bottleneck with certain demand, the conventional deterministic capacity concept may suggest that breakdown will never occur under this demand level (if the demand is less than the deterministic capacity value) at this bottleneck, while in the stochastic capacity environment, the breakdown may occur with certain probability, which depends on the demand level. Although stochastic capacities have been observed and discussed by several researchers, there are not stochastic capacity models readily available for real-world application. Therefore, continued research is needed to increase understanding and provide realistic, implementable stochastic capacity models for the physical bottlenecks.

As discussed above, the stochastic capacity concept will significantly change the way that we look at the traffic network. Therefore, some research hypothesis include: how can we quantify the effects of stochastic capacity on traffic conditions in terms of performance

measures, such as travel time or travel time variability? For example, observations in Figure 1.1, would seek to explore the extent to which the stochastic capacity contribute to the observed travel time variability. Does the stochastic capacity really play an important role in the travel time estimation? Furthermore, in the DTA simulation environment, travel time is the key criterion for route switching in traffic assignment models. How will the travel time variance introduced by stochastic capacity impact the traffic assignment models? Therefore, a theoretical approach is needed to account for the travel time variability due to stochastic capacity. This is a critical intermediate step to incorporate stochastic capacity into DTA simulation tools.

1.3 Research Objectives

The objective of this study is to analyze stochastic characteristics of road capacity for freeway physical bottlenecks and develop a theoretical approach to account for the travel time variance introduced by stochastic capacity. More specific, this study will try to answer following questions:

- Does the stochastic capacity exist?
- How to quantify the stochastic capacity and the corresponding queue discharge?
- What is the possible underlying reason of the stochastic characteristics?
- Is stochastic capacity important for the traffic analysis (ex., travel time analysis)?

This research is expected to produce a better understanding of stochastic capacity and queue discharge for freeway bottlenecks and a realistic assessment of its impacts in the transportation network. It is expected to improve the capability of analytical or simulation models in terms of addressing travel time variation caused by stochastic capacity and then produce better estimations from these models for the travel time studies. It is also expected that the results of this study will contribute to a more valid benefit/cost analysis of capacity enhancement strategies so as to support the decision making by transportation planners.

1.4 Dissertation Organization

This dissertation is organized in six chapters:

Chapter 1 introduces background, problem statement, and objectives.

Chapter 2 presents a literature review of stochastic capacity concept, state of the practice of breakdown identification, stochastic capacity models and the effects of stochastic capacity on dynamic traffic assignment models.

Chapter 3 describes the analysis of stochastic capacity models at macro level, including data description, study site selection, breakdown determination, stochastic capacity model for freeway bottlenecks, stochastic queue discharge model and the implementation of stochastic capacity model into DTA simulation tool.

Chapter 4 presents the analysis of stochastic capacity at micro level with the focus on explaining the underlying phenomena of stochastic capacity.

Chapter 5 presents the importance of stochastic capacity and queue discharge concept in traffic operational analysis by demonstrating to what extent the stochastic capacity can contribute to the observed travel time variability.

Chapter 6 summarized conclusions and recommendations for future study.

2. LITERATURE REVIEW

In this chapter, studies on stochastic capacity as well as the state of the practice of DTA models are reviewed.

2.1 Stochastic Capacity Concept

In the 2000 edition of the *Highway Capacity Manual* (HCM 2000), freeway capacity is defined as "the maximum hourly rate at which vehicles reasonably can be expected to traverse a point or a uniform section of a roadway during a given time period under prevailing roadway, traffic, and control conditions" (*5*). In keeping with this definition of freeway capacity, it is widely accepted by most traffic analysts that the facility will experience breakdown (i.e. a transition from an uncongested state to a congested state) only if the traffic demand exceeds a specified capacity value. In other words, the breakdown is treated as a deterministic phenomenon, and the freeway capacity is taken to be a constant value. However, an emerging body of research (*6-11*) indicates that the traffic flow rate during the time intervals preceding observed instances of freeway breakdown (called pre-breakdown flow rate in this study) is better represented as a random variable than a fixed value. For example, Lorenz and Elefteriadou (*10*) clearly described the stochastic freeway capacity concept. The findings described in their paper indicate that breakdown is not a deterministic event and that it could occur at any given flow rate with a finite probability (zero probability at many low flow rates). This suggests that breakdown could occur across a wide range of volumes and the probability of the breakdown occurrence varies by the volumes: higher volume results in higher probability of breakdown. Due to the stochastic

nature of freeway capacity, Lorenz and Elefteriadou (*10*) also suggested a new terminology, called sustainable flow rate, as the substituent of conventional deterministic capacity. The sustainable flow rate could be defined as the maximum flow rate up to which tolerable traffic performance (i.e. certain breakdown probability) of the facility is achieved and beyond which intolerable traffic conditions are likely to arise. As the tolerable traffic performance is defined differently, the sustainable flow rate may vary correspondingly even for a same roadway segment, which makes the sustainable flow rate a stochastic variable in contrast to the conventional deterministic capacity. Although these studies did not quantify the capacity variations, they do demonstrate the stochastic nature of freeway capacity through the analysis of real-world traffic data.

2.2 State of the Practice of Breakdown Identification

Breakdown determination is the critical starting point for both stochastic capacity and queue discharge studies. In current practice, the flow rates just preceding the breakdown condition are used to analyze the freeway stochastic capacity. The flow rate data are typically time indexed data aggregated at five- or fifteen-minute intervals. The studies specified a critical speed or a critical speed drop to define the freeway breakdown. However, while such a speed-based threshold can be well defined in reference to representative traffic flow characteristics, the threshold value will vary by location. For example, extensive analysis of Los Angeles freeway data suggests that free flow speed is around 60 mph and that at breakdown the operating speed rapidly drops below 40mph (*12*). Researchers in Los Angeles therefore specified a minimum speed differential of 20 mph and a speed threshold of 40 mph

to identify a breakdown event using five-minute data. Using data obtained from Toronto freeways, on the other hand, Elefteriadou defined that breakdown occurred "when the average speed of all lanes on the freeway dropped below 90 km/hr (56mph) for a period of at least five minutes" (*13*). These examples clearly illustrate that setting a specific, universal speed threshold is not advisable and the threshold for breakdown identification requires local calibration. Instead freeway breakdown analyses should be based upon speed thresholds extracted from the speed flow observations. Moreover, a recent study by Jia et al. (*14*) suggests that it is problematic to use speed as the only criterion to define breakdown. Based on the 15-minute sensor data from I-880 in the San Francisco Bay Area (Figure 2.1), they found that a single speed threshold was not considered sufficient for determining congested conditions. As shown in Figure 2.1, by applying a single speed threshold (speed differential of 20 mph), observed conditions exhibiting a flow rate lower than 1000 vph per lane but with speeds higher than 40 mph were considered to be reflective of anomalous free-flow conditions rather than congested conditions. The presence of low flow observations below the single speed threshold creates the need for a robust phase boundary for defining congested conditions.

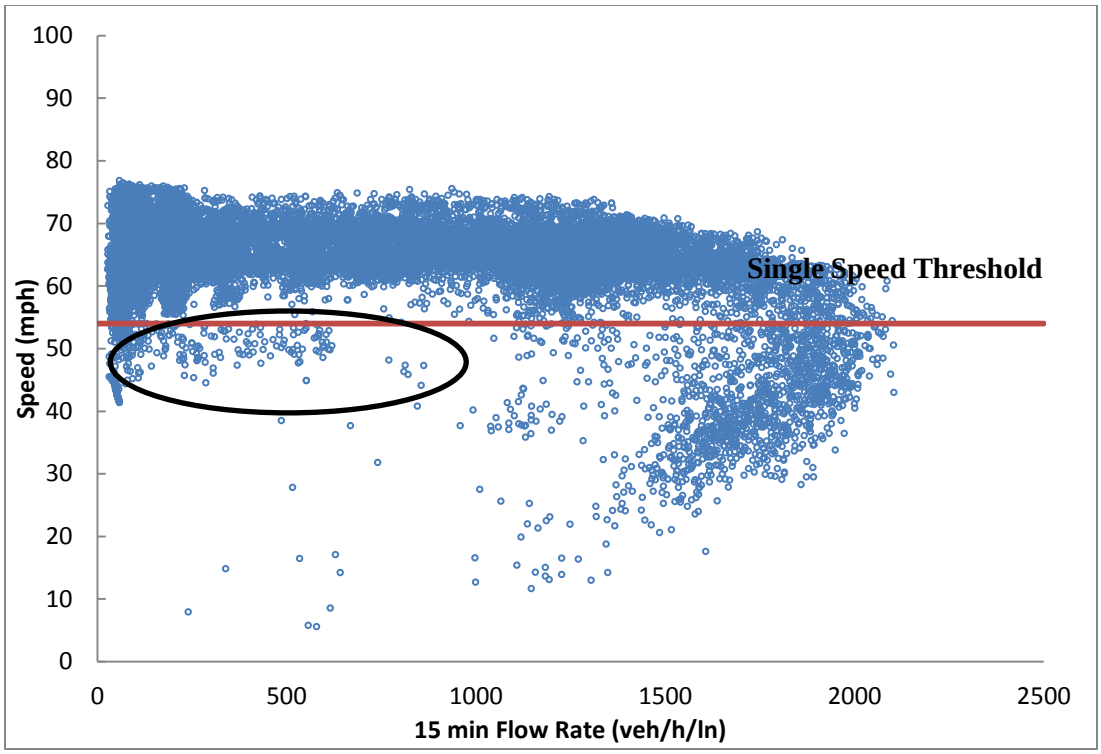

Figure 2.1 I-880 Speed Flow Data

2.3 Stochastic Capacity Models

Zurlinden (*15*) and Brilon (*16*) developed a methodology to derive roadway pre-breakdown distribution functions for the purpose of implementing the stochastic capacity concept. In the most recent study, Brilon (*17*) suggested the Weibull distribution for characterizing the stochastic capacity based on traffic data from German freeways. Based on the probabilistic nature of freeway capacity, Dong and Mahmassani (*18*) first illustrated the significant effects of the stochastic concept on travel time reliability. Figure 2.2 illustrates the estimated stochastic capacity distribution for Freeway A1, a two-lane freeway segment in Germany, developed in Brilon's study *(17)*.

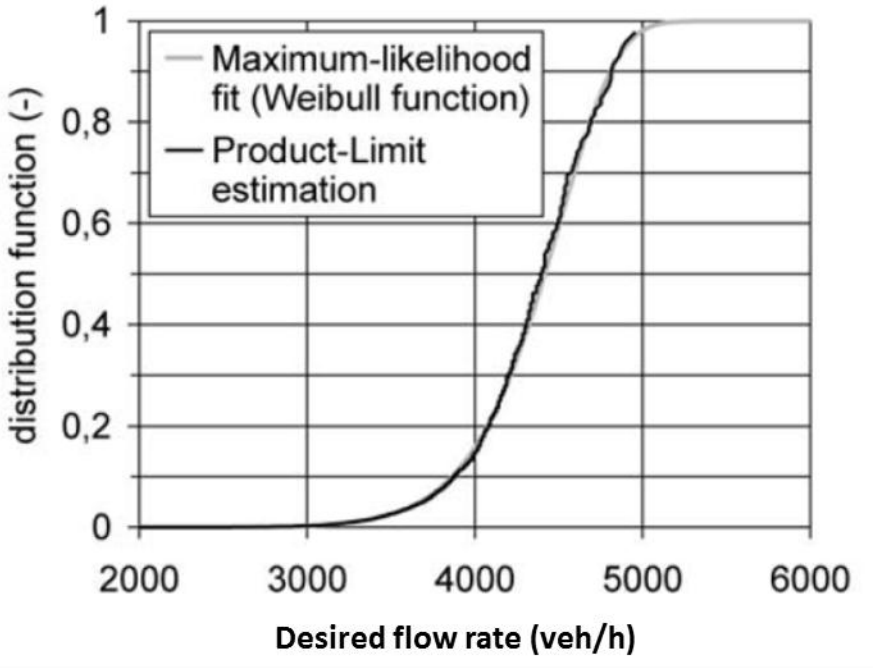

(Source: http://www.ruhr-uni-bochum.de/verkehrswesen/vk/deutsch/Mitarbeiter/Brilon/ISTTT16_Brilon_Geistefeldt_Regler_final_citation.pdf)

Figure 2.2 Estimated Capacity Distribution for Freeway A1

As shown in the figure, a single capacity value is not appropriate for defining breakdown on freeway bottlenecks. The trend illustrated by the figure also indicates that the slope of the cumulative density function continually increase with increasing values of flow rate. This trend is consistent with findings from previous studies (*10, 17*), which show the probability of breakdown increasing with increasing flow rate. Therefore, the freeway data calibration results indicate that the HCM capacity levels are more representative of the upper tail of the capacity observations and conversely are not representative of the expected or mean capacity values for freeway segments downstream of the freeway bottleneck.

Similar to the traditional definition of capacity in the HCM, the queue discharge flow rate is also typically characterized in a deterministic manner. In other words, after a breakdown occurs, the queue will discharge at a constant flow rate. Based on field data, Lorenz and Elefteriadou (*10*) have clearly demonstrated that the queue discharge flow rate is also stochastic in nature. Further, Dong and Mahmassani (*19*) suggested a linear relationship between queue discharge rate and the pre-breakdown flow rate. In a most recent study, Jia et.al, (*14*) concluded that the queue discharge rate series are strongly time-correlated and developed a recursive queue discharge model. In their model, the queue discharge rates converge to the mean discharge rate for breakdowns that are initiated with stochastic average pre-breakdown headway probability distribution.

2.4 Effects of Stochastic Capacity on Dynamic Traffic Assignment Models

As stated previously, conventional traffic assignment methods assume static, deterministic segment capacity. Therefore, travel time on a path only depends on the flow pattern on that path. In other words, for a fixed network-wide path flow pattern, the corresponding path travel times do not change. Within the stochastic capacity concept, however, real-world road capacities vary with time over a certain range, and a driver's travel experience on a single day can be dramatically affected by the underlying realized capacity values on that particular day. In other words, travelers will experience different travel times on the same path over different days even under the same path flow pattern because of the inherent travel time variability introduced by stochastic capacity. As a result, conventional "within-day" or iterative route choice methods for reaching user equilibrium, such as the

method of successive averaging (MSA *(20)*), may not enable drivers to recognize and appropriately respond to the travel time variability/unreliability resulting from capacity fluctuation. A theoretically rigorous and practically useful traveler route choice model is crucially needed in order to adaptively capture the stochastic day-to-day travel time evolution process and also to maintain robustness under disruptions due to stochastic capacity reductions.

To better describe adaptive traveler behavior and simulate the resulting travel flow pattern in an environment where roadway capacity varies within single day and over multiple days, a day-to-day learning framework is needed to allow a realistic consideration and evaluation of different capacity-enhancing and traffic management scenarios. A wide variety of day-to-day learning models have been proposed to understand and simulate the medium-term traffic evolution process under various advanced traveler information provision strategies. An early study by Hu and Mahmassani (*21*) took into account both route and departure time choices as the sources of day-to-day traffic dynamics. Srinivasan and Guo (*22*) examined network evolution (i.e., the network traffic condition or performance) and user response characteristics under varying market penetration levels of traveler information. Jha et al. (*23*) adapted a Bayesian framework to model the traveler perception updating process. Chen and Mahmassani (*24*) further studied triggering mechanism and termination conditions for the travel time learning process. All existing day-to-day learning frameworks assume a constant road capacity, and the variability sources considered in those models are limited to route and departure time choices only. As discussed before, however, based on field data,

road capacities vary with time over a certain range. In order to represent the traffic network in a more realistic way, capacity variance should be incorporated with other variability source. Correspondingly, the simulation frameworks should be improved to account for the new variance introduced by stochastic capacity.

2.4.1 Conceptual Framework

The day-to-day learning framework proposed by Hu and Mahmassani (*21*) and Jha et al. (*23*), as shown in equation 2-1, 2-2 and 2-3, provides a promising path for seamlessly integrating stochastic capacity models in the DTA simulator for large-scale networks. Generally speaking, the learning behavior in such a day-to-day learning framework is determined by each vehicle's historical travel experiences, the traveler information obtained before and during the trip, as well as newly experienced travel times on the current day.

Conceptually, the model includes three components:

Traffic flow assignment model: $f^{d+1} = A(f^d, T^d, w^d)$ (2-1)

Stochastic traffic system simulation process: $t^d = S(f^d) + w^d$ (2-2)

Travel time perception model: $T^d = t^d + \varepsilon^d$ (2-3)

Where:

f^d = assigned route flow pattern on day *d*, determined by traffic assignment model/function $A(\cdot)$,

t^d = true travel time on day *d*, determined by dynamic assignment/simulation function $S(\cdot)$,

w^d = the system noise introduced by the stochastic capacity,

T^d = the observed travel time by a traveler,

ε^d = the traveler perception error associated with perceived travel time in the network, introduced by sampling error associated with personal experience and quality of information.

It should be noted that most existing day-to-day learning models are implemented assuming stable road capacity, and therefore no system noise, i.e. $w^d = 0$, so the travel time t^d is a deterministic vector for a given set of route flows, f^d in Equation 2-2. Accordingly, the focus in previous research has been on how to reach the deterministic steady-state conditions, and how to construct realistic learning/updating models for the travel time perception error term ε^d related to Equation 2-3.

2.4.2 Route Choice Utility Function and Route Switching Rule

A behaviorally sound route choice utility function was proposed and calibrated by Brownstone and Small (*25*) and Lam and Small (*26*), which considers the stochastic nature of traffic systems.

$$GT = T + \frac{VOR}{VOT} \times TSD + \frac{TOLL}{VOT} = T + \beta \times TSD + \frac{TOLL}{VOT} \quad (2\text{-}4)$$

Where,

GT= generalized travel time (hour),

T = the expected travel time for a traveler,

TSD = perceived travel time variability.

β = reliability ratio (computed as the ratio of Value of Reliability (VOR) and Value of Time (VOT)).

TOLL = road toll charge; assumed to be zero in the following discussion as no toll-related strategies will be evaluated in this research.

It has been well recognized that travel time variability and reliability are important measures of service quality for travelers. In the above utility function, Equation 2-4, the travel time standard deviation (*TSD*) is used to measure system travel time variability associated with the underlying stochastic traffic process. This contrasts with the perception error variance in a deterministic assignment model. For a single traveler *v*, the route choice decision is made by comparing the generalized travel time of habitual path, GT_v^h, and that of alternate path, GT_v^a. The traveler will switch to the alternative path from his/her habitual path only if the following condition were met:

$$GT_v^h > GT_v^a \tag{2-5}$$

Where,

v = traveler index,

h=index for habitual path, and

a=index for potential alternative path.

According to Equation 2-4, if the generalized travel time of the habitual path, GT_v^h, is greater than that of alternate path, GT_v^a, as shown in Equation 2-5, a driver should switch his/her route from the habitual path to the alternative path. The resulting decision rule could be derived as:

$$T_v^h - T_v^a > \beta(TSD_v^a - TSD_v^h) \tag{2-6}$$

A bounded rationality model, which states that a driver's decision depends on their desired satisfaction level, is usually adapted to make the route choice comparison. The bounded rationality concept is employed because there has been growing attention (starting

from the early work by Mahmassani and Herman (*27*)) since Herbert Simon (*28*) pointed out that perfectly rational decisions are often not feasible given the limits of human cognition.

Based on the minimum acceptable absolute tolerance and the relative acceptable tolerance, a set of bounded rationality rules, shown in Equation 2-7, are used to describe users' route switching behavior. As opposed to the optimization theory in which users select the best option from *all possible* decisions, in the bounded rationality approach, users perform limited searches, accepting the first satisfactory decision.

$$\delta \begin{cases} 1 & \text{if } \bar{T}_v^{d-K,d-1} - T_v^a > MAX[\alpha, \lambda * T_v^h)] \\ 0 & \text{otherwise} \end{cases} \quad (2\text{-}7)$$

Where,

$\boldsymbol{\delta}$ =1, switch to an alternative path; 0, remain on the habitual/ current path,

α = Minimum acceptable absolute tolerance needed for a switch *and* $\alpha = \beta(TSD_v^a - TSD_v^h)$,

λ = Relative acceptable tolerance (i.e. relative improvement threshold).

However, by assuming constant demand level and stable road capacity (i.e., no system noise, $w^d = 0$), it is impossible to calculate the perceived travel time variability. Therefore, in most studies, the above minimum acceptable absolute tolerance is always assumed as a constant value in order to apply the bounded rationality approach. The models proposed in the past to describe drivers' travel choice behavior are based on the assumption that drivers select paths to minimize their perceived travel times (*29*).

As a result, most previous study efforts only focus on how to estimate the updated travel time and the travel time variability is assumed as zero. For example, Horowitz (*30*) suggested an equilibrium model in which travel choices on each day are based on weighted

averages of measured travel times on previous days. A simple extension of the above approach would be to allow the weights to vary across individuals. Under the myopic adjustment approach, Mahmassani and Chang (*31*) modeled drivers' travel choices based on the previous day's experience. The updating process is given by the following equation:

$$\tau_{i,d} = t_{i,d-1} + a_i\lambda^c_{i,d-1}E_{i,d-1} + b_i\lambda^l_{i,d-1}E_{i,d-1} \quad (2\text{-}8)$$

Where,

$\tau_{i,d}$ = updated travel time by driver i;

$t_{i,d-1}$ = experienced trip time by driver i on day d-1;

$E_{i,d-1}$ = schedule delay of driver i on day d-1;

a, b = parameters reflecting the relative weights of earliness and lateness

$\lambda^c_{i,d-1}$ = binary variable such that $\lambda^c_{i,d-1} = -1$ for early arrival and otherwise $\lambda^c_{i,d-1} = 0$;

$\lambda^l_{i,d-1}$ = binary variable such that $\lambda^l_{i,d-1} = -1$ for late arrival and otherwise $\lambda^l_{i,d-1} = 0$;

Jhe et al. (*23*) proposed a perceived travel time updating model based on Bayesian updating. The perceived travel time is given by:

$$\tau_{i,d} = \beta\left(\tau^u_{i,d}\right) + (1-\beta)T^{ed}_{i,d} \quad (2\text{-}9)$$

Where,

$\tau^u_{i,d}$ = prior mean;

$T^{ed}_{i,d}$ = Mean of the sample

β = parameter based on the updated variance.

Although it is not well known how the travel variability will impact the accuracy of dynamic traffic assignment simulation, researchers do realized that ignorance of travel time

variability already constrains the analysis capability of the dynamic traffic assignment simulation tools. For example, it is difficult to evaluate the travel variability, which has become a very important operational criterion to assess the transportation network performance.

Therefore, several studies have considered the stochastic demand in the simulation, for example, by incorporating dynamic departure time choice. However, travel time is a function of both demand and supply. It is also important to investigate whether the incorporation of stochastic capacity will improve the estimation of travel time variability. Within the stochastic capacity environment, it is reasonable to expect that drivers' perception of travel time would change across different days.

2.5 Impacts of Stochastic Capacity on Travel Time Prediction

The researchers have realized that the incorporation of stochastic inputs (i.e., demand and capacity) into the traffic system will significantly alter the characteristics of travel time, especially the travel time variance. Focusing on analytical Bureau of Public Roads (BPR) functions, which is widely used U.S., several studies have developed numerical approximation methods to predict travel time variability distributions due to the stochastic capacity or the stochastic demand. Lo and Tung (*32*) implemented the Mellin transforms-based method to estimate the mean and variance of travel time distribution due to the stochastic capacity, which is modeled as a uniform probability distribution function. Through a sensitivity analysis of the link representation in a network based on a multivariate normal distribution, Clark and Watling (*33*) proposed a procedure to develop the probability density

function of link travel times within stochastic demand environment. Ng and Waller (*34*) calculated the probability density function of travel time within stochastic capacity environment by using a Fourier transformation approach. Recently, Zhou et al. (*35*) has derived the distribution of the link travel time based on BPR function. If demand, *d*, is assumed constant and the stochastic link capacity *C* follows a Lognormal distribution ($C \sim LogNormal\ (\mu_c, \sigma_c^2)$), the link travel time can be estimated as:

$$t - t_0 \sim LogNormal\left(\ln(\alpha\, t_0) + \beta(d - \mu_c)\,, \beta^2 \sigma_c^2\right) \quad (2\text{-}10)$$

Where,

t_0 = link free-flow travel time

d = traffic demand

μ_c = mean of stochastic link capacity

σ_c = standard deviation of stochastic link capacity

α = coefficient of BPR function (often set at 0.15)

β = exponent of BPR function (often set at 4.0)

Although several analytical studies have been conducted focusing on the BPR function, it has been well known that the BPR function cannot effectively describe the dynamic buildup and dissipation of traffic system congestion. Therefore, the travel time estimation studies above based on BPR function are more suitable for analyzing long-term steady-state traffic equilibrium results (*35*). A robust theoretical approach is required to account for the travel time variability introduced by stochastic capacity, especially under heavy congestion conditions. Moreover, travel time is a function of both demand and supply

and therefore the approach should incorporate both stochastic demand and capacity simultaneously.

3. STOCHASTIC CAPACITY MODELS AT MACRO-LEVEL

In this chapter, the stochastic capacity models developed at Marco-level are summarized. This chapter is organized as follows. Section 3.1 first introduces the field dataset used to develop the stochastic capacity models. This is followed by the breakdown identification procedure (section 3.2), and the stochastic capacity models in terms of pre-breakdown flow and queue discharge (section 3.3).

3.1 Data and Study Site Description

In this study, data were assembled from the TransGuide system (36) in San Antonio, Texas, and from PeMS data (37) archived for the San Francisco Bay Area (CALTRANS District 4) in California. Data for both locations are available from online databases. The TransGuide database provides traffic volume, speed, and occupancy data gathered from the initial 26 miles of instrumented highways within the Texas Department of Transportation TransGuide project. The extracted data set for this study is the daily raw data (20 sec. intervals) from 01/01/2007 to 09/30/2008. The information provided by TransGuide database is summarized in the Table 3.1.

The Bay Area data used in this study are processed traffic data, which include volume, speed, and occupancy. The data covered the period from 01/01/2007 to 09/30/2008 aggregated at a five-minute interval. The information provided by the PeMS database is summarized in the Table 3.2.

Table 3.1 Information provided in Transguide database

Column	Units	Description
Date		Date of data as MM/DD/YYYY
Time		Time of data as HH24:MI:SS
Lane		Lane N, N ranges from 1 to the number of lanes at the location
Roadway		Route # and direction
ID		Unique detector identifier
Speed	Mph	Format: Speed=**
Volume	Veh	Format: Volume=***
Occ	%	Format: Occ=***

Since the Bay area data were pre-processed and aggregated by PeMS, there are no missing observations in the dataset. For TransGuide data, however, there are a small number of missing observations. Therefore, before performing the data aggregation, the corresponding days with missing observations were removed from the dataset. Because the entire dataset covers twenty-one months and the missing observations represented a small portion of the data set, deletion of the missing values is a reasonable approach. Both TransGuide and PeMS databases provide detailed location information for each sensor on the freeway system. As discussed below, this detailed location data are important for selecting appropriate bottleneck locations for this study.

Table 3.2 Information provided in Bay Area database

Column	Units	Description
Timestamp		Date of data as MM/DD/YYYY HH24:MI:SS. Note that the indicates the beginning of the summary period. For example, a time of 08:00:00 reports measurements from between 08:00:00 and 08:59:59.
Station		Unique station identifier. Use this value to cross-reference with *Metadata* files.
District		District #
Route		Route #
Direction of Travel		N | S | E | W
Station Type		CD = Coll/Dist FF = Fwy-Fwy HV = HOV FR = Off Ramp OR = On Ramp ML = Mainline
Station Length		Segment length covered by the station in Miles/km.
Samples		Total number of samples received for all lanes.
% Observed	%	Percentage of individual lane points at this location that were observed (e.g. not imputed).
Total Flow	Veh/5-min	Sum of flows over the 5-minute period across all lanes. Note that the basic 5-minute rollup normalizes flow by the number of good samples received from the controller.
Avg Occupancy	%	Average occupancy across all lanes over the 5-minute period expressed as a decimal number between 0 and 1.
Avg Speed	Mph	Flow-weighted average speed over the 5-minute period across all lanes. If flow is 0, mathematical average of 5-minute station speeds.
Lane N Samples		Number of good samples received for lane N. N ranges from 1 to the number of lanes at the location.
Lane N Flow	Veh/Hour	Total flow for lane N over the 5-minute period normalized by the number of good samples.
Lane N Avg Occ	%	Average occupancy for lane N expressed as a decimal number between 0 and 1. N ranges from 1 to the number of lanes at the location.
Lane N Avg Speed	Mph	Flow-weighted average of lane N speeds. If flow is 0, mathematical average of 5-minute lane speeds. N ranges from 1 to the number of lanes
Lane N Observed		1 indicates observed data, 0 indicates imputed.

As a basis for developing and demonstrating the stochastic freeway bottleneck models, the most common freeway bottleneck feature, i.e. on-ramp junctions, was selected for detailed study. The ideal bottlenecks for this study should be the on-ramp junctions with a sufficient number of breakdown observations. PeMS system has listed the active bottlenecks in Bay Area. The analyst selected the locations where congestion occurs more than during 10 or more days per month as the candidate study sites in Bay Area. Compared with PeMS system, the TransGuide database did not indicate the active bottlenecks in the freeway network. Therefore, what the analyst did firstly is to record all geometric bottlenecks through Google Map in the areas covered by TransGuide detectors. The candidate study sites in both Bay Area and San Antonio Area are summarized in the Appendix A. The next step is to identify the appropriate study sites from the candidates for the pre-breakdown model and queue discharge model development. In order to control for possible confounding operational effects and isolate ramp merge bottleneck effects, a systematic process was developed for study site selection. The site selection criteria were:

- Sufficient distance between the on-ramp and the nearest downstream bottleneck. The longer the distance to a potential downstream bottleneck (e.g. on-ramp), the greater the likelihood that the data will not be confounded by the presence of downstream queues regularly spilling back to the bottleneck location under consideration;
- Suitably placed sensor data. Ideal detector is the one just downstream of the bottleneck; and

- Presence of traffic demand high enough to yield regular freeway breakdown. This criterion ensures an adequate freeway breakdown sample size.

The first and second criteria are applied to identify the potential on-ramp bottlenecks with appropriate detectors. The third criterion is then applied to make sure that there is enough traffic demand to result in regular traffic breakdown. Since the candidate sites in the Bay Area are real bottlenecks, the third criterion is not a problem. In the San Antonio Area, however, the analyst needs to apply the first and second criteria and then retrieve the traffic data from the detectors to verify the third one. For every bottleneck and detector, their location information is either longitude/latitude or mile point. Therefore, ArcMap was used here to facilitate the examination of first two criteria. The following ArcMap image (Figure 3.1) illustrates the candidate bottlenecks and the detectors in the San Antonio Area.

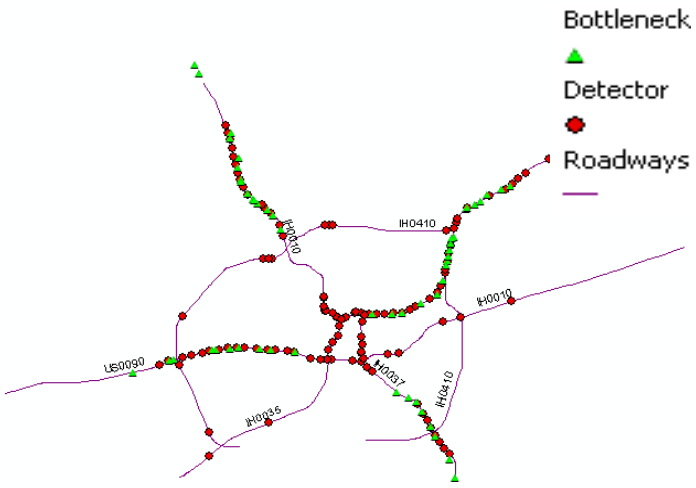

Figure 3.1 Location of bottlenecks and Detectors in San Antonio Area

Based on the three criteria above, seven on-ramp bottlenecks were selected as the study sample. Two of the sites are in the San Antonio area, and the remaining five are from the Bay area. The basic information for each on-ramp bottleneck site is summarized in Table 3.3.

Table 3.3 Basic Information for the Study Sites

Site #	Highway*	Direction	# Lanes	Dis. to downstream Bottleneck (KM)	Dis. to Detector (KM)
1	I-880 (BA)	S	4	3.0	0.1
2	I-680 (BA)	S	3	2.6	0.1
3	I-280 (BA)	N	4	N.A*	0.36
4	I-580 (BA)	W	4	N.A	0.25
5	I-680 (BA)	N	4	6.1	0.12
6	I-35 (SAT)	N	3	3.6	0.18
7	I-35 (SAT)	S	3	2.2	0.38

*Notes: “N.A” indicates there is no adjacent downstream bottleneck within 10 kilometers;
*Highway (BA=Bay Area; SAT=San Antonio)

3.2 Breakdown Determination

Breakdown determination is the critical starting point for both stochastic capacity and queue discharge studies. As mentioned earlier, although most previous studies used speed as the threshold, a single speed threshold was not considered appropriate for determining congested conditions based on the speed-flow diagram from field data. Figure 3.2 shows 21 months of 15-minute freeway data from the I-880 in Bay Area in CA. The horizontal line superimposed on the plot indicates the speed boundary that was used to isolate congested conditions. As is apparent from the graph, a single speed threshold was not considered sufficient for determining congested conditions. Observed conditions exhibiting a flow rate lower than 1000 vph per lane but with speeds higher than 40 mph were considered to be reflective of anomalous free-flow conditions rather than congested conditions. The data pattern shown in Figure 3.2 is typical of the seven on-ramp sites, and the presence of low flow observations below the critical speed threshold creates the need for a robust phase boundary for defining congested conditions.

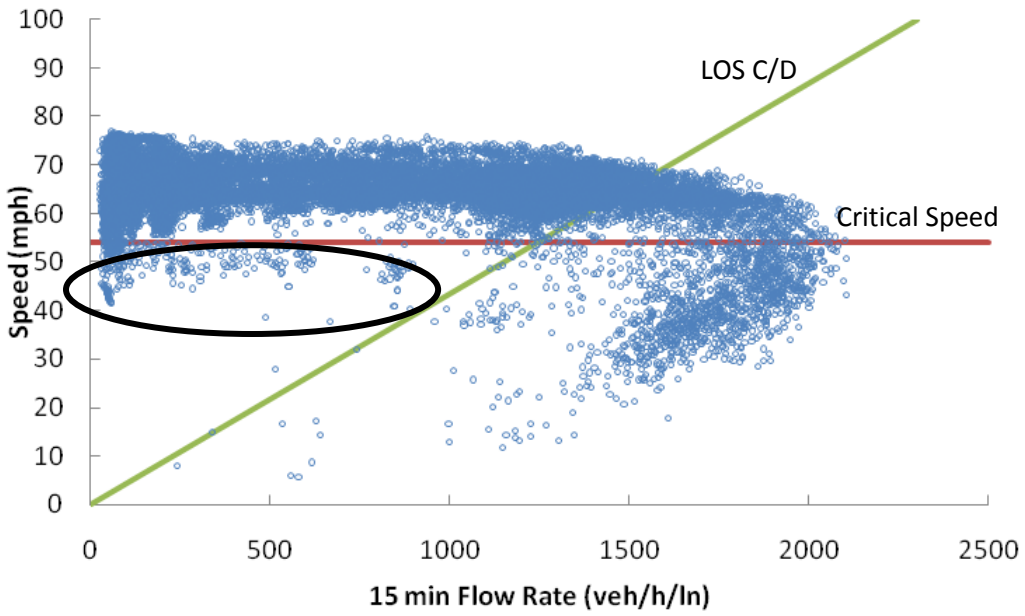

Figure 3.2 I-880 Speed Flow Data

Therefore, a combination of speed and density (diagonal line in Figure 3.2) threshold was applied to identify congested conditions, thereby avoiding the inclusion of anomalous low speed data such as the observations identified within the oval in Figure 3.2. The observed traffic states are considered to represent congested conditions only when:

a) The observed speed is below the critical speed **AND**

b) The observed density is greater than or equal to boundary between level of service C and D (LOS C/D).

As mentioned above, the critical speed and the density at the LOS C/D boundary are locally calibrated for each of the specific study sites. The procedure for calculating these site specific thresholds is described in the following paragraphs.

First, 15-minute flow rate values, q, in the top one percentile tail are identified. The average of this sample of near maximum flows was found to be generally equivalent to the traditional capacity defined in the HCM. Secondly, the density for each 15-minute observation is then calculated by:

$$k = q/\bar{u} \tag{3-1}$$

Where,

k: Density for each 15-min. observation (veh/mi/ln)

q: 15-min. flow rate for the top one percentile flows (veh/h/ln)

$\bar{u}$: Space mean speed (mph)

The critical speed is then calculated as:

$$\bar{u}_{critical} = \frac{\sum q}{\sum k} \tag{3-2}$$

Where,

q: 15 min. flow rate in the top one percentile flows;

k: 15 min. density corresponding to flow q.

The equivalent density at capacity based on HCM definition is calculated by

$$k_{capacity} = \frac{1}{n}\sum k \tag{3-3}$$

Where,

n: Number of 15-min. observations in the top one percentile flow region

Finally, the adjusted *HCM*-based, critical density threshold (LOS C/D boundary) is calculated by

$$\boldsymbol{k_{critical} = \frac{26(k_{capacity})}{45}} \quad (3\text{-}4)$$

Where,

26 pc/mi/ln represents the maximum density per lane passenger car equivalent density for LOS C for basic freeway segments per *HCM 2000*

45 pc/mi/ln respresents the corresponding per lane passenger car density at capacity

It should be noted that the equation above provides adjusted values for the LOS C/D thresholds based on the observed density at capacity. In summary, traffic condition observations are identified as representing congested flow when the observed 15-minute speed, $\overline{\mu}$, is less than the critical speed, $\overline{\mu}_{Critical}$, **and** the observed 15-minute density, $k = Q/\bar{u}$, is greater than the critical density, $k_{Critical}$, as specified in Equation 3-2 and 3-4, respectively.

Each of the study sites was analyzed independently. At each site, the speed and vehicle count data were summarized in 15-min. intervals across all lanes. The vehicle count data were then expressed as equivalent hourly flow rates per lane. Based on the above methodology, the traffic parameters for each study site are summarized in Table 3.4. The corresponding flow-speed curves (Appendix B) for each study site were plotted and illustrated for three different traffic states ("Free Flow", "Congestion", and "Pre-Breakdown Flow").

Table 3.4 Calibrated Traffic Parameters for Each Study Site

Site #	Highway	Average Top 1 percentile Flow Rate (veh/h/ln)	Critical Speed (mph)	Density (C/D) (veh/mi/ln)
1	I-880 (BA)	2052	56	21
2	I-680 (BA)	2093	53	23
3	I-280 (BA)	2183	53	24
4	I-580 (BA)	1982	49	23
5	I-680 (BA)	2127	54	23
6	I-35 (SAT)	1992	47	23
7	I-35 (SAT)	2172	63	20

In order to ensure the identified breakdown was not due to the downstream queue spillback, traffic data from the next downstream sensor were also analyzed following the same procedure above. The breakdown observations at the study sites were screened out from the study sample whenever there were simultaneous downstream breakdown observations. Moreover, based on the information provided by PeMS, there is no long-term work zone closure to the study sites during the analysis period.

Taking traffic observations of site 1 on January 3rd , 2007 from 15:00 to 18:15 as an example, the way how pre-breakdown flow rate and breakdown are identified is demonstrated in Figure 3.3. Based on the speed and density of the traffic observations at 15 minute interval, the breakdowns (highlighted in green cycles) are identified as the observed

speed is below the critical speed (56 mph in this example) **and** the observed density is greater than or equal to boundary between level of service C and D (21 veh/mi/ln in this example). The uncongested state just preceding the breakdown state (highlighted in yellow cycle) is then identified as pre-breakdown flow rate.

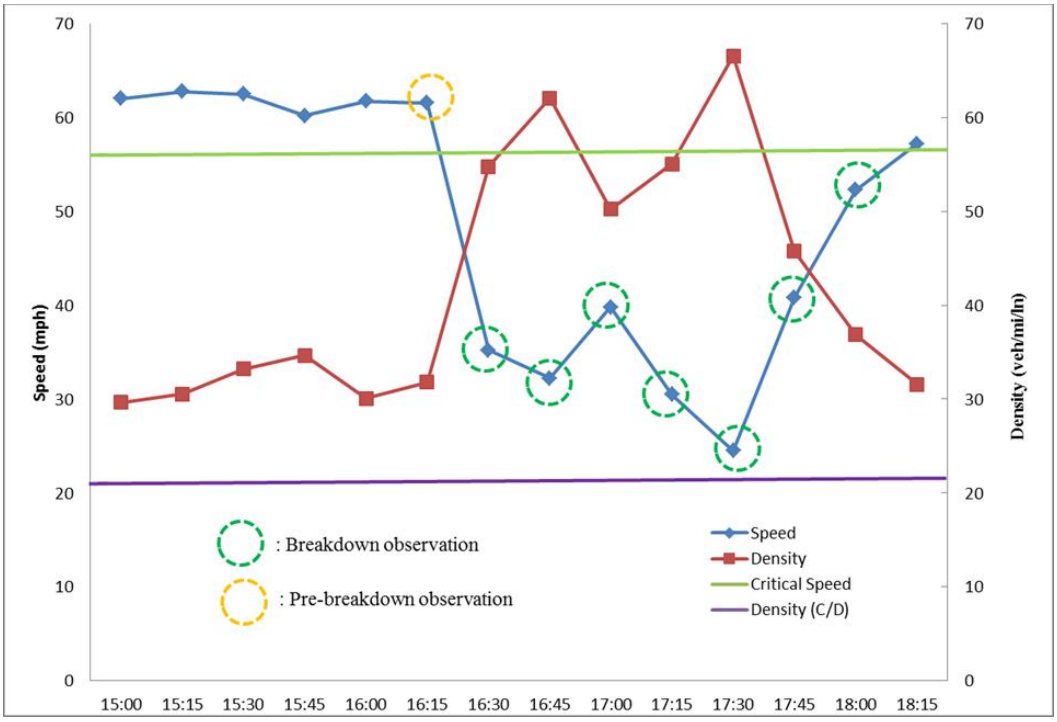

Figure 3.3 Illustrations of the Identification of Pre-breakdown and Breakdown

3.3 Models for Stochastic Capacity and Queue Discharge

The introduction of stochastic capacity at critical points within the network that suffer from queue and congestion more frequently, i.e. freeway bottlenecks and signalized intersections, enables reasonable and realistic modeling of travel time variability and the concept of sustainable flow rates. In deterministic traffic models, such as the HCM, there are

two basic traffic states in uninterrupted freeway operation: uncongested and congested flow. In defining stochastic capacity, the focus lies on the pre-breakdown state, i.e., the uncongested states just preceding the breakdown state. Once the breakdown states were identified, all the corresponding pre-breakdown states were selected from each data set. However, it should be noted that it is important to exclude the pre-breakdown flow rate under non-recurring conditions as much as possible. The possible impacts of severe weather and incidents should be screened from the dataset. Regarding the impacts of incidents, if an incident occurs between the target sensor and the next downstream sensor, the corresponding pre-breakdown observations should be excluded. Based on the incident logs provided by PeMS, several pre-breakdown observations were excluded from the dataset. Unfortunately, Transguide does not provide any incident information, which prevents us to screen out the impacts of incident on the three study site in San Antonio. Moreover, the two-year weather data were also downloaded from weatherundergroud.com. When there are unrecursive conditions, such rain, snow, and poor visibility, the corresponding pre-breakdown observations were also identified and then removed from the dataset of pre-breakdown observations. The criteria used to remove unrecursive pre-breakdown observations are:

1. Precipitation > 0 mm **OR**
2. Wind speed > 16 mph **OR**
3. Visibility < 1mile

Table 3.5 summarizes the number of unrecursive pre-breakdown observations screened by above criteria and the number of recursive pre-breakdown observations for develop stochastic capacity models.

Table 3.5 Summary of Pre-breakdown Observations Screening Results

Site #	Highway	Incident	Precipitation	Wind	Visibility	Pre-breakdown
1	I-880 (BA)	42	110	137	13	1436
2	I-680 (BA)	17	29	30	5	511
3	I-280 (BA)	16	51	84	8	619
4	I-580 (BA)	28	22	42	5	994
5	I-680 (BA)	5	86	251	11	604
6	I-35 (SAT)	N.A.	64	93	20	377
7	I-35 (SAT)	N.A.	68	82	17	372

Based on Table 3.5, it seems that incident and visibility have fewer impacts on the quality of the sample of pre-breakdown observation than the precipitation and wind. Therefore, it is necessary to account for the potential weather impacts in order to study the stochastic capacity under recursive condition.

For the sites discussed above, heavy vehicle count data was not available. Therefore, the HCM 2000 default of 5% heavy vehicles and the level general freeway segment passenger car equivalent for trucks and buses of 1.5 was used to convert the Transguide and

PeMS data to passenger car equivalent flow rates. It should be acknowledged that such assumptions could be a cause of the variation of pre-breakdown flow rates as well and therefore may bias the analysis result and model development. The only way to address this issue is to use the sensor data with vehicle classification, although it really depends on the real-world traffic monitoring system. It should also be noted that by using the data with vehicle classification and then excluding the impact of heavy vehicles (refer to Chapter 5), the values of pre-breakdown flow rates still vary in a wide range.

Due to the lack of the incident logs and weather information, a statistical approach was initially proposed to exclude outlying pre-breakdown flow rates. A pre-breakdown flow rate q, is identified as an outlier if:

$$q < Q_{0.25} - 1.5IQR \; or \; q > Q_{0.75} + 1.5IQR \tag{3-5}$$

Where,

$Q_{0.75}$: 75thpercentile flow rate (pc/h/ln);

$Q_{0.25}$: 25th percentile flow rate (pc/h/ln);

IQR: $Q_{0.75}$ -$Q_{0.25.}$

The speed-flow diagram in Figure 3.4 shows the pre-breakdown and outlier observations for one study site (I-880). Almost all of flow rates above the HCM equivalent LOS C/D density boundary were identified as outliers. For the 15 minute aggregated traffic data, it looks reasonable that the pre-breakdown flow rates would not occur at LOS C or better under the prevailing roadway, traffic, and control conditions. However, by comparing

the screening results above, only 56% of the unrecursive pre-breakdown observations were identified as the outliers for this specific study site. It may suggest that the simplified statistical method is not sufficient to screen out the impacts of unrecursive pre-breakdown observations when people try to develop the stochastic capacity model and carefully examining the incident logs and weather information is necessary.

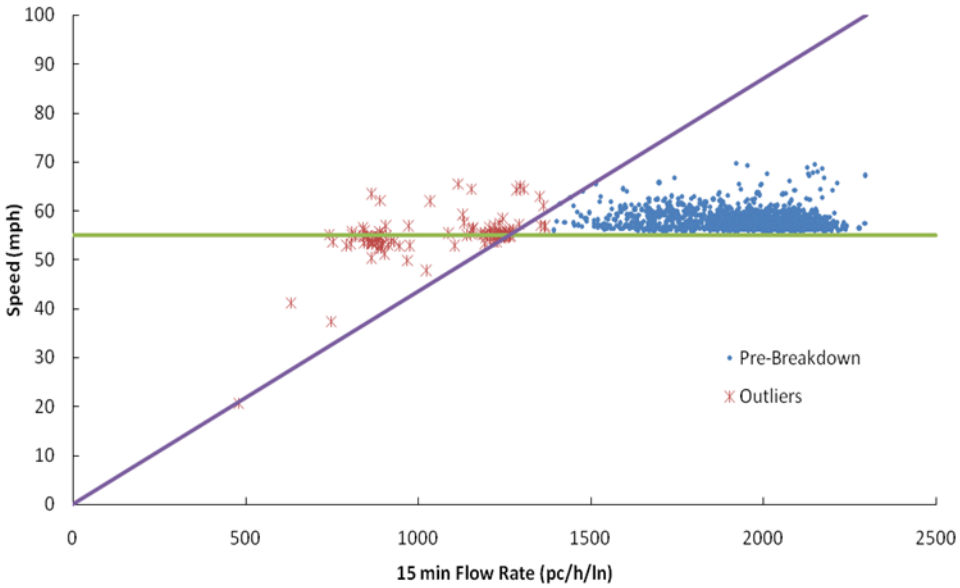

Figure 3.4 Pre-breakdown Flows and Outliers for I-880

3.3.1 Stochastic Capacity Model for Freeway On-ramp Bottlenecks

After removing the possible outliers, the remaining pre-breakdown flow rates were then used to develop the probability distributions that reflect the stochastic characteristics of freeway average pre-breakdown headway. The most common tests for goodness-of-fit are the Kolmogorov-Smirnov (K-S) test, Chi-Square test, and Anderson-Darling (A-D) test. Each is

used to decide whether a data sample belongs to a population with a specific distribution. The chi-square test could be applied to test any univariate distribution; however, the values of the chi-square statistic are quite sensitive to how the data are binned (*38*). The Anderson-Darling statistic is a measure of how far the data points are from the fitted distribution. However, the A-D test is not a distribution free test. The critical values for A-D test must be calculated for each distribution, and they are only available for a very limited number of distributions (*39*). The K-S statistic also quantifies a distance between the empirical distribution function of the sample and the cumulative distribution function of the reference distribution. The K-S test is distribution-free in the sense that it makes no assumption about the underlying distribution of data (*40*). In this study, all three tests were used to examine which distribution functions provide the best fit to the pre-breakdown flow rates. The distribution with minimum summation of ranks of above three tests will be used. By examining 65 possible distribution function, Generalized Logistic Distribution whose probability density function is shown in the following equation, provides the best fit across all study sites. The details of the tests for goodness-of-fit are listed in Appendix C.

$$f(x) = \frac{(1+kz)^{-1-1/k}}{\sigma(1+(1+kz)^{-1/k})^2} \tag{3-6}$$

Where,

k : continuous shape parameter

$$z = \frac{x-\mu}{\sigma}$$

x : pre-breakdown flow rate

μ : continuous location parameter

σ : continuous scale parameter (σ >0)

Similar to the site-specific process for identifying breakdown observations, there is no basis for assuming that pre-breakdown flow rate probability distribution parameters will be consistent between different ramp merge sites. Therefore, a local pre-breakdown flow rate probability distribution was estimated independently for each on-ramp site. The distribution parameters for the seven sites are summarized in Table 3.6. Figure 3.5 illustrates a sample pre-breakdown flow rate distribution for one study site on I-880 in Bay area, CA. The distributions of other study sites are listed in Appendix D. As shown in the figure, a single flow rate value is not appropriate for defining breakdown on freeways. The trend illustrated by the figure also indicates that the slope continually decreases with decreasing values of flow rate. This trend is consistent with findings from previous studies (*10, 17*), which show the probability of breakdown increasing with increasing flow rate. The figure also gives the corresponding 15^{th}, 50^{th} and 85^{th} percentile flow rates derived from the distribution. For example, if one defined capacity as a 15-minute flow rate that is sustainable 85% of the time, the corresponding capacity value could be 2029 pc/h/ln.

Table 3.6 Summary of Pre-breakdown Flow Rate Distribution Parameters

Site	Area	Gen. Logistic			Max. Pre-Breakdown Flow (pc/h/ln)
		k	μ	σ	
1	I-880 (BA)	-0.054	1951	47.34	2343
2	I-680 (BA)	-0.229	1955	75.92	2422
3	I-280 (BA)	-0.212	1875	65.44	2214
4	I-580 (BA)	-0.054	1951	47.34	2418
5	I-680 (BA)	-0.177	1791	53.89	2358
6	I-35 (SAT)	-0.222	1811	49.12	2371
7	I-35 (SAT)	-0.207	2010	74.57	2449

Although the distribution parameters estimates varied among study sites, it was found that the average pre-breakdown flow rate of all seven sites is best modeled as a Generalized Logistic random variable. The mean pre-breakdown flow rate at the seven study sites is 1910 pc/h/ln. The scale parameters vary among different sites and may depend on the specific characteristics of the analyzed freeway section, local differences in driver behavior, prevailing weather conditions, etc.

As discussed above, 15 minute time frame is chosen in this study to aggregate the sensor data. It should be noted that using different time frame may result in different stochastic capacity models. However, shorter time frame is usually not recommended because of the possible impacts of extreme or unreasonable field observations (i.e., outliers). In the literature and practice, there is no criterion to determine the best time frame for such

analysis. Therefore, 15 minute time frame is chosen in this study, which is consistent with the time frame suggested by HCM for the roadway capacity analysis.

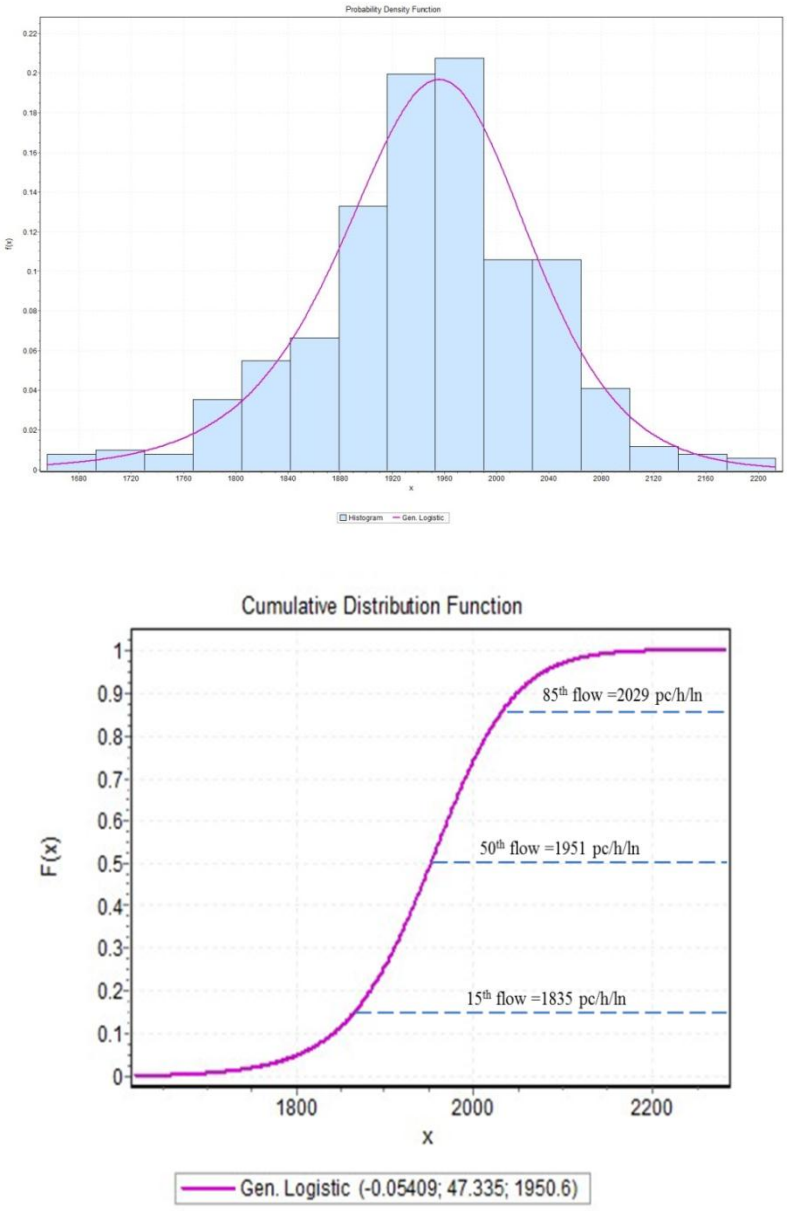

Figure 3.5 Probability Density and Cumulative Distribution of Pre-Breakdown Flow Rate for I-880

3.3.2 Stochastic Queue Discharge Model

As mentioned earlier, queue discharge flow rate is also known to be a random variable (*19*). Considering the stochastic nature of freeway capacity, it is quite possible that the queue discharge flow rate is correlated with the stochastic pre-breakdown flow rate preceding the queue existence. In addition, the 15-min. field data have shown that the queue could be discharged over multiple time intervals. By examining the observational data, it was found that the queue discharge rate could be updated with stochastic time-correlated recursions. A simple first order autoregressive model is proposed as following:

$$\boldsymbol{C_t = \alpha C_{t-1} + \mu + \varepsilon_t, \quad t \geq 1} \tag{3-7}$$

Where,

C_t: Queue discharge rate at time interval t in pc/h/ln;

α: Coefficient;

μ: Intercept;

$\varepsilon_t \sim N(0, \sigma^2)$: Random error.

When t=1, C_0 is the pre-breakdown flow rate. If we assume β=1-α, the first two terms of the model above can be rewritten as:

$$\boldsymbol{C_t = C_{t-1} + \beta(\mu_c - C_{t-1}) \quad t \geq 1} \tag{3-8}$$

Where,

β: A linear parameter that models the strength of regression to the mean;

μ_c: The average discharge rate in pc/h/ln;

$\mu = \beta\mu_c$.

For the dynamic traffic simulation model implementation, a random error term is added based on the error distribution of the fitted model. As shown in the equation (3-9), a stochastic innovation term $\varepsilon_t \sim N(0, \sigma^2)$ is proposed. Therefore, the recursive model to update the queue discharge rate (per lane) is:

$$C_t = C_{t-1} + \beta(\mu_c - C_{t-1}) + \varepsilon_t, \quad t \geq 1 \tag{3-9}$$

The traffic data from the study site on I-880 in Bay Area were used to fit the proposed queue discharge model. The fitting procedure began with the series only having two time intervals, i.e., pre-breakdown time interval and queue discharge interval with duration of one time interval and then extended to longer duration of queues by adding one interval at a time. Table 3.7 shows fitted parameters for the various cumulative queue duration lengths. The results indicate that there is a statistically significant relationship between C_t and C_{t-1}**.** The relatively high R^2 value also suggested that the proposed model match the data very well. At least 73% (the minimum R^2 value in Table 3.7) of the variation in the response variable C_t, can be explained by the proposed model. Moreover, by using an average discharge rate of 1850 pc/h/ln and β as 0.2 for all the queue duration lengths, a simple overall queue discharge model could be generated with few impacts on the goodness of fit of each subgroup. Based on the model fitting results, a stochastic innovation term $\varepsilon_t \sim N(0, \sigma^2)$ is also proposed with σ=100 pc/h/ln. Figure 3.6 illustrates the proposed simplified recursive queue discharge model.

Above recursive queue discharge model suggests that when the breakdown occurs, the queue discharge flow rate is correlated with the stochastic pre-breakdown flow rate just preceding the queue existence at beginning and then converges to the mean discharge rate,

i.e., 1850 pc/h/ln. One important implication of this queue discharge model is that the stochastic capacity is dominated by driver behavior effects. When the traffic breakdown just occurs, certain driver behavior that results in the traffic breakdown still maintains its impact on the traffic flow, and therefore the discharge flow rate is correlated with the stochastic pre-breakdown flow rate at the very beginning. As the queue built up, the driver behaviors of queued vehicles become "uniformization" and therefore the queue discharge rates begin to converge to the mean discharge rate.

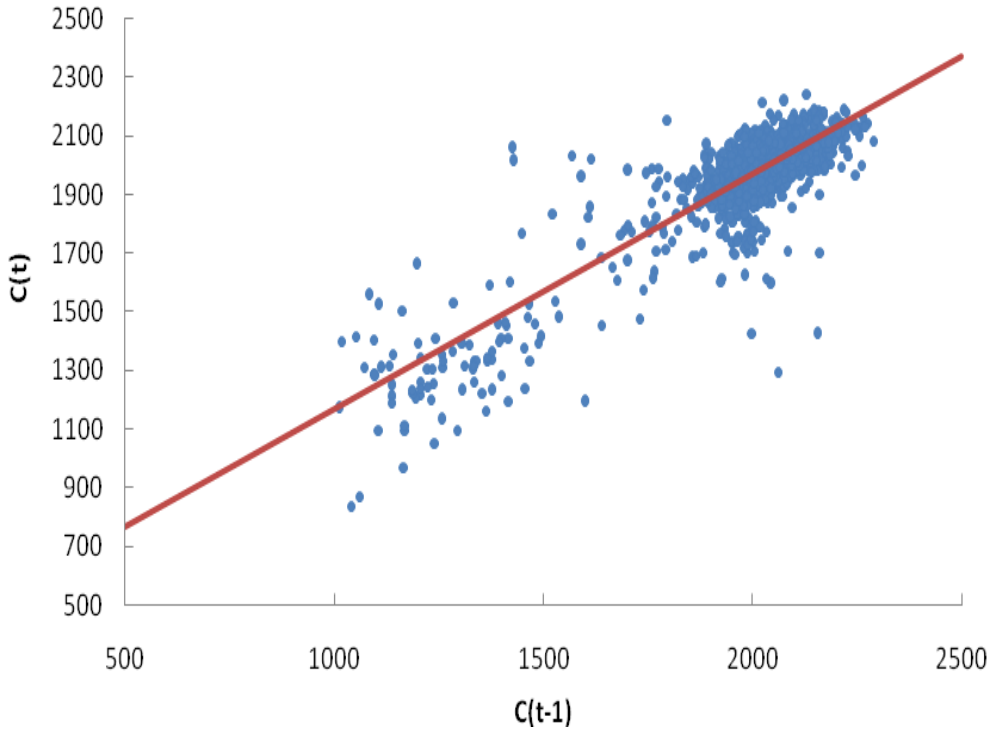

Figure 3.6 Simplified Recursive Queue Discharge Model

In summary, the queue discharge model is based on all breakdown flow observations with three primary characteristics:

- The queue discharge rate series are strongly time correlated;
- The queue discharge rates have a stochastic, random innovation component;
- The queue discharge rates converge to the mean discharge rate for breakdowns that are initiated with stochastic average pre-breakdown headway probability distribution.

Table 3.7 Summary of Fitted Queue Discharge Model

Queue Duration Intervals (Pre-Breakdown)	Number Instances (=queue duration)	Number Instances (≤ queue duration)	Fitted Parameters and GOF*				GOF with μ_c = 1850 (pc/h/ln) and β = 0.2	
			μ_c	β	R^2	MSE	R^2	MSE
2	94	94	1934	0.195	0.912	97.6	0.909	98.9
3	54	148	1876	0.159	0.868	131.9	0.866	132.9
4	39	187	1872	0.172	0.866	121.8	0.865	122.2
5	53	240	1843	0.179	0.842	111.2	0.841	111.4
6	56	296	1838	0.186	0.823	103.9	0.823	104.0
7	108	404	1840	0.204	0.776	95.8	0.776	95.8
8	53	457	1848	0.213	0.744	98.5	0.744	98.5
9	15	472	1842	0.212	0.738	99.0	0.738	99.1
10	6	478	1842	0.213	0.731	100.2	0.730	100.3
11	6	484	1838	0.212	0.728	100.5	0.728	100.6
12	5	489	1832	0.207	0.732	102.4	0.731	102.5
13	4	493	1822	0.199	0.745	103.5	0.744	103.7
14	1	494	1817	0.195	0.747	103.7	0.746	103.9
19	1	495	1798	0.177	0.772	104.3	0.771	104.6

Besides the stochastic queue discharge rate, it is also of interest to note that the duration of breakdown varies case by case as well: from one 15-minute interval to nineteen 15-minute intervals based on Table 3.7. Since the breakdown results from the pre-breakdown flow rate, it is reasonable to assume that the pre-breakdown flow rate may also have some impacts on the duration of the breakdown. Therefore, the relationship between the pre-breakdown flow rate and the duration of the breakdown is studies below.

First of all, based on Table 3.7, it has been realized that the instances of the duration of breakdown greater than eight 15-minute intervals (i.e., two hours) only comprise 5% of the entire observations. Considering that two-hour breakdown is usually very rare in the real-world, these instances are removed from the sample before doing any further analysis. In this study, cumulative logistic regression is used to model the relationship between the duration of breakdown and the pre-breakdown flow rate. The cumulative logistic regression model aims to predict the probabilities of the duration of breakdown, whose value varies from 1 to 8, based on the value of the pre-breakdown flow rate. Table 3.8 summarizes the statistics of the duration of breakdown, such as frequency, percentage, cumulative frequency and cumulative percentage.

Table 3.8 Statistics of the Duration of Breakdown

Duration (number of 15 minutes)	Frequency	Percentage	Cumulative Frequency	Cumulative Percentage
1	94	19.92	94	19.92
2	54	11.44	148	31.36
3	39	8.26	187	39.62
4	53	11.23	240	50.85
5	56	11.86	296	62.71
6	108	22.88	404	85.59
7	53	11.23	457	96.82
8	15	3.18	472	100

The parameters of the cumulative logistic regression model are estimated by the maximum likelihood method and shown in Table 3.9. As shown in Table 3.9, the p-values for all the estimates of the parameters are less than 0.0001, which indicates that the null hypothesis, i.e., the parameter is equal to "0", is rejected. There is statistically significant relationship between the dependent variable (the duration of breakdown) and the independent variable (the pre-breakdown flow rate).

Based on the model described in Table 3.9, one can easily predict the probability of certain duration of breakdown in respond to the given pre-breakdown flow rate. Let α_i (i=1, 2, …, 8) denotes the intercept for different duration of breakdown. For example, α_8 represent the intercept for the duration of breakdown equal to "8". Let β denotes the coefficient of the independent variable, pre-breakdown flow rate and x denotes the pre-breakdown flow rate. Therefore, at the given pre-breakdown flow rate x, the probability of the duration of breakdown can be estimated as:

Table 3.9 Parameter Estimation of the Cumulative Logistic Regression

Parameter	Duration	DF	Estimate	Standard Error	Wald Chi-Square	Pr > ChiSq
Intercept	8	1	-7.9051	0.6829	133.987	<.0001
Intercept	7	1	-6.2674	0.6411	95.5789	<.0001
Intercept	6	1	-4.9516	0.6274	62.2811	<.0001
Intercept	5	1	-4.4148	0.6218	50.4112	<.0001
Intercept	4	1	-3.8992	0.6155	40.1259	<.0001
Intercept	3	1	-3.48	0.61	32.5499	<.0001
Intercept	2	1	-2.7975	0.601	21.6644	<.0001
Pre-breakdown	-	1	0.00221	0.00031	51.1963	<.0001

$$
\begin{aligned}
P(duration = 8) &= \frac{\exp(\alpha_8 + \beta x)}{1 + \exp(\alpha_8 + \beta x)} \\
P(duration = 7) &= \frac{\exp(\alpha_7 + \beta x)}{1 + \exp(\alpha_7 + \beta x)} - \frac{\exp(\alpha_8 + \beta x)}{1 + \exp(\alpha_8 + \beta x)} \\
&\vdots \\
P(duration = 2) &= \frac{\exp(\alpha_2 + \beta x)}{1 + \exp(\alpha_2 + \beta x)} - \frac{\exp(\alpha_3 + \beta x)}{1 + \exp(\alpha_3 + \beta x)} \\
P(duration = 1) &= 1 - \frac{\exp(\alpha_2 + \beta x)}{1 + \exp(\alpha_2 + \beta x)}
\end{aligned}
\tag{3-10}
$$

For example, if the pre-breakdown flow rate, *x*, is 2,000 pc/h/ln, the corresponding probabilities of the duration of breakdown from 8 to 1 are 3.0%, 10.6%, 23.4%, 13.1%, 12.6%, 9.2%, 11.6%, and 16.5%.

3.4 Implementation of Stochastic Capacity Model into DTA Simulation Tool

The stochastic capacity and queue discharge model are prototyped through a mesoscopic DTA simulator, DYNASMART-P and tested on a real-world subarea network within the Portland, Oregon metropolitan area in order to demonstrate the model applicability and usefulness. The case study is designed to demonstrate the impacts of the stochastic capacity on the evaluation of various operational strategies in the dynamic traffic assignment simulation tool. The detailed conceptual simulation framework is discussed in Appendix F. The subarea network selected for this purposes is illustrated in Figure 3.7. It is relatively large in size and therefore represents a good opportunity to test scaling issues associated with the method applications.

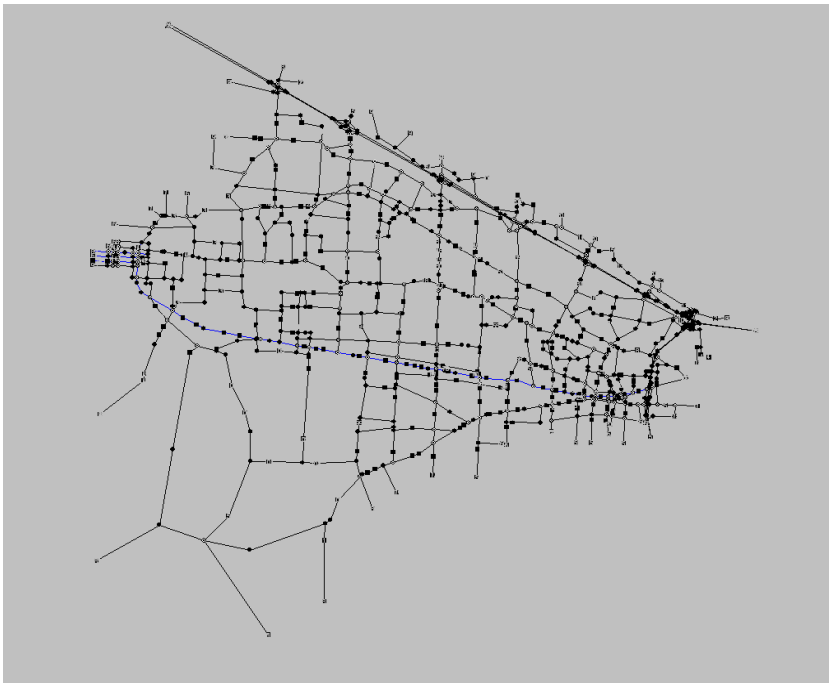

Figure 3.7 Portland Network Study Area

The above network includes 858 nodes, 2000 links, and 208 origin-destination zones. Among the 858 nodes, 169 of them are modeled as signalized intersections with actuated control and the remaining are modeled at uncontrolled nodes with capacity constraints. In this case study, the stochastic capacity is randomly generated every 15 minute interval and applied on all the on-ramp bottlenecks. Conventional traffic assignment methods assume static, deterministic road capacity. Therefore, the travel time of a path only depends on the flow pattern on that path. In other words, for a fixed network-wide path flow pattern, the corresponding path travel times do not change. After incorporating stochastic capacity, however, a driver's travelling experience on a single day can be dramatically affected by the underlying realized capacity values on that particular day. In other words, travelers will experience different travel times on the same path over different days even for the same path flow pattern because of the inherent travel time variability introduced by stochastic capacity. As a result, conventional "within-day" or iterative route choice methods for reaching user equilibrium, such as the method of successive averaging (MSA), may not enable drivers to recognize and appropriately respond to the travel time variability/unreliability resulting from capacity fluctuation. A theoretically rigorous and practically useful traveler route choice model is crucially needed in order to adaptively capture the stochastic day-to-day travel time evolution process and also to maintain robustness under disruptions due to stochastic capacity reductions. To this end, a new route choice mechanism is proposed to simulate the drivers' route choice behavior under stochastic traffic process noise. By comparison, conversional stochastic assignment models focus on traveler perception errors under a

deterministic traffic environment. The proposed mechanism includes two key components: a route choice learning module and a route choice decision module.

This study adapts a behaviorally sound route choice utility function, proposed and calibrated by Brownstone and Small (*25*) and Lam and Small (*26*), to consider the stochastic nature of traffic systems.

$$GT = T + \frac{VOR}{VOT} \times TSD + \frac{TOLL}{VOT} = T + \beta \times TSD + \frac{TOLL}{VOT} \quad (3\text{-}11)$$

Where,

GT= the generalized travel time,

T = the expected travel time for traveler,

TSD = perceived travel time variability.

β = reliability ratio (computed as the ratio of Value of Reliability (VOR) and Value of Time (VOT)).

TOLL = road toll charge, and it is assumed to be zero in the following discussions as no toll-related strategies will be evaluated in this study.

It has been well recognized that travel time variability and reliability are important measures of service quality for travelers. In the above utility function, Equation 7, the travel time standard deviation (*TSD*) is used to measure system travel time variability associated with the underlying stochastic traffic process. This contrasts with the perception error variance in a deterministic assignment model. For a single traveler v, the route choice decision is made by comparing the generalized travel time of habitual path, GT_v^h, and that of alternate path, GT_v^a.

$$GT_v^h > GT_v^a \tag{3-12}$$

Where,

v = traveler index,

h=index for habitual path, and

a=index for potential alternative path.

According to Equation 7, if the generalized travel time of the habitual path, GT_v^h, is greater than that of alternate path, GT_v^a, as shown in Equation 8, a vehicle should switch his route from the habitual path to the alternative path. The resulting decision rule could be derived as:

$$T_v^h - T_v^a > \beta\left(TSD_v^a - TSD_v^h\right) \tag{3-13}$$

In this study, T_v^h is equal to $\overline{T}_v^{d-K,d-1}$ as calculated in Equation 10. In order to take a traveler's multi-day travel time experience into account. T_v^a is calculated using the estimated travel time on the shortest path. It should be noted that the calculation of T_v^a varies for different user classes, which will be discussed in section 3.3.

$$\overline{T}_v^{d-K,d-1} = \frac{T\left(P_v^{d-K}\right)+T\left(P_v^{d-K+1}\right)+\cdots+T\left(P_v^{d-1}\right)}{K} \tag{3-14}$$

Where,

d = day index

K = number of days in the learning memory window

$\overline{T}_v^{d-K,d-1}$= traveling experience (i.e., average travel time) for traveler v from day d-K to day d-1, on a particular path,

$T\left(P_v^{d-1}\right)$ = travel time on path P_v^{d-1}, and P_v^{d-1} is the path traveled by vehicle v on day d-1.

The right side of Equation 9 can be viewed as the minimum acceptable absolute tolerance needed for a route switch decision. This value arises from three components: the reliability ratio β, the standard deviation of travel time on the habitual path TSD_v^h, and the standard deviation of travel time on the alternative path TSD_v^a. The setting of parameter K depends on the signal-to-noise ratio in the traffic system. Specifically, the more stable the travel time process, the smaller the K can be and still yield a reliable mean travel time estimate. In general, K must be large enough to filter out the process noise from the stochastic traffic system.

The travel time variability measure, TSD_v^h, for the habitual path can be calculated from multi-day travel times experienced by the traveler. The remaining challenge is how to estimate the standard deviation of travel time on the alternative path, TSD_v^a, where the traveler has little or no experience on this path. When there is no external pre-trip or en-route information available, TSD_v^a needs to be calculated from the traveler's prior experience. To our knowledge, there is no widely accepted method to calibrate the standard deviation of perceived travel times on alternative paths for travelers without access to advanced traveler information systems and relying on prior knowledge only. In this research, we assume TSD_v^a is significantly larger than TSD_v^h due to the lack of precise information and the high level of uncertainty associated with the perceived alternative travel time. The calibration of the minimum acceptable absolute tolerance was beyond the scope of this study. Therefore, this research uses a simplified, single term model, $\beta\left(TSD_v^a - TSD_v^h\right)$, to represent the minimum

acceptable absolute tolerance needed for a route switch decision. This simple model is intuitively sound, and using it eliminates the need for extensive calibration efforts.

In this study, a bounded rationality model, which states that a driver's decision depends on their desired satisfaction level, is adapted to make the route choice comparison. The bounded rationality concept is employed because there has been growing attention (starting from the early work by Mahmassani and Herman(*27*)) to bounded rationality since Herbert Simon (*28*) pointed out that perfectly rational decisions are often not feasible given the limits of human cognition.

Based on the minimum acceptable absolute tolerance and the relative acceptable tolerance, a set of bounded rationality rules, shown in Equation 11, are used to describe users' route switching behavior. As opposed to the optimization theory in which users select the best option from all possible decisions, in the bounded rationality approach, users perform limited searches, accepting the first satisfactory decision.

$$\delta = \begin{cases} 1 & \text{if } \overline{T}_v^{d-K,d-1} - T_v^a > \text{MAX}[\alpha, \lambda * T_v^h)] \\ 0 & \text{otherwise} \end{cases} \quad (3\text{-}15)$$

Where,

$\boldsymbol{\delta}$ =1, switch to an alternative path; 0, remain on the habitual/ current path,

α = Minimum acceptable absolute tolerance needed for a switch and $\alpha = \beta\left(\text{TSD}_v^a - \text{TSD}_v^h\right)$,

λ = Relative acceptable tolerance (i.e. relative improvement threshold).

The percentage of drivers who are willing to make a route change in any given day was set to 15%. The number of days in the learning window was set to K = 5. Therefore the mean travel time was calculated from the experience of day *d-5* to day *d-1*. This mean travel

time represents each driver's historical traveling experience. The calibrated parameters of the stochastic models described in section 3 were applied to generate stochastic capacity and queue discharge flow rates for freeway bottlenecks (i.e., on-ramp and lane drop segments). For simplicity, the minimum acceptable absolute tolerances used in bounded rationality rule are 5 minutes.

In the case study, the analyst performed the simulation run over 100 days of simulated time in order to effectively generate realistic results. Figure 3.8 shows the network-wide average travel time and route switching rate of total vehicles segmented in three time regimes. In this study, for example, during the baseline stabilization period (Regime I in Figure 3.6) 50 days are simulated to achieve a stable baseline scenario. The average travel time diminishes significantly during the first 40 days and stabilizes afterwards.

After the baseline stabilization period was completed, the operational and/or construction strategies to be evaluated were introduced into the network, and we carried out the simulation process for additional 30 days to allow driver adjustments and achieve stable conditions under the new scenario. This is referred to as the strategy stabilization period and is illustrated as Regime II. Immediately following upon this 30-day period was a simulation of an additional 20 days (Regime III in Figure 3.8) that formed the basis for the summary results output associated with the particular strategy being investigated. In regime III, although the average travel time or switching rate is relatively stable, there are still obvious day-to-day fluctuations, because the travel time experience on a single day can be dramatically affected by the underlying stochastic capacity features. Therefore, the

evaluation of network performance only based on the last simulation day (last iteration) is not recommended and new reliability-oriented system performance measures should be applied to take multiple days into account. In this study, for example, the simulation results from the last 20 days were used to report the network performance.

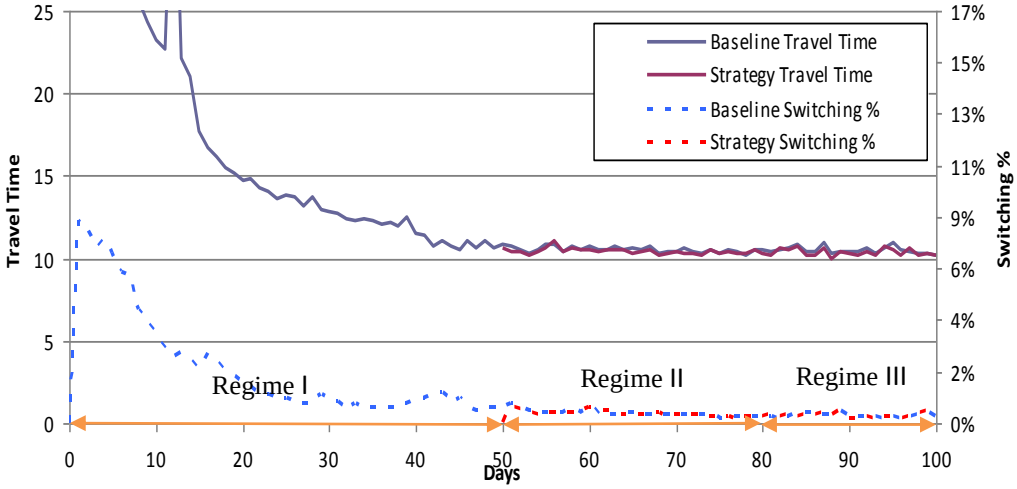

Figure 3.8 Network-Wide Simulation Results

In this case study, various capacity-enhancing construction and operational strategies were evaluated on the Portland subarea network. The hypothesis of the case study is that after introducing the stochastic capacity into the simulation tool, the corresponding network performance is significantly different from that with deterministic capacity which is widely used by practitioners before. These strategies are discussed in detail as follows:

- Baseline Scenario

  Scenario 0: Baseline condition without any strategies.

- Construction Strategy Scenarios

  Scenario 1: Construct a new through lane on TV highway (each direction).

  Scenario 2: Construct a new through lane on OR-217 northbound.

- Operational Strategy Scenarios

  Scenario 3: Increase the percentage of users who access to pre-trip information from 1% to 10%.

  Scenario 4: Increase the percentage of users who access to en-route information from 2% to 10%.

Figure 3.9 demonstrates the locations of OR-217 and TV highway in the network of Portland, Oregon metropolitan area.

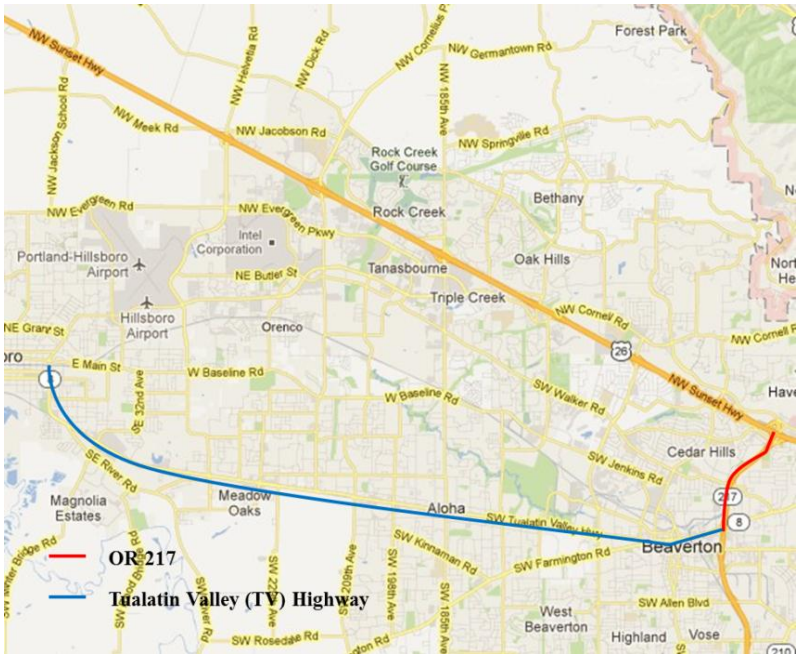

Figure 3.9 Locations of OR-217 and TV Highway in the Network

Each of the four improvement strategies identified above, in addition to a "no change" baseline scenario, was analyzed. Scenario 1 and 2 are the capacity improvement strategies in which the number of lanes of the roadway increases. Scenario 3 and 4 are the ITS strategies in which the percentage of users who access to real-time travel information increases. Table 3.10 summarizes the performance at network-wide level of above five scenarios in terms of average network-wide travel time, standard deviation (SD) of travel time, and buffer index (BI). For comparison purpose, the corresponding results under deterministic capacity condition were also summarized. It should be noted that all the results are calculated on the 20-day simulation basis. The BI is defined as follows:

$$BI = \frac{(TT_{95th} - TT_{avg})}{TT_{avg}} \quad (3\text{-}16)$$

Where

TT_{95th}=95 percentile travel time among twenty day simulation results.

TT_{avg} = average travel time of two day simulation results.

Table 3.10 Network-wide Travel Time Characteristics of Alternative Improvement Strategies

Scenario #	Stochastic Capacity (Enhanced DYNASMART-P)				Deterministic Capacity (Original DYNASMART-P)			
	TT_{avg}	Improvement	SD	BI	TT_{avg}	Improvement	SD	BI
0	11.50	-	1.43	0.25	10.12	-	0.63	0.11
1	11.03	4%	1.36	0.23	9.53	6%	0.60	0.09
2	9.98	13%	1.21	0.21	8.58	15%	0.52	0.09
3	9.87	14%	1.21	0.20	9.45	7%	0.58	0.10
4	9.58	17%	1.20	0.18	9.17	9%	0.58	0.09

'-': data not applicable

As expected, each strategy improved the network performance in terms of average travel time with the stochastic capacity or deterministic capacity simulation settings. However, average network travel time (minute), SD, and BI in the stochastic capacity environment are consistently higher than their counterpart in the deterministic capacity environment. This pattern is consistent with the previous assertion that deterministic network modeling platforms are likely to be under-represent the traffic operational impact of freeway system bottlenecks. Therefore, the proposed simulation framework, which incorporates stochastic capacity models and a compatible route choice mechanism, hold the promise of providing significant different representation of network performance under various alternative scenarios, especially in terms of travel time variance. It is expected to provide transportation practitioners and planners alternative views of the system performance and then support their decision-making. Within the stochastic capacity environment, the network

performance benefited the most from increasing the percent of drivers who make use of pre-trip/en-route information in terms of both average travel time and travel time reliability. In contrast, within the deterministic capacity environment, the network performance benefited the most from the physical capacity additions. The implication of the results suggests that conventional deterministic DTA platforms are likely to misestimate the effectiveness of physical road capacity enhancement strategies, and the benefits from information provision services.

3.5 Summary

Based on the empirical traffic data, the freeway breakdown phenomenon is stochastic, not deterministic. In other words, breakdown is a probabilistic event and can occur over a range of flow values. The incorporation of stochastic characteristics of capacity and queue discharge rate at freeway on-ramp bottlenecks will significantly change the system performance when evaluating the transportation network or traffic improvement strategies. This provides researchers and practitioners an efficient way to model the system variations that have been observed from the field data. In this study, the possible impacts of weather and incident are excluded from the data for the development of stochastic capacity and queue discharge. However, it should be noted that the drivers' and vehicles' characteristics cannot be measured using the aggregated sensor data. It is quite possible that the underlying reasons of the variations of capacity/queue discharge observed in the sensor data can be explained by the variations between drivers and vehicles. Therefore, in the next chapter (i.e., chapter 4), the vehicle trajectory data at micro-level will be analyzed. The hypothesis is that the

heterogeneity of driver behavior in terms of vehicles' car following behavior at congestion condition (at least partially) contributes to the capacity variations observed at macro-level.

4. INVESTIGATING STOCHASTIC CAPACITY AT MICRO-LEVEL

In this chapter, the stochastic characteristics of freeway bottleneck are investigated at the micro-level. The primary purpose of this chapter is to study the underlying reason of stochastic capacity using micro-level analysis. This chapter is organized as follows. Section 4.1 first introduces the field dataset. This is followed by the methodology used to determine the key parameters (section 4.2), the experimental distributions of stochastic wave speed and jam density (section 4.3) and the correlation with the stochastic model at the macro-level.

4.1 Data Description

The vehicle trajectory data are collected from the NGSIM program (*41*), which is used to develop a core of open behavioral algorithms for improving the quality and performance of traffic simulation tools. The datasets include detailed vehicle trajectory data and thus the NGSIM data can be utilized to evaluate the individual drivers' behavior in the traffic system. The field data selected from the NGSIM datasets consist of U.S. Highway 101 (US 101) data and Interstate 80 prototype data.

The vehicle trajectory data on a segment of U.S. Highway 101 (the Hollywood Freeway) in Los Angeles, California were collected by the NGSIM team using video cameras. Figure 4.1 demonstrates the location for this dataset. The data were collected between 7:50 AM and 8:35 AM on June 15, 2005. The detection site is 2100 feet in length, with an on-ramp at Ventura Boulevard and an off-ramp at Cahuenga Boulevard. There are five freeway lanes and an auxiliary lane between the two ramps. Video data were collected by using eight

video cameras. Complete vehicle trajectory data were transcribed at a resolution of 10 frames per second.

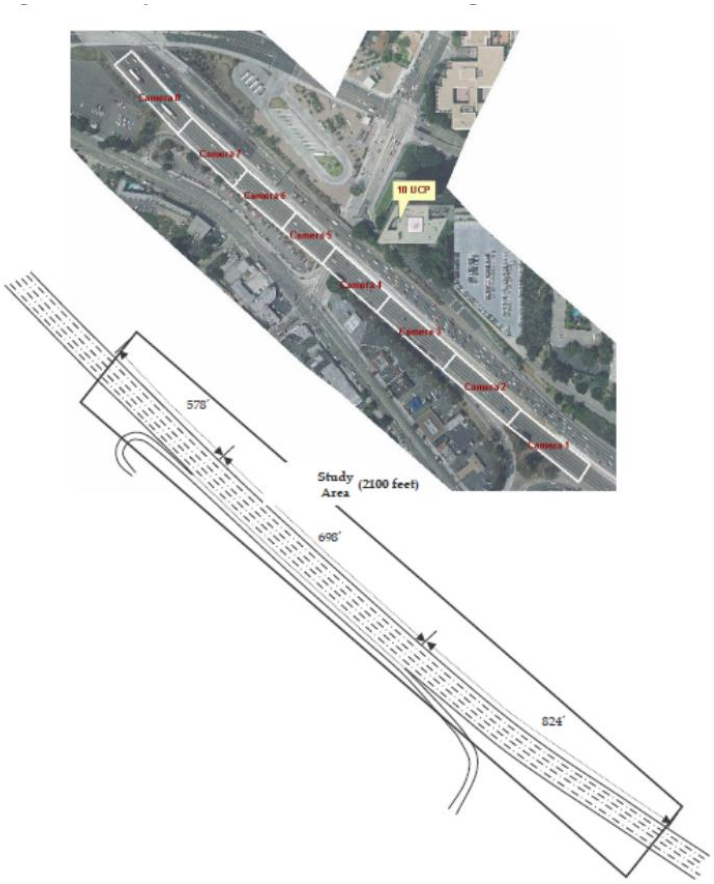

Figure 4.1 Study Area for NGSIM US 101 Data (Source: (*42*))

The I-80 vehicle trajectory data were collected as part of the NGSIM data collection by Cambridge Systematic, Inc. These vehicle trajectory data were collected at the Berkeley Highway Laboratory (BHL) site, which is located at a segment of eastbound I-80 in Emeryville, California. Figure 4.2 shows the detection location for this prototype I-80 dataset.

The detection site is approximately 1650 feet in length, with an on-ramp at Powell Street and an off-ramp at Ashby Avenue. There are six lanes in this section before the off-ramp and five lanes at the downstream of the off-ramp. Video data were collected using seven video cameras, and the vehicle trajectory data were transcribed at a temporal resolution of 15 frames per second. The data collection time is approximately 30 minutes, from 4:00 PM to 5:30 PM.

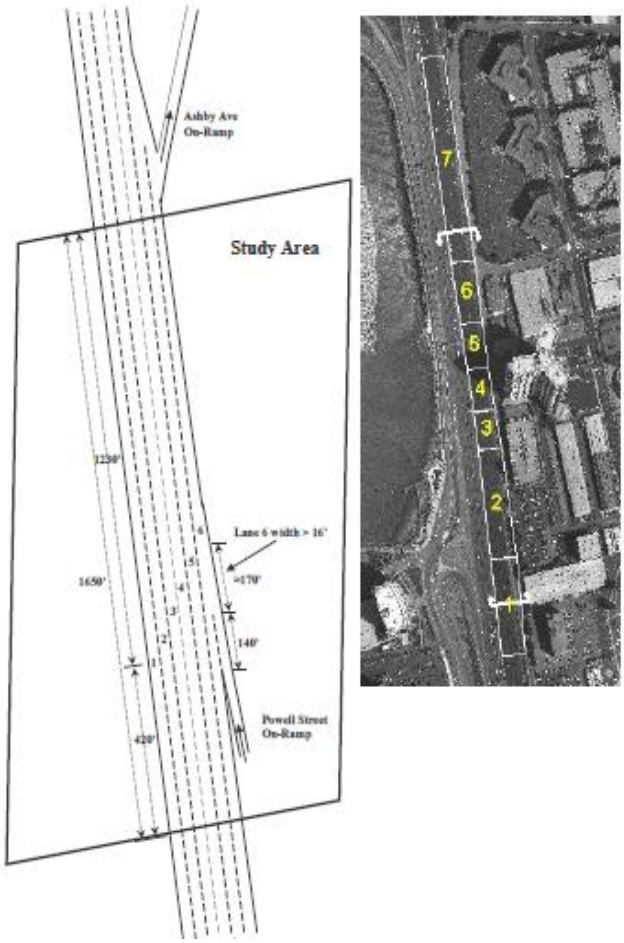

Figure 4.2 Study Area for NGSIM I-80 data (Source: (*42*))

4.2 Methodology

Newell's car following model (*43*) is a simplified linear car-following model, which considers two traffic conditions. Under uncongested traffic conditions, vehicles are travelling at the free-flow speed; while under congested traffic conditions, a following vehicle adjusts the speed to maintain a minimum jam spacing and reaction time lag with respect to the leading vehicle's trajectory. Among a number of well-known car-following models, Newell's simplified car-following model demonstrated reasonable performance with limited calibration efforts (*44*).

In Newell's car following model, under the congested traffic condition, the position of the following vehicle is determined by a space and time offset (d_n, τ_n), as shown in the following equation.

$$x_n(t+\tau_n) = x_{n-1}(t) - d_n \tag{4-1}$$

Where,

$x_n(t+\tau_n)$=the position of following vehicle at time $t+\tau_n$

$x_{n-1}(t)$=the position of the leading vehicle at time *t.*

In the above equation, the key point is that two consecutive vehicles are related in congestion by a shift $-w$ (d_n, τ_n), as shown in figure 4.3. Note that d_n is the minimal or jam spacing between two vehicles that is observed at zero speed and the w is the wave speed in the congestion condition.

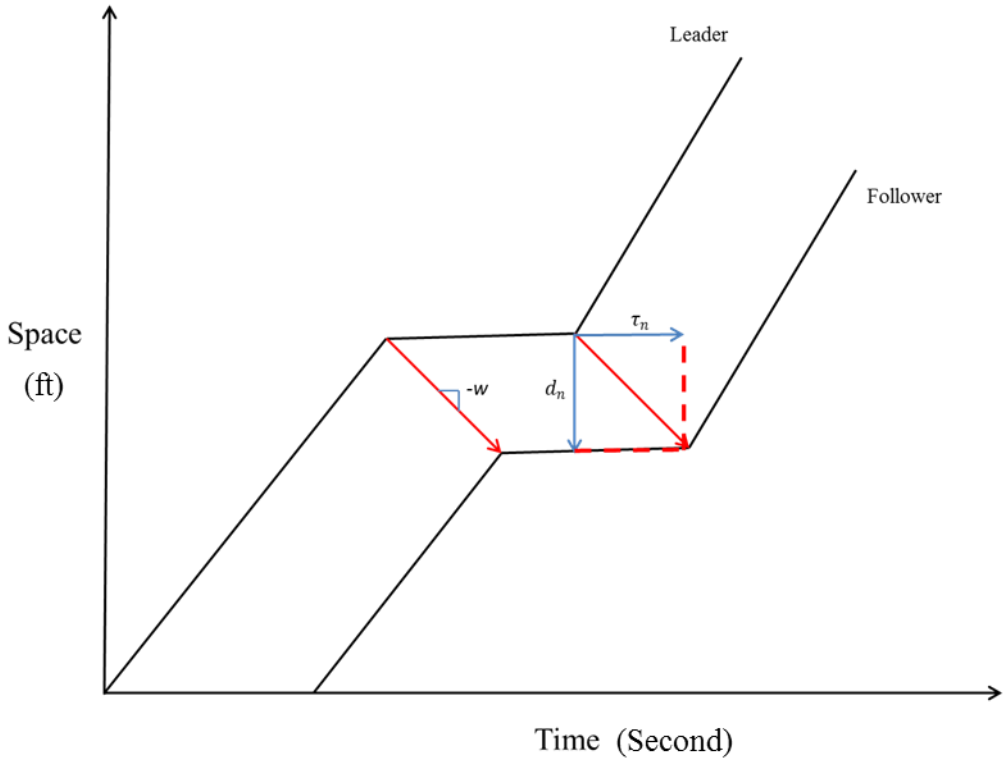

Figure 4.3 Vehicles' Trajectories according to Newell's Car Following Model

In literature, there are a lot of studies conducted to calibrate Newell's car following model. A common method adopted by researchers is to find the optimal alignment between two or more time-dependent vehicle trajectories. The optimal process aims to determine the best fit between the simulated trajectories and the measured trajectories of the followers. The car following model is usually calibrated by minimizing the root mean square error between the simulated trajectories and the measured trajectories. However, Ossen and Hoogendoorn (*45*) found that the optimal parameters obtained from such optimization method usually do not best capture the leader-follower dynamics and then result in significant bias in the estimations. By searching the vehicle trajectory data downloaded from NGSIM, the stop-and-

go conditions similar as Figure 4.3 are identified, and then the vehicles' trajectory break points are identified. In this study, the shift $-w$ $(d_{n,}\ \tau_n)$ between leader and follower are only measured at the break points instead of using the optimization method. It should be noted that the shifts are measured for every leader-follower pair in the platoon within the stop-and-go conditions. Figure 4.4 illustrates an example of vehicle trajectory data for the stop-and-go condition from US 101 between 7:50 AM to 8:05 AM. Moreover, only the stable situations, i.e., vehicles pairs driving in the same lane without lane changing, will be studies. Finally, 148 pairs of leader and follower vehicles have been identified from several different platoons and then used for the analysis.

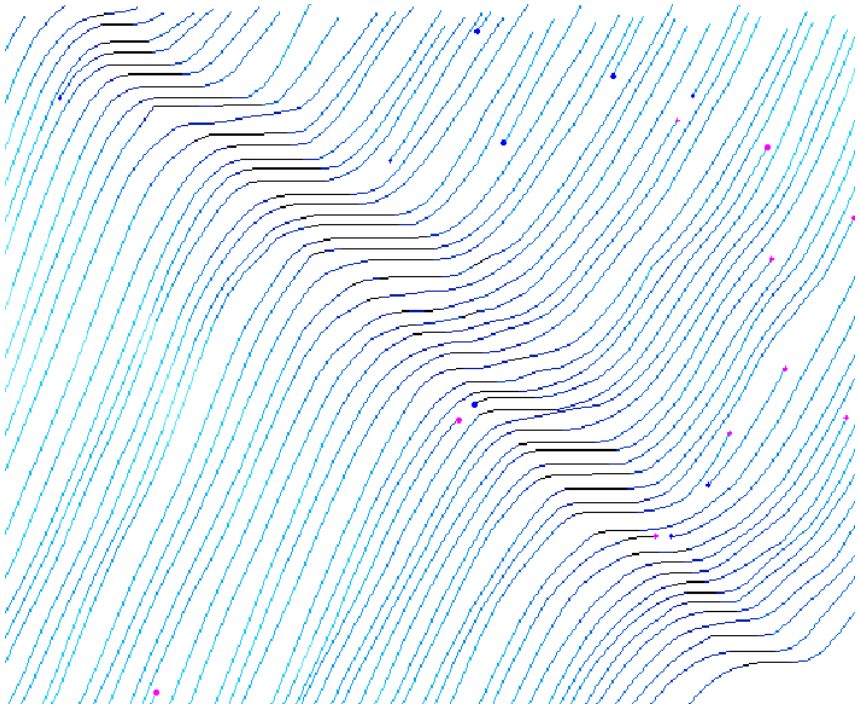

Figure 4.4 An Example of Stop-and-go Condition from NGSIM Data

Based on the triangular flow-density model (as shown in Figure 4.5), Newell's car following model can be expressed into its corresponding simplified kinematic wave model.

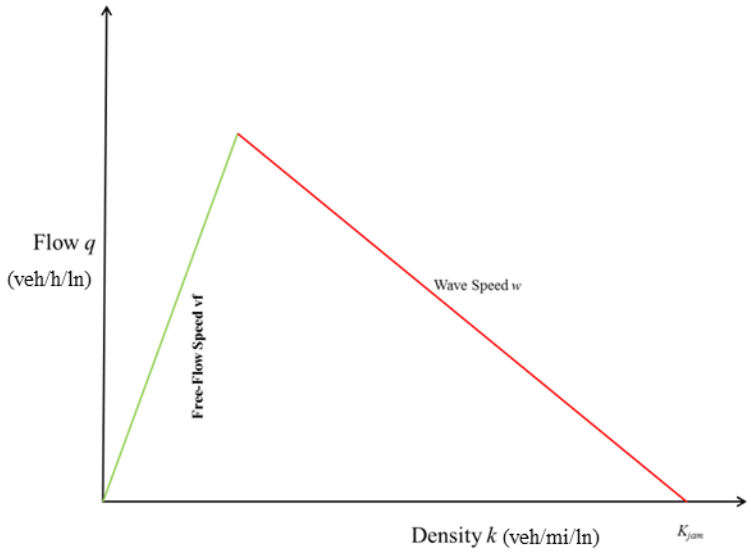

Figure 4.5 Typical Triangular Flow-Density Diagram

The jam density is the inverse of the critical jam spacing:

$$k_{jam} = \frac{1}{d_n} \tag{4-2}$$

The backward wave speed is calculated as:

$$w = \frac{d_n}{\tau_n} \tag{4-3}$$

4.3 Stochastic Wave Speed and Jam Density

Based on the 148 pairs of space and time offsets ($d_{n,}$ τ_n), the corresponding individual wave speed and jam density are calculated for each leader and follower vehicle pairs. Figure 4.6 and Figure 4.7 show the distribution of k_{jam} and w for the 148 vehicle pairs.

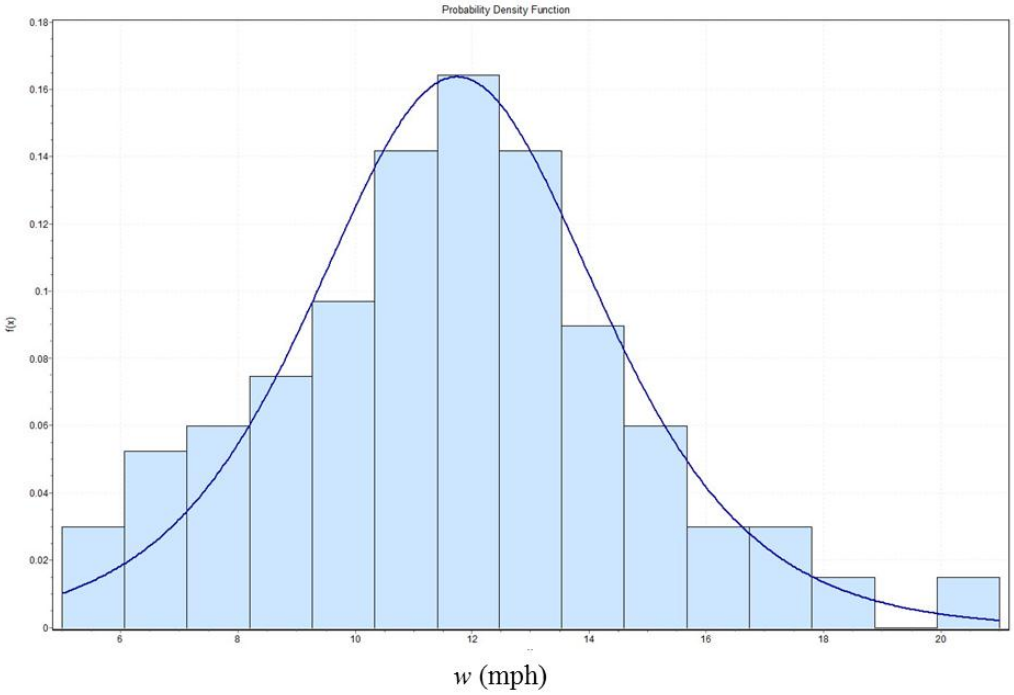

Figure 4.6 Distribution of *w*

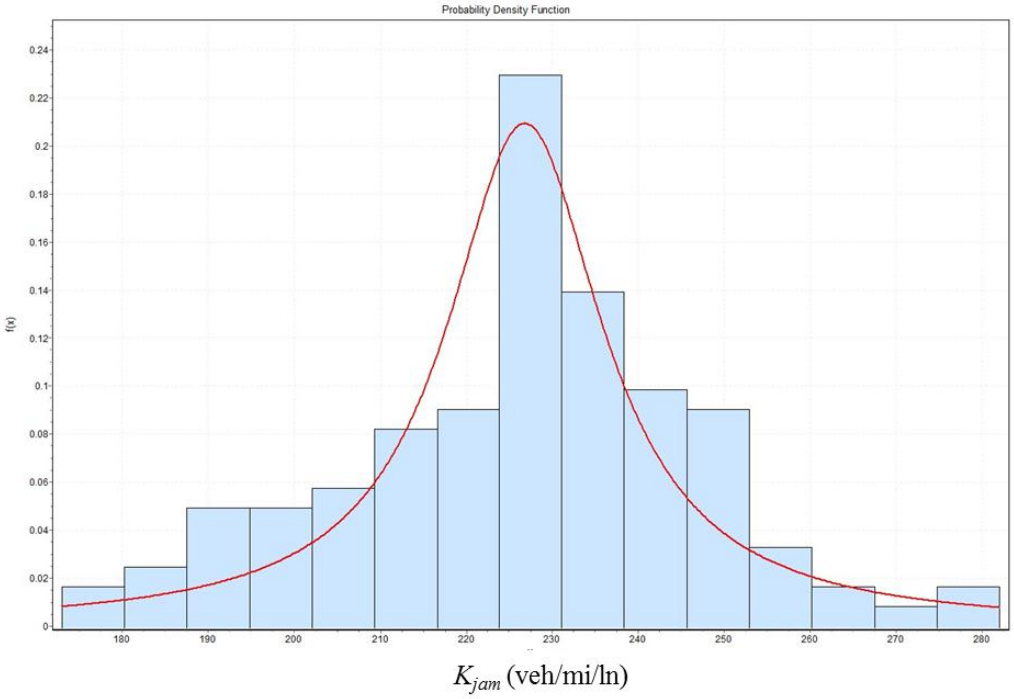

Figure 4.7 Distribution of k_{jam}

The waving speed, *w*, can be represented as a random variable with the Logistic distribution as:

$$f(w) = \frac{\exp(-\frac{w-11.74}{1.63})}{1.63[1+\exp(-\frac{w-11.74}{1.63})]^2} \quad (4\text{-}4)$$

The mean of the waving speed is 11.74 mph, which matches what can be found in the literature (between 6 mph and 15 mph, (*46-48)*) ; while the standard deviation of the waving speed is 2.96 mph.

The jam density, k_{jam}, can be represented as a random variable with the Cauchy distribution as:

$$f(k) = (11.05\pi(1+\left(\frac{k-227}{11.05}\right)^2))^{-1} \tag{4-5}$$

The mean of the jam density is 227 veh/mile and the standard deviation is 21.2 vehicle/mile.

If assume the free-flow speed, v_f, is constant, the value of capacity can be derived as a function of k_{jam} and w. Based on Figure 4.5, if the density at the capacity is k_c, it is clear that:

$$v_{f=}\frac{c}{k_c} \tag{4-6}$$

$$w = \frac{c}{k_{jam} - k_c} \tag{4-7}$$

Combing above two equations, the capacity, c, could be expressed as:

$$c = \frac{wk_{jam}}{1 + w/v_f} \tag{4-8}$$

It is clear that the capacity, c, is a function of free-flow speed, backward wave, and jam density. If the free-flow speed, v_f, is assumed constant, capacity is fully determined by the wave speed and jam density. Since both wave speed and jam density is a random variable, the capacity, c, is mostly likely a random variable as well instead of a constant value. It should be noted that the index of dispersion for wave speed, $\frac{\sigma}{w}$, is 0.25, which indicates that the value of wave speeds are not far from the mean but that heterogeneity exists at a

microscopic scale. The index of dispersion for jam density, $\frac{\sigma}{k_{jam}}$, is 0.1, which is much smaller than its wave speed counterpart. The distribution is sharply centered on the mean value of k_{jam}.

As discussed above, both of k_{jam} and w are measured from the vehicle pairs at stop-and-go conditions (the impacts of optimization error are excluded) and the impacts of lane changing and heavy vehicles are excluded from the dataset. Therefore, it is reasonable to conclude that the heterogeneity of k_{jam} and w at the micro-level results from individual driving behavior and the corresponding stochastic capacity and queue discharge rate observed in the field data (marco-level) are also generated by the heterogeneity between individual driving behaviors.

A Monte Carlo simulation is performed to generate the stochastic k_{jam} and w based on their distributions calibrated above and the corresponding capacity values are calculated. Before doing this, it is reasonable to check whether there is strong correlation between the variables, jam density (veh/mile/ln) and wave speed (mph). Based on the definition, the correlation between two variables exists when they have a linear relationship. The measurement of correlation commonly used in practice is the "Pearson-Moment Correlation Coefficient", which is calculated as:

$$\rho_{x,y} = \frac{\mathrm{cov}(x, y)}{\sigma_x \sigma_y} \tag{4-9}$$

Where,

$\rho_{x,y}$: the correlation coefficient of the two variables, x and y

cov(x,y) : the covariance between the two variables

σ_x, σ_y : the standard deviation of variable *x* and *y*

The value of $\rho_{x,y}$ ranges from -1 to 1. A value of *-1* implies that a perfect negative relationship between *x* and *y;* while a value of *1* implies that a perfect positive relationship between the two variables. A value of *0* suggests that there is no linear correlation between the variables. In this study, the correlation coefficient between *w* and k_{jam} is -0.359 and the scatter plot of the two variables (with 95% prediction ellipse) is shown in Figure 4.8. The correlation coefficient and the scatter plot suggest that there is a negative relationship between *w* and k_{jam} : as wave speed increases, the jam density tends to decrease. However, the correlation between the two variables is not significant (-0.359 is close to 0 and far away from -1) and therefore may be considered negligible in practice.

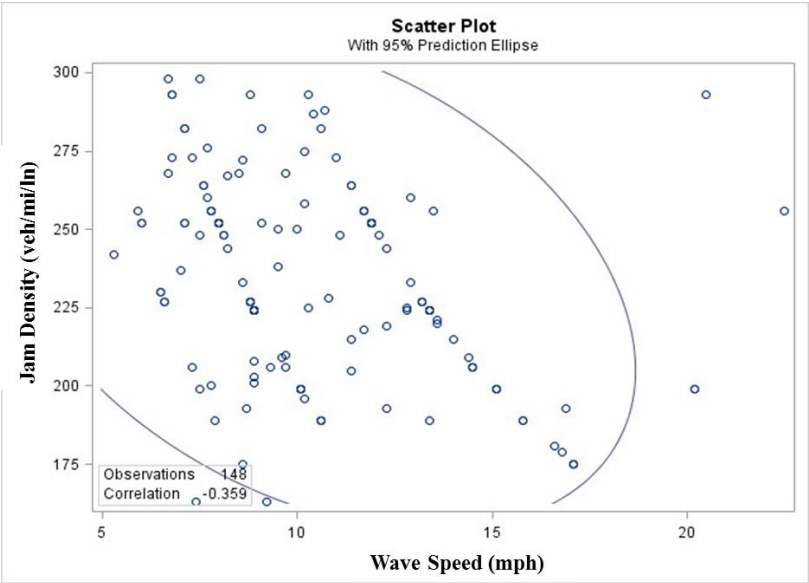

Figure 4.8 Scatter Plot of Jam Density and Wave Speed

However, the stochastic k_{jam} and w should not be generated totally randomly; otherwise unreasonable capacity will be obtained. The basic logic is that the follower will follow the leader but keep the minimum time space. Therefore, a constraint is applied to the Monte Carlo simulation as follows:

$$\frac{d_n}{v_f} + \tau_n \geq a \tag{4-10}$$

Where,

v_f = free-flow speed

a = constant value, representing the minimum required time space between two vehicles (a=2 second in this study).

Since

$$k_{jam} = \frac{1}{d_n} \text{ and } w = \frac{d_n}{\tau_n} \tag{4-11}$$

It is easy to derive the constraint equation as:

$$\frac{1}{v_f k_{jam}} + \frac{1}{w k_{jam}} \geq a \tag{4-12}$$

Therefore, the constraint equation only depends on the values of k_{jam} and w.

Figure 4.9 shows the distribution of the calculated capacity values based on different values of k_{jam} and w calibrated from vehicle trajectory data. The blue bars represent the frequencies of different stochastic capacity values, and the red line represents the cumulative percentage of different stochastic capacity values.

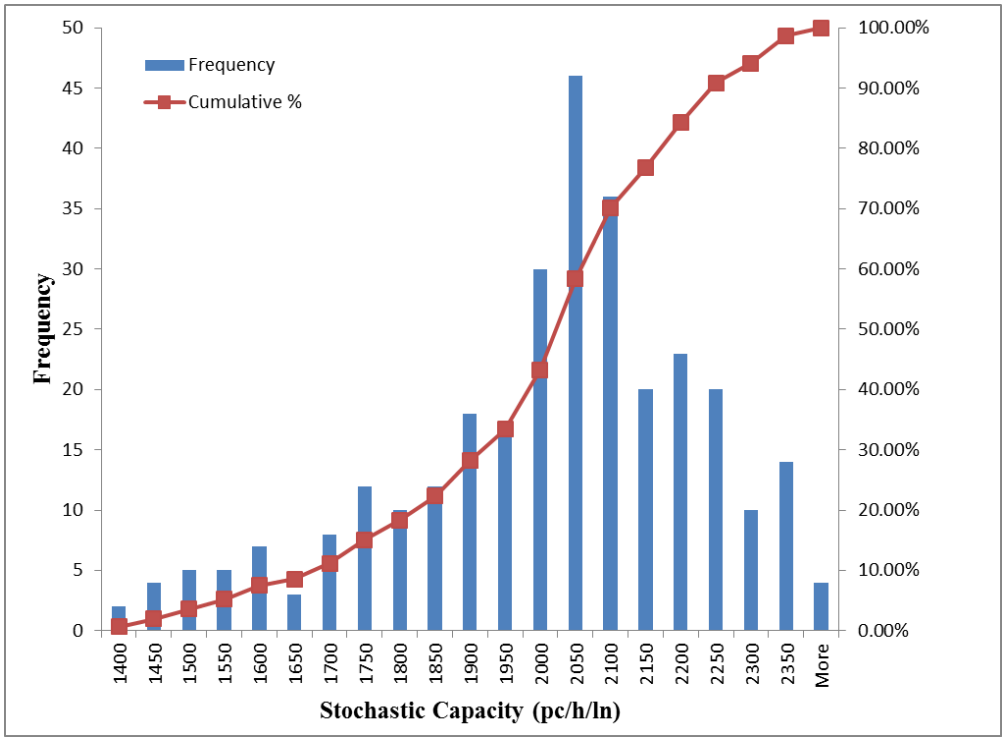

Figure 4.9 The Distribution of Stochastic Capacity in Respond to the Distribution of k_{jam} and w

It is also necessary to compare the stochastic capacities estimated above with the values calibrated at the macro-level. Sensor data were downloaded at I-80 from 01/01/2007 to 09/30/2008 at 15 minute interval. Following the same procedure described in Chapter 3, the values of stochastic capacity at macro-level are estimated. Figure 4.10 demonstrates the distribution of the capacities estimated at the macro-level.

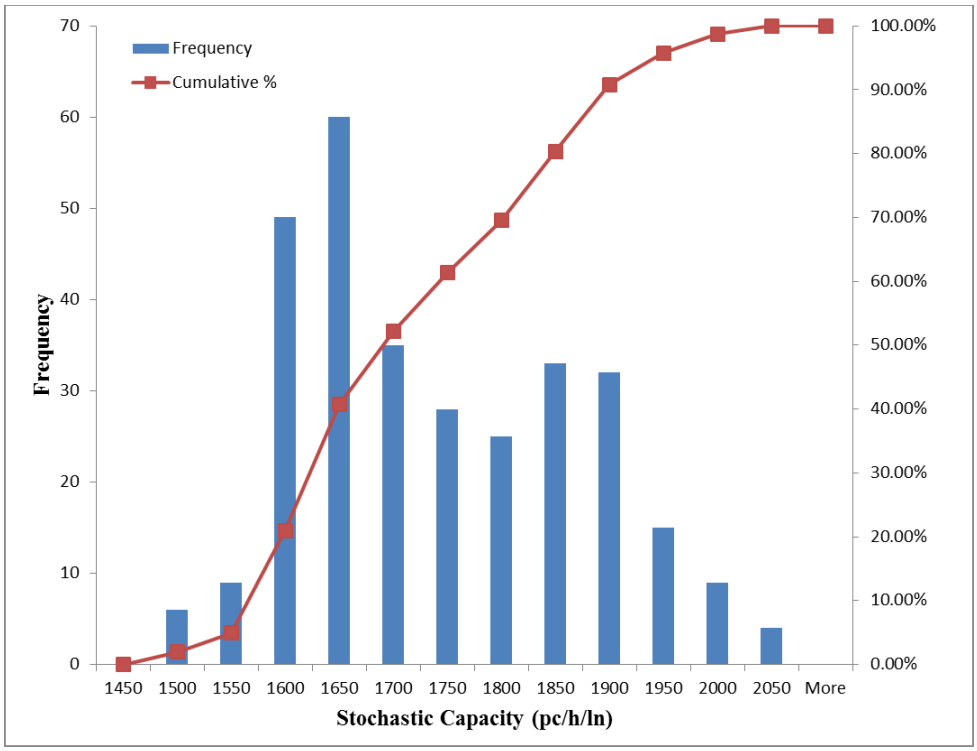

Figure 4.10 The Distribution of Stochastic Capacity at Macro-level

As shown in Figure 4.9, the capacities estimated at the macro-level are in the interval [1480, 2035]. The mean value is 1747 veh/h/ln and the standard deviation is 129 veh/h/ln. The index of dispersion for capacity is 0.08. In contrast, the capacities estimated at the micro-level are in the interval [1385, 2359]. The mean value is 1967 veh/h/ln and the standard deviation is 249 veh/h/ln. The index of dispersion for capacity is 0.12. As expected, the capacities estimated by kjam and w calibrated from individual vehicle trajectory data have bigger range and standard deviation. The underlying reasons are: (1) the variance between individual vehicles is going to be averaged out at the macro-level analysis; and (2) the measurement error involved in the micro-level analysis may result in higher variance of the

capacity estimation. Moreover, the mean of the capacities estimated at micro-level is higher than that estimated at macro-level. Based on their distributions, it is obvious that the distribution of the capacities estimated at micro-level is skewed to the left; while the distribution of the capacities estimated at macro-level is skewed to the right. The possible reason could be that the impacts of lane change and heavy vehicles were excluded from the data analysis at micro-level. It should be also noted that the corresponding speed observations of the capacities estimated at the macro-level fluctuate near the free-flow speed as shown in Figure 4.11. Therefore, the assumption of drivers' heterogeneity having no impact on the free-flow traffic condition should be released in future study. Further research should be conducted to study free-flow conations and nearly congested conditions.

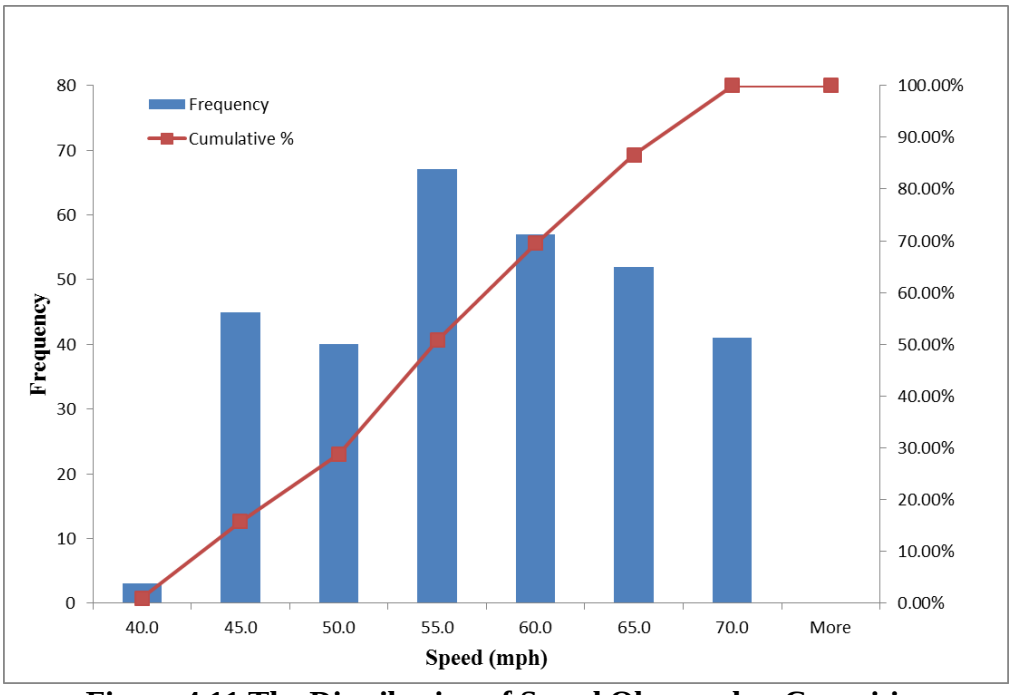

Figure 4.11 The Distribution of Speed Observed at Capacities

4.4 Correlation with the Deterministic Capacity at Marco-Level

As discussed above, the leader and follower are related by the shift $-w\ (d_n, \tau_n)$. In this section, the analyst try to demonstrate the how the stochastic car-following model can be related to the traditional deterministic capacity at Macro-Level. Assume w_i is the shift associated with vehicle i, Newell (*43*) found that the shift w_i follows a random walk in the *t-x* plane. Figure 4.12 illustrates how wave propagates at a microscopic scale along a platoon.

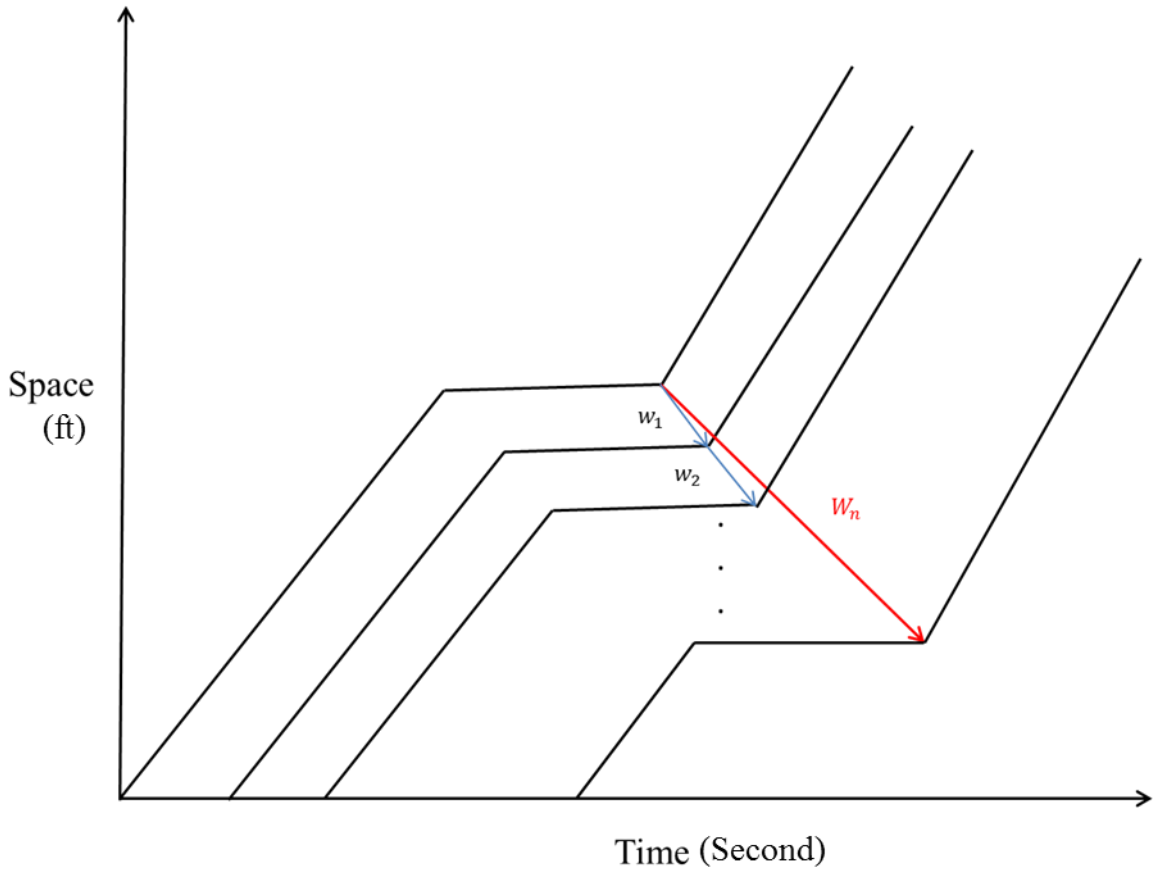

Figure 4.12 Wave Propagation along a Platoon

Let $\boldsymbol{W}_n$ represents the mean shift between vehicle 1 and $n+1$ and the coordinates of $\boldsymbol{W}_n$ is $(\sum_{i=1}^{n} d_n, \sum_{i=1}^{n} \tau_n)$.

The jam density along a platoon with n vehicles, K_{jam}, can be expressed as:

$$K_{jam} = \frac{n}{\sum d_i} = \frac{1}{\frac{1}{n}\sum d_i} \tag{4-13}$$

The backward wave speed along a platoon, W, is calculated as:

$$W = \frac{\sum d_i}{\sum \tau_i} \tag{4-14}$$

Therefore, if the triangular flow-density model is assumed, then the K_{jam} can be easily estimated by the arithmetic mean of d_i when the sample size of d_i is large enough. Chiabaut et. al (*49*) have proved that the wave speed, W, can be estimated by the harmonic mean of individual wave speed w_i as:

$$W = \frac{1}{\frac{1}{n}\sum \frac{1}{w_i}} \tag{4-15}$$

Based on the data measured from individual vehicle trajectories, the jam density and wave speed corresponding to the macro-level model can be estimated as 224 veh/mile and 10.4 mph, respectively. The value of capacity related to these jam density and wave speed is 1985 vphpl, which is consistent with the mean value of the capacities from the Monte Carlo simulation.

4.5 Summary

In this chapter, the stochastic characteristics of freeway bottleneck are investigated at the micro-level. Based on the vehicle trajectory data are collected from the NGSIM program, 148 pairs of trajectories have been identified at the stop-and-go. According to Newell's car following model, the corresponding jam density and wave speed of vehicle pairs are calibrated at micro-level. Both of the jam density and wave speed are stochastic variables. The jam density can be represented as a random variable with the Cauchy distribution and the wave speed can be represented as a random variable with the Logistic distribution. Since the impacts of lane changing and heavy vehicles are excluded from the dataset, it is reasonable to conclude that the heterogeneity of jam density and wave speed at the micro-level results from individual driving behavior. If the free-flow speed is assumed constant, capacity is fully determined by the wave speed and jam density. Therefore, capacity is mostly likely a random variable as well instead of a constant value and the corresponding stochastic capacity and queue discharge rate observed at marco-level are also generated by the heterogeneity between individual driving behaviors. A Monte Carlo simulation is performed to generate the stochastic jam density and wave speed based on their distributions. The corresponding capacity values are calculated and then compared with the stochastic capacities calibrated at the macro-level from aggregated sensor data. The capacity calculated at micro-level is reasonably compatible with the one measured at macro-level. However, it should be noted that the assumption of drivers' heterogeneity having no impact on the free

flow traffic condition should be released in future study. Further research should be conducted to study free-flow conations and nearly congested conditions.

5. INVESTIGATING TRAVEL TIME VARIABILITY WITH EMPRIRICAL STUDY

The primary objective of this research is to develop the stochastic capacity and queue discharge models for freeway physical bottlenecks and develop a theoretical approach to account for the travel time variance introduced by stochastic capacity. This could be used in travel time reliability studies and route choice models for real-world application or DTA simulation in the future. So far, the stochastic capacity and queue discharge models have been developed and implemented in a mesoscopic DTA simulator, DYNASMART-P, with a simplified bounded rationality route choice model. However, some methodology development and modeling improvements still need to be addressed. There is an obvious gap for the applications of stochastic capacity model in the field of traffic state prediction and assignment: lack of theoretical approach that can account for travel time variability. For example, as discussed before, the proposed simplified bounded rationality route choice model does not theoretically take into account the travel time variability caused by stochastic capacity, although it is intuitively sound. Therefore, this chapter aims to apply theoretically rigorous approaches to explicitly account for the travel time variability caused by stochastic capacity and demonstrate the travel time variability in an empirical study. Moreover, a comparison will be made between the travel time predictions from stochastic and deterministic (HCM level) capacity under same demand level. It is expected to demonstrate to what extent the stochastic capacity contributes to the observed travel time variability.

5.1 Study Site

A 0.85-mile freeway link with 3 lanes (as shown in Figure 5.1) in Raleigh, North Carolina, is selected for the empirical study to evaluate the effectiveness of the travel time prediction functions derived from several different theories, which are discussed later. The Raleigh area is selected for two major reasons:

1) The high level of recurrent congestion within this region during peak hours;

2) This region is monitored under two different traffic data systems, Traffic.com (*50*) and Inrix (*51*).

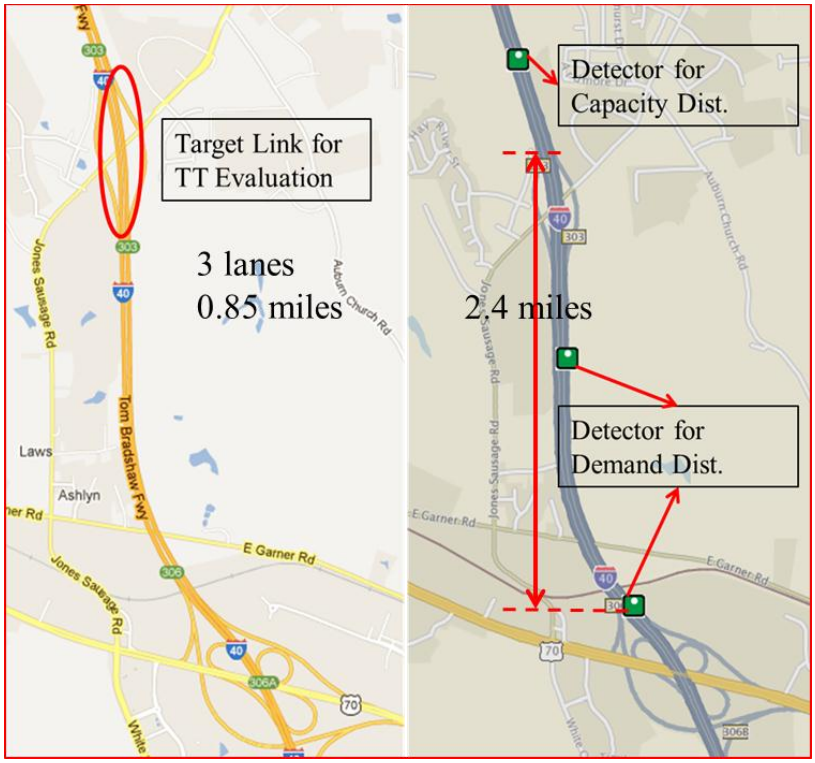

Figure 5.1 Study Site

Specifically, Traffic.com provides traffic data from microwave detectors, which could be used to develop stochastic capacity and demand distributions and the travel time prediction function. Inrix provides travel time data for freeway links from probe vehicles, which could be used to validate the travel time prediction function.

As shown in above figure, the freeway link highlighted in the red circle will be used to evaluate the travel variability due to stochastic capacity. Since the travel time is a function of both demand and supply (i.e., capacity), besides the stochastic capacity distribution, the demand distribution is also needed. During free-flow traffic conditions, traffic demand for certain freeway link could be directly attained from detectors. During congested traffic conditions, however, traffic demand may be not readily available. In order to get a good representation of the demand distribution and then assess the travel time variability caused by stochastic capacity, traffic demand is formulated by using the procedure described in section 5.2. Three detectors from traffic.com will be used to retrieve the data necessary to calibrate the stochastic capacity and demand. As shown in Figure 5.1, the detector just downstream of the target link is used to develop the stochastic capacity distribution and the other two are used to estimate the demand distributions. The data (both traffic.com and Inrix) were downloaded from 01/01/2011 to 08/31/2012 and the holidays were excluded from the dataset. Figure 5.2 shows the average travel time of the target link from Inrix from 6:00 AM to 8:00 AM and Figure 5.3 shows the standard deviation of travel time during the same time period.

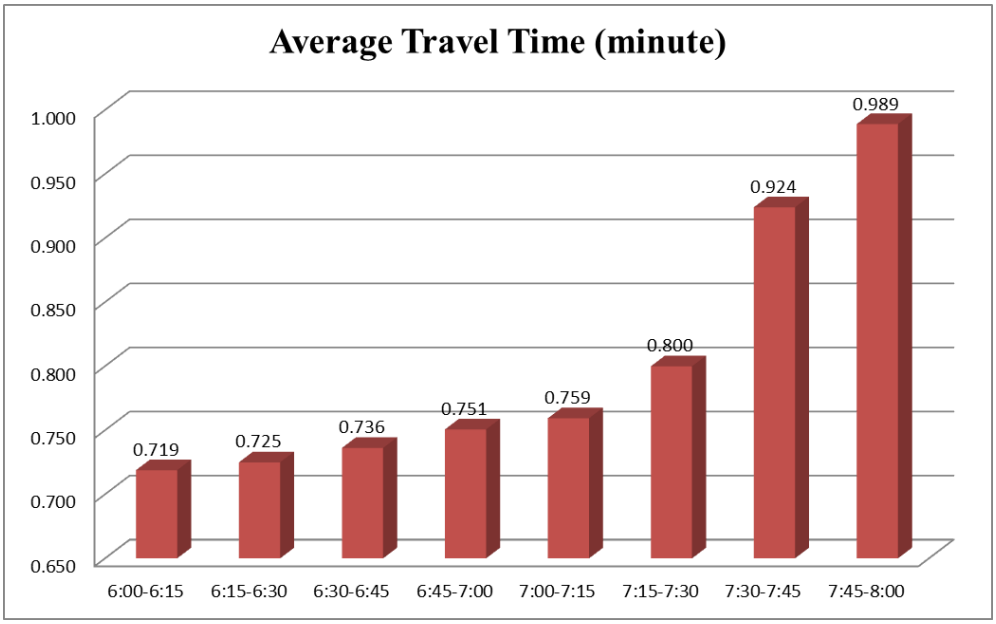

Figure 5.2 Average Travel Time of the Target Link from Inrix

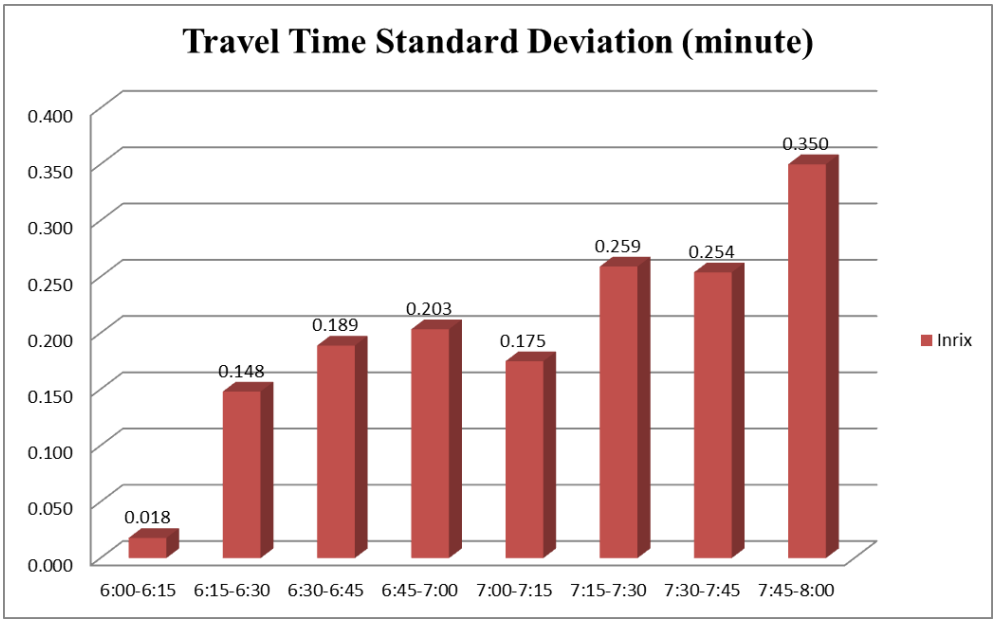

Figure 5.3 Travel Time Standard Deviation of the Target Link from Inrix

5.2 Formulate Demand and Capacity distribution

The stochastic capacity will be developed in the same method described in Chapter 3; while stochastic demand calibration procedure will be discussed in this section.

5.2.1 Stochastic Capacity Distribution

Following the methodology described in Chapter 3, the stochastic capacity model for the target link is developed. Again, generalized logistic distribution provides the best fit for this study sites. The corresponding parameters are: k=-0.254, μ=2165 and σ=69.6. Figure 5.4 demonstrates the capacity distribution of the target link.

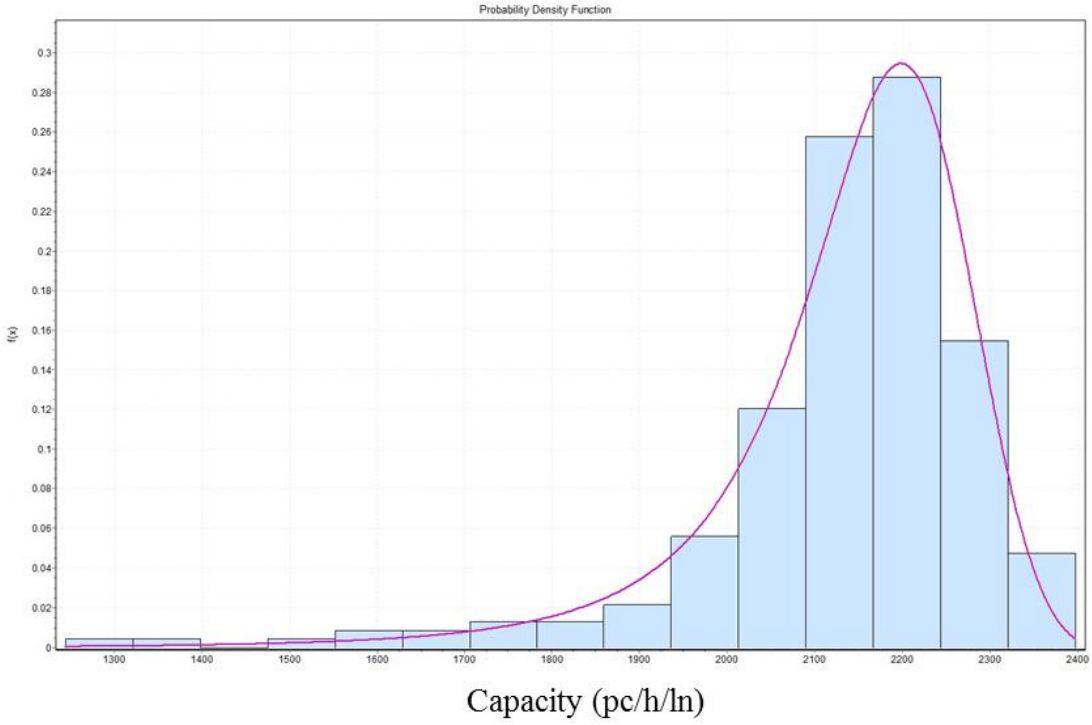

Figure 5.4 Stochastic Capacity Distribution of Target Link

5.2.2 Demand Distribution

Traffic demand is usually defined as the number of vehicles that wish to pass a roadway section in a given time period. If the traffic demand does not exceed the corresponding roadway capacity, the measured flow rate in the field is the traffic demand rate. However, if traffic demand rates exceed the roadway capacity, there are vehicle stored in the transportation systems and the measured flow rate by sensor only represent the number of vehicles that can be handled by the transportation system, but not the demand rate. Therefore, it is clear that it is impossible to measure the traffic demand by just using single detector in the system.

In order to quantify the link travel time and travel time variability, it is important that the analyst can estimate traffic demand in the congestion condition. In the congestion condition, high densities are quite possibly observed upstream of the bottleneck, which could be used to estimate to what extent the traffic demand is underestimated. Therefore, in this study, two sensors at the upstream of the bottleneck, as shown in Figure 5.1, are used to estimate the demand on the target link. Based on the data from the two sensors, the "excess lane density" method developed by May (*52*) is applied to estimate the demand of the target link. The excess lane density can then be converted to the number of excess vehicles for each demand time period (15 minutes in this study) by the following equation:

$$(V_{EXC})_t = \sum_{i=1}^{n} (k_{it} - k_0) L_i N_i \qquad (5\text{-}1)$$

Where,

$(V_{EXC})_t$ =number of excess vehicles in the system at time t

n = number of subsections in the system (n=2 in this study)

k_{it} =density in subsection i at time t

k_0 = density at capacity in vehicles per lane-mile

L_i =length of subsection i in miles

N_i =number of lanes in subsection i

$k_{it} - k_0$ represents the excess lane density.

The next step is to convert excess number of vehicles at certain time interval into unserved flow rates due to capacity constraints of the downstream bottleneck for different time interval by following equation:

$$(q_{EXC})_{t,t+1} = \frac{(V_{EXC})_{t+1} - (V_{EXC})_t}{TI} \quad (5\text{-}2)$$

Where,

$(q_{EXC})_{t,t+1}$ =unserved flow rate between time t and $t+1$

TI =time interval between time t and $t+1$ in hours (in this study, TI=0.25)

Finally, the estimated traffic demand can be calculated as:

$$D_{t,t+1} = q_{t,t+1} + (q_{EXC})_{t,t+1} \quad (5\text{-}3)$$

Where,

$D_{t,t+1}$ = estimated demand between time t and $t+1$

$q_{t,t+1}$=observed flow rate by sensor between time *t* and *t+1*

Figure 5.5 is an example of the demand estimation procedure from 6:00 AM to 8:00 AM. As shown in the figure, from 6:00 AM to 6:30 AM, the observed flow rate is actually the demand which wishes to pass the downstream roadway segment; while starting from 6:30, vehicles have been stored in the network and the actual traffic demand is actually greater than the observed flow rate until 8:00 AM.

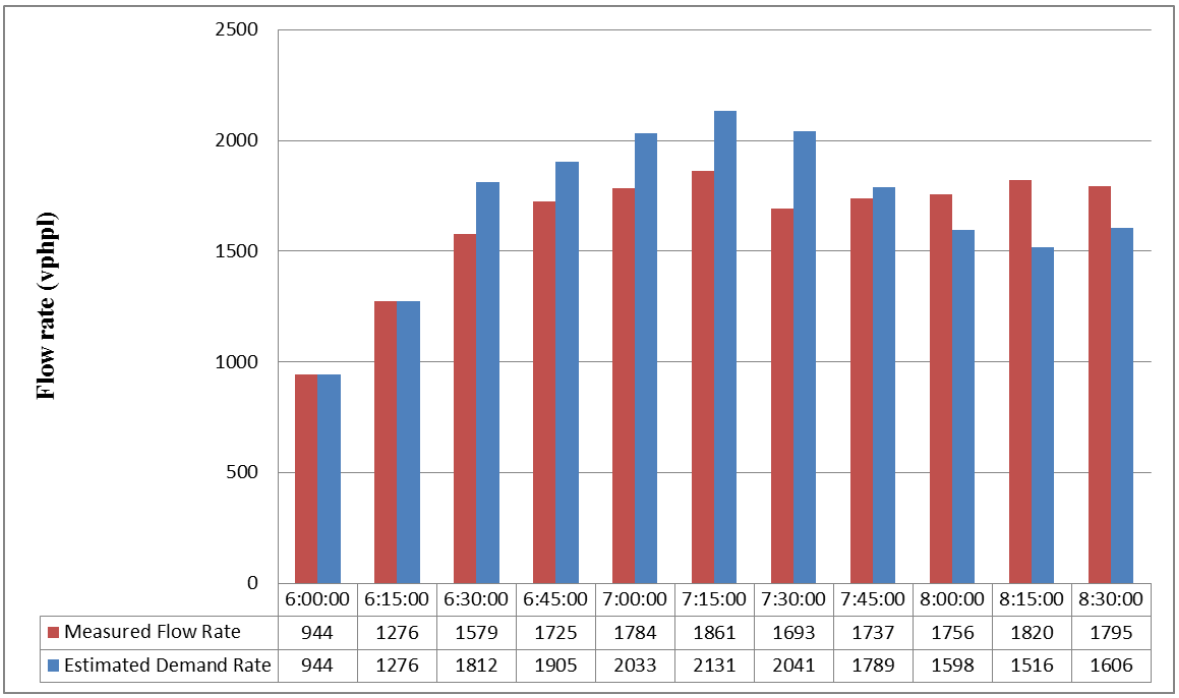

	6:00:00	6:15:00	6:30:00	6:45:00	7:00:00	7:15:00	7:30:00	7:45:00	8:00:00	8:15:00	8:30:00
Measured Flow Rate	944	1276	1579	1725	1784	1861	1693	1737	1756	1820	1795
Estimated Demand Rate	944	1276	1812	1905	2033	2131	2041	1789	1598	1516	1606

Figure 5.5 Example of Traffic Demand Estimation

By repeating the above process, the traffic demand of 357 days (excluding holidays and missing data) between 6:00 AM and 8:00 AM are estimated. The next step is to formulate the traffic demand distribution for each 15 minute time period. In general, the

generalized logistic distribution provides the best fit for all demand time period. The corresponding parameters of each time period are summarized in Table 5.1. Figure 5.6 shows the demand distribution for the time period 6:00 – 6:15 and the rest are listed in Appendix E.

Table 5.1 Parameters of Demand Distribution for Different time Periods

Time Period	Gen. Logistic		
	k	μ (pc/h/ln)	σ (pc/h/ln)
6:00 – 6:15	-0.207	1010	38.09
6:15 – 6:30	-0.265	1462	50.04
6:30 – 6:45	-0.254	1750	65.84
6:45 – 7:00	-0.326	1865	66.41
7:00 – 7:15	-0.317	1919	73.57
7:15 – 7:30	-0.332	2029	70.47
7:30 – 7:45	-0.280	1955	68.17
7:45 – 8:00	-0.253	1815	80.83

However, an important question arises here: are the demands between different time intervals independent? In other words, during the simulation, can one just simply randomly generate the demand for each time interval? Therefore, it is necessary to investigate whether the demand level at certain time interval is correlated with a subsequent demand level. Figure 5.7 demonstrate the demand at time interval *i* against the demand at time interval *i+1*.

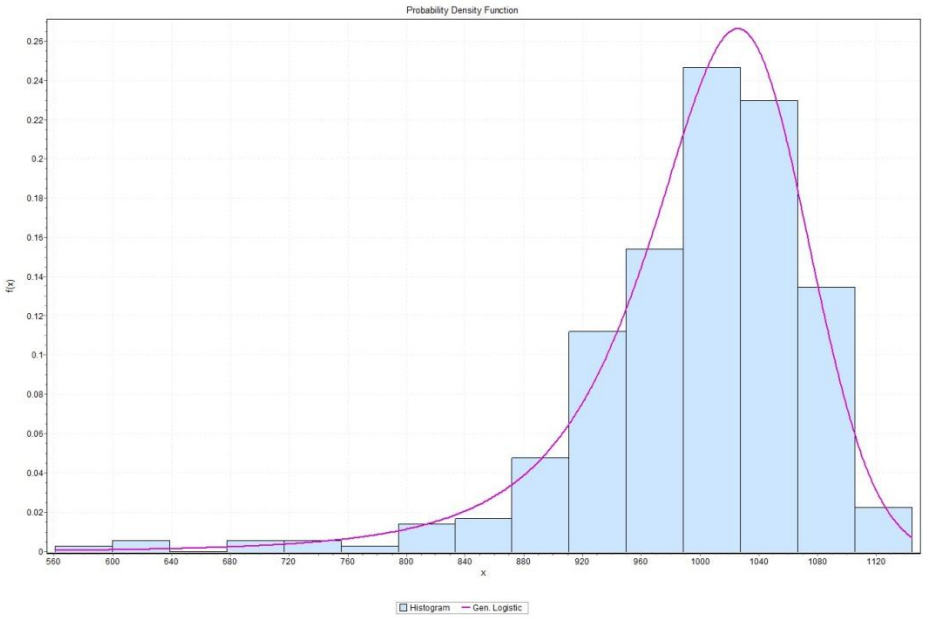

Figure 5.6 Demand Distribution for Time Period 6:00 – 6:15

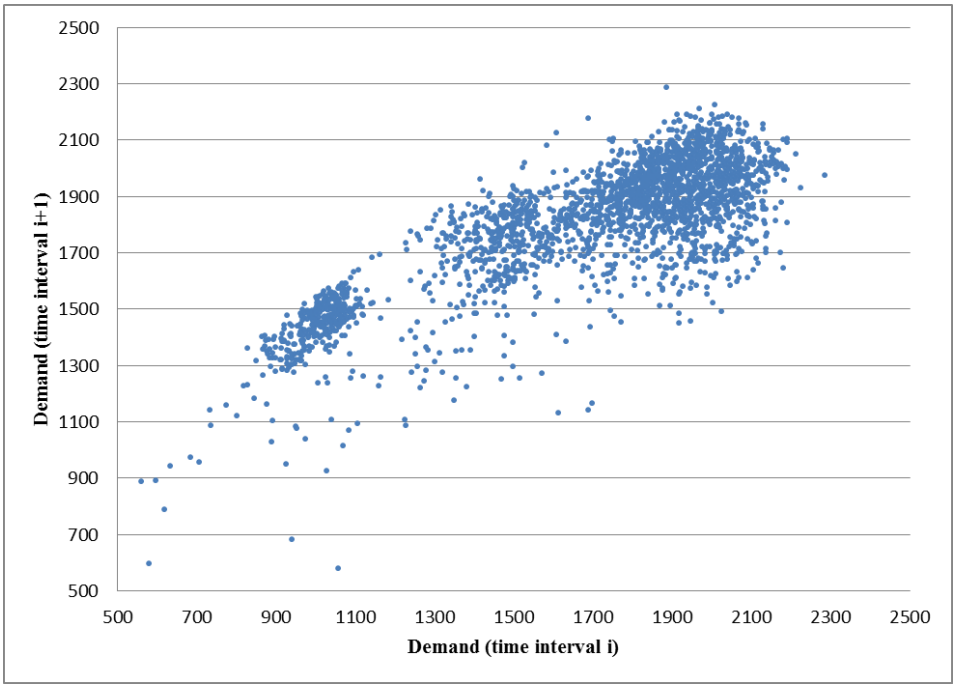

Figure 5.7 Correlation between Demands at Two Consecutive Time Intervals

As shown in Figure 5.7, for the traffic demand between 6:00 AM and 8:00 AM, there is an obvious trend between two consecutive time intervals: the higher the demand at time *i*, the higher the demand at time *i+1*. Therefore, during the simulation, it is incorrect to just simply randomly generate the traffic demand for each time interval. Instead, a simple first order autoregressive model is proposed as follows.

$$D_{i+1} = \alpha D_i + \mu + \varepsilon_i \tag{5-4}$$

Where,

D_{i+1}: Traffic demands at interval *i+1* in pc/h/ln;

α: Coefficient;

μ: Intercept;

$\varepsilon_i \sim N(0, \sigma^2)$: Random error.

Based on the demand observations, the above parameters can be estimated as α=0.516 and μ=929 pcphpl. At least 65% (the R^2 value of this model) of the variation in the response variable $D_{i+1,}$ can be explained by the proposed model. Based on the discussion above, the fact is that the demand at different 15-minute interval has their own distribution and the demand at time interval *t+1* is strongly correlated with the demand at time interval *t*. Therefore, an appropriate approach is required to generate the stochastic demands, D_t, at different time interval *t*, which are consistent with their own distribution, i.e., D_t ~ generalized logistic distribution F_t, and strongly time-related with each other. The simulation approach is proposed as follows:

Step 1: Generate random variable, $x_{0,}$ and $x_0 \sim N(0,1)$

Step 2: For $t>0$, $x_t=\varphi_i x_{t-1}+\varepsilon_t$, $\varepsilon_t \sim N(0,1-\varphi_i^2)$, where φ_i (i=0,1,…) is the coefficient of the first order autoregressive model for the x_t recursion. For i=0, let $\varphi_0 = \alpha = 0.516$, which is the same coefficient of the first order autoregressive model for the observed demand. Since $Var(x_t)=1$, for all t, $x_t \sim N(0,1)$

Step 3: Calculate $\phi(x_t)$, where $\phi(.)$ is the inverse cumulative distribution function. It is clear that $\phi(x_t) \sim$ Uniform (0,1)

Step 4: Calculate D_t: $D_t = F_t^{-1}(\Phi(x_t))$. It is clear that $D_t \sim F_t$.

Step 5: Build the first order autoregressive model for the D_t calculated at step 4 and obtain the coefficient β of the first order autoregressive model of the demand

Step 6: Check whether the β is in the 95% confidence interval of the α, which is [0.500483, 0.530673]. If true, then **STOP.** Otherwise, go to step 2 and repeat the whole process by adjusting the value of φ_i until the β calculated in step 5 within the 95% confidence interval of the α.

In this study, through trail-and-error, it was found that when $\varphi_i = 0.85$, the coefficient β of the first order autoregressive model of the demand calculated at step 5 is 0.5188, which is in the 95% confidence interval, [0.500483, 0.530673]. Therefore, the corresponding demand, D_t, generated based on $\varphi_i = 0.85$, will be used as the stochastic demand in this study.

Besides the generation of the stochastic demand, the implementation framework of the stochastic capacity is demonstrated in Figure 5.8.

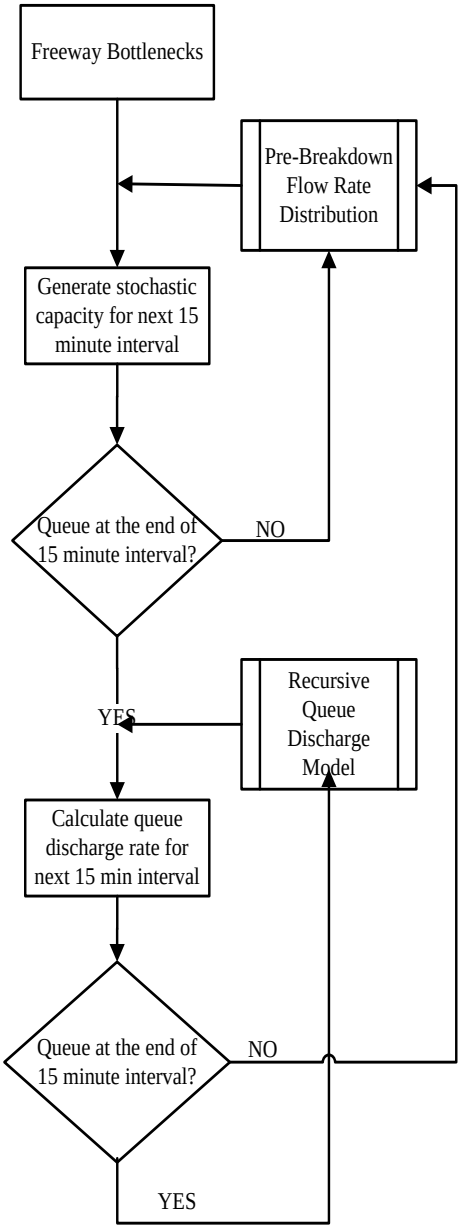

Figure 5.8 Implementation Framework of Stochastic Capacity Generation

5.3 Formulate travel time prediction function

Travel time is a function of both demand and supply. Considering a freeway bottleneck *A* and a freeway link *L* just upstream of *A*, the average travel time for vehicles passing through link *L* can be denoted as follows:

$$T = f(D, C) \tag{5-5}$$

Where,

T = average travel time for freeway link *L*;

D = traffic demand for link *L*;

C = capacity of bottleneck *A*.

Therefore, an appropriate $f(.)$ should be formulated to establish the relationship between demand and supply. Three alternatives, namely BPR function, queuing theory and kinematic wave theory will be used to establish such relationship, respectively. All are widely used for highway traffic analysis. Regarding the BPR function and queuing theory, the computation is relatively simple compared to kinematic wave theory. However, the drawback of BPR function and queuing theory is that it overlooks the speed difference between free-flow traffic state and congested traffic state and the vehicle queues as well. Therefore, the kinematic wave theory is expected to be more accurate. After formulating the travel time functions, the corresponding travel time variance can be estimated. Their effectiveness will be evaluated through a real-world empirical study.

5.3.1 BPR Function

In most traffic assignment models, the effect of road capacity on travel time is expressed as volume-delay function:

$$t = t_0 * f\left(\frac{v}{c}\right) \tag{5-6}$$

Where,

t_0 = free-flow travel time

v = traffic demand

c = link capacity

Various types of volume-delay functions have been proposed before and the most widely used one is the BPR functions (*53*):

$$t = t_0 * (1 + \alpha\left(\frac{v}{c}\right)^{\beta}) \tag{5-7}$$

Where,

α = coefficient (often set at 0.15)

β = exponent (often set at 4.0)

It should be noted that in such volume-delay functions, the vehicle queuing phenomenon is not modeled at the bottleneck. All the traffic demand at certain time interval can pass the bottleneck with certain delay with no vehicles stored at the upstream of the bottleneck. Before evaluating the effects of stochastic capacity on the travel time variability, constant capacity value combined with the demand distribution calibrated above will be

applied first to demonstrate the travel time variability due to the traffic demand variance. Based on the traffic.com data, the constant roadway capacity of the target link is calculated as 2220 vphpl based on the conventional definition of the deterministic capacity.

A Monte Carlo simulation is performed to generate the stochastic capacity and demand based on the capacity/demand distributions calibrated above. Within deterministic capacity environment (stochastic demand only), Figure 5.9 demonstrates the comparison between the simulated average link travel time and real-world average link travel time reported by Inrix for different time intervals. Figure 5.10 shows the corresponding travel time standard deviation comparison.

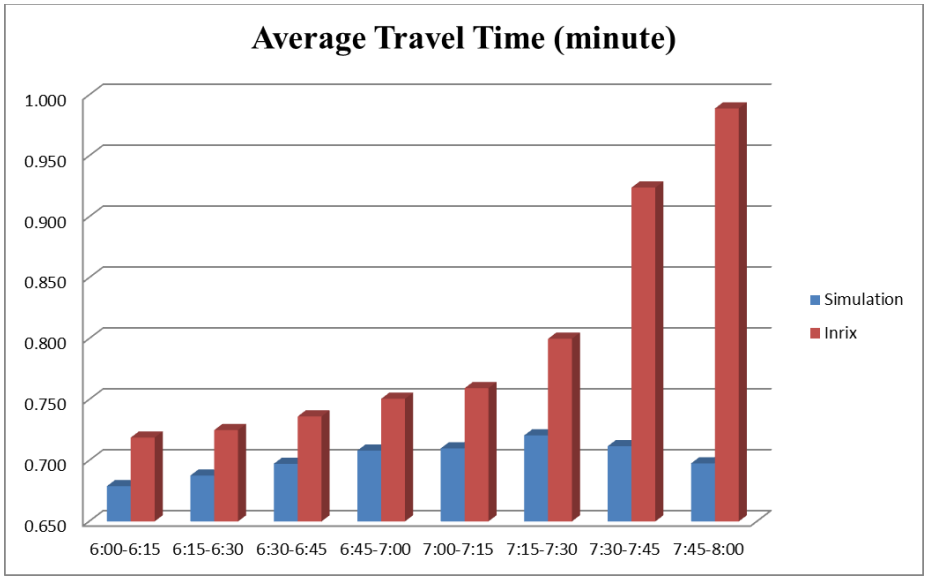

Figure 5.9 Average Travel Time: BPR Simulation vs. Inrix (Deterministic Capacity)

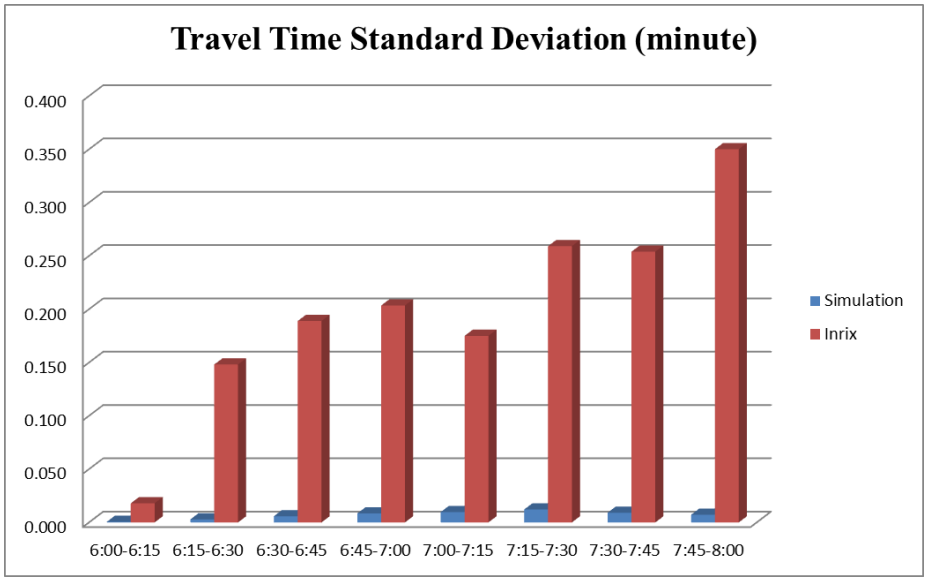

Figure 5.10 Travel Time Standard Deviation: BPR Simulation vs. Inrix (Deterministic Capacity)

As shown in Figure 5.9, within the deterministic capacity environment, the simulated link travel time is systematically and significantly lower than the Inrix estimates, especially during the peak period (7:30 AM ~ 8:00 AM). More importantly, as demonstrated in Figure 5.10, the simulated link travel time standard deviation is much lower than the real-world observations, which suggests that the demand variability is far from adequate to explain the travel time variability observed in the field.

Within the stochastic capacity environment, Figure 5.11 demonstrates the comparison between the simulated average link travel time and real-world average link travel time measured by Inrix for different time interval. Figure 5.12 shows the corresponding travel time standard deviation comparison.

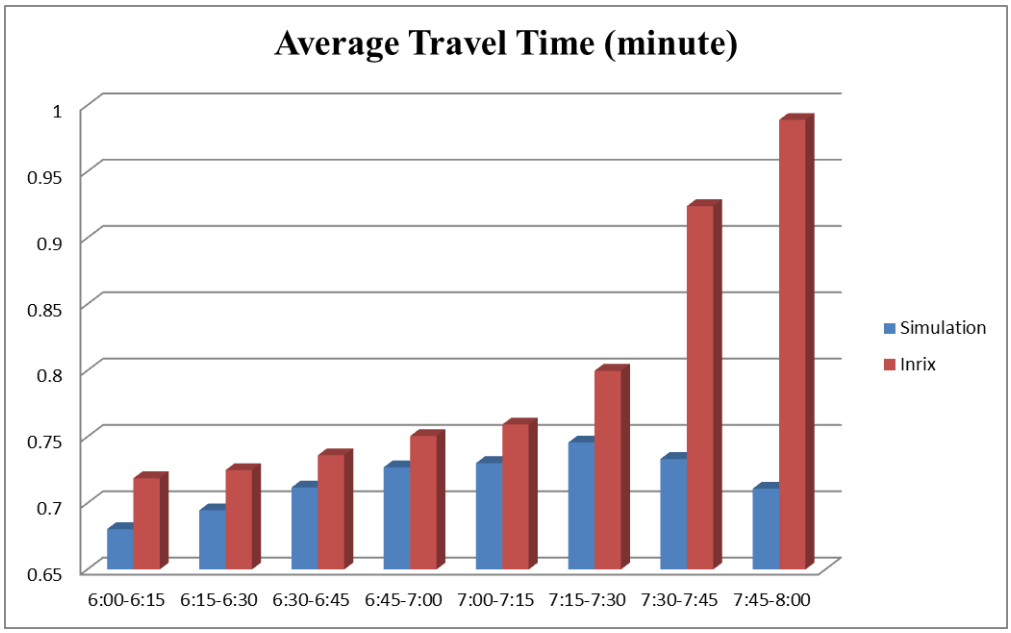

Figure 5.11 Average Travel Time: BPR Simulation vs. Inrix (Stochastic Capacity)

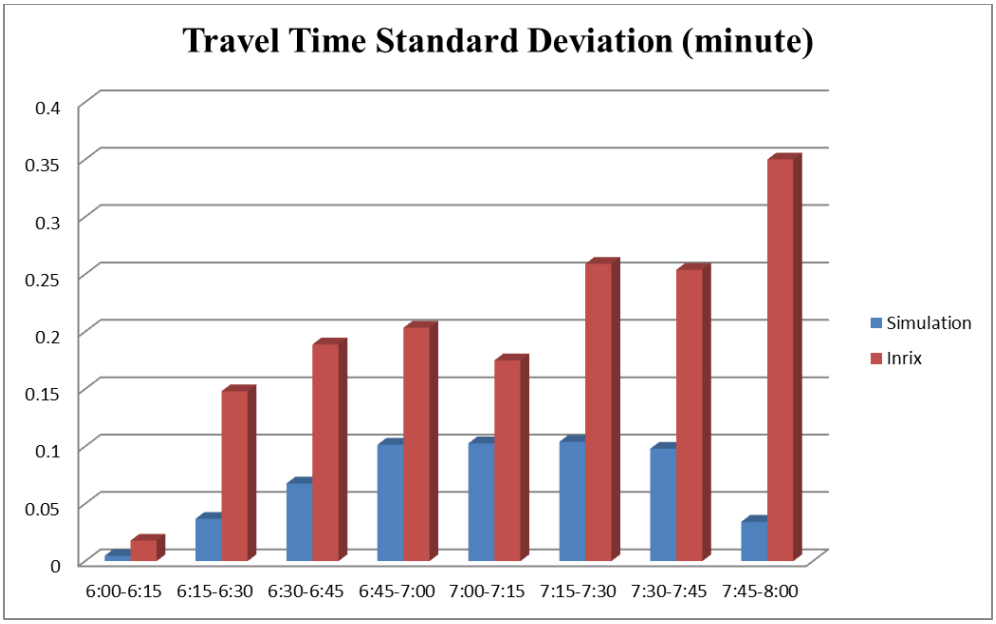

Figure 5.12 Travel Time Standard Deviation: BPR Simulation vs. Inrix (Stochastic Capacity)

As shown in Figure 5.11, after introducing the stochastic capacity into the BPR function, the simulated link travel time begins to get closer to the field travel time observations during the time period from 6:00 AM to 7:30 AM. During the time period 7:30 AM to 8:00 AM, the simulated link travel time is still much lower than the Inrix observation. The underlying reason is that the vehicle queuing phenomenon is not modeled in the BPR function. During 7:15~7:30, the traffic demand usually reaches its peak values and vehicles begin to be stored at the upstream of the bottleneck. Therefore, the travel times between 7:30 AM to 8:00 AM are underestimated by the BPR function compared with the Inrix observation. The results are consistent with findings from previous study: BPR function will leads to an underestimation of travel time if the V/C ratio is greater than 1.0 (*54*), which is the inherent drawback of BPR function. Therefore, the BPR function requires enhancement that could address the issues caused by the oversaturated conditions (demand exceeds capacity). Using the freeway detector data, Huntsinger (*55*) applied the method of bottleneck analysis and queue length estimation to enhance the BPR function. The calibrated BPR function performs really well when compared with field observations.

Comparing Figure 5.10 and Figure 5.12, after introducing the stochastic capacity into the BPR function, the variability of the link travel time is modeled more accurately, which suggests that the variability of traffic demand itself is not able to explain the travel time variance measured in the real-world. Again, during the time period 7:30 AM to 8:00 AM, the variability of travel time is underestimated due to the limitation of BPR function.

5.3.2 Queuing Theory Approach

When demand exceeds capacity for a period of time, a queue will be formed: the excess vehicles are stored upstream of the bottleneck and their departure is delayed to a later time period. The inputs for a queuing analysis described in this section include the following three elements:

- Arrival distribution (demand distribution discussed in section 5.2.2)
- Service distribution (capacity distribution discussed in section 5.2.1)
- Queue discipline

The queue discipline used here is "first in, first out", i.e., the vehicles are served in the order in which they arrive. Therefore, in the queuing theory, the link travel time for a period of time is essential the summation of free-flow travel time and the delay due to the queues as follows:

$$T_i = FFTT + d_i \tag{5-8}$$

Where,

T_i = travel time for a time period of i

$FFTT$ = free-flow travel time

d_i = delay due to the vehicle queue

For each time period, the average vehicle delay is calculated based on the arrival rate (demand) and the departure rate (capacity). In this study, both demand and capacity are random variables and can be expressed as: *D(i)* and *C(i)*. Assuming there is no queue in the

system at the beginning and in a time period of *i* (from t_0 to t_1), the traffic demand is greater than the roadway capacity, the average vehicle delay can be calculated as:

$$d_i = \frac{(D(i) - C(i)}{2D(i)}(t_1 - t_0) \tag{5-9}$$

Where,

d_i = average vehicle delay for a time period of *i*

D(i): traffic demand during time period *i*

C(i): roadway capacity during time period *i*

For the next time period, *i+1* (from t_1 to t_2), the traffic demand needed to be served becomes the summation of the new arriving traffic and the number of vehicles stored at the bottleneck during time period, *i*. The average vehicle delay for the time period *i+1* can be calculated as:

$$\text{Case 1: } d_{i+1} = \frac{(D(i) + D(i+1) - C(i) - C(i+1)}{2D(t+1)}(t_2 - t_1) \text{ If } (D(i) + D(i+1) > C(i) + C(i+1) \tag{5-10}$$

$$\text{Case 2: } d_{i+1} = \frac{[(D(i) - C(i)]^2}{2[C(i+1) - D(i+1)]D(i+1)}(t_2 - t_1) \text{ If } (D(i) + D(i+1) \le C(i) + C(i+1) \tag{5-11}$$

In case 1, there is still vehicles stored at the end of time period *i+1*; while in case 2, there is no vehicle queued at the end of time period *i+1*. In contrast to the BPR function discussed in section 5.3.1, vehicles will be stored at the upstream of the bottleneck if the demand rate is greater than the capacity rate, which is the primary advantage of queuing theory. However, it should be noted that the queue is stored in a vertical form, called point

queue and there is no constraint applied on the number of vehicles which can be stored at the bottleneck.

Similarly, constant capacity value combined with the demand distribution will be applied first to demonstrate the travel time variability due to the traffic demand variance. The combination of stochastic capacity and demand will be evaluated subsequently. Again, a Monte Carlo simulation is performed to generate the stochastic capacity and demand based on the capacity/demand distributions calibrated above. Within the deterministic capacity environment, Figure 5.13 demonstrates the comparison between the simulated average link travel time and real-world average link travel time measured by Inrix for different time interval. Figure 5.14 shows the corresponding travel time standard deviation comparison.

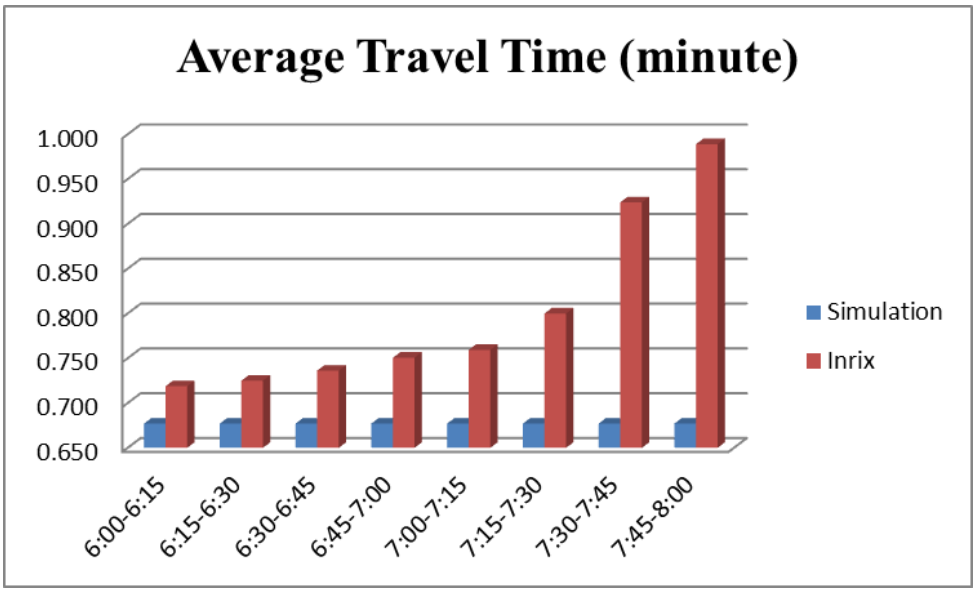

Figure 5.13 Average Travel Time: Queuing Simulation vs. Inrix (Deterministic Capacity)

As shown in Figure 5.13, within the deterministic capacity environment, the simulated link travel time is systematically lower than the Inrix observations. There is even no significant difference between the simulated link travel time over different time period, which indicates that the queuing model significantly underestimate the delays not only for the peak periods but also the non-peak periods. More importantly, as demonstrated in Figure 5.14, the simulated link travel time standard deviation is much lower than the real-world observations, although its performance is slightly better than the BPR function during the peak period. In general, consistent with the results of BPR function, it suggests that the demand variability does not explain the travel time variability observed in the field.

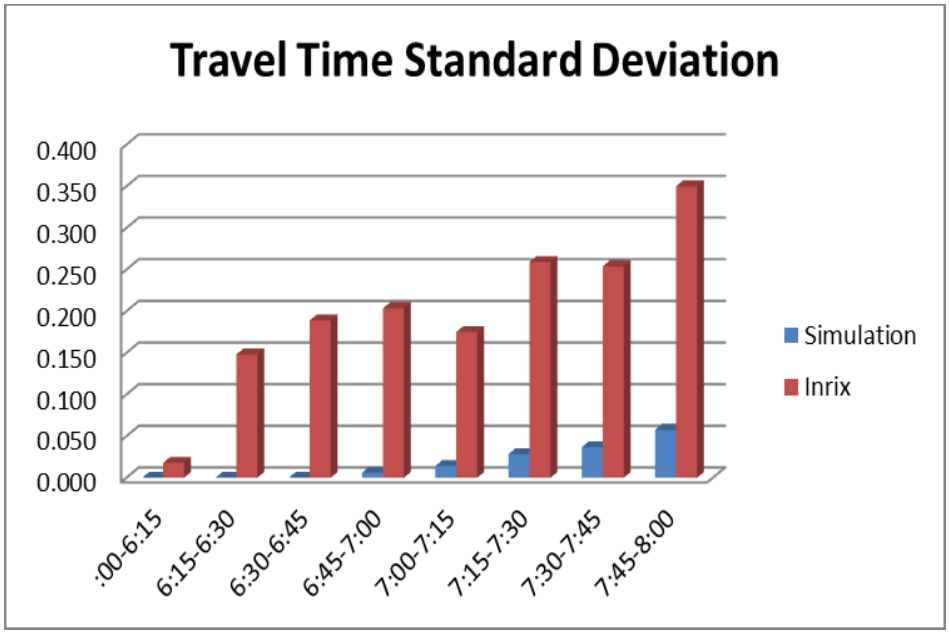

Figure 5.14 Travel Time Standard Deviation: Queuing Simulation vs. Inrix (Deterministic Capacity)

Within stochastic capacity environment, Figure 5.15 demonstrates the comparison between the simulated average link travel time and real-world average link travel time measured by Inrix for different time intervals. Figure 5.16 shows the corresponding travel time standard deviation comparison.

As shown in Figure 5.15, after introducing the stochastic capacity into the queuing model, the simulated link travel time begins to get closer to the field travel time observations during the time period from 6:00 AM to 7:30 AM. During the time period 7:30 AM to 8:00 AM, the simulated link travel time is still much lower than the Inrix observation; while its performance is slightly better than BPR function. The underlying reason is that compared with the BPR function, the vehicle queuing phenomenon is modeled in the queuing theory; while since the queue spill-back phenomenon is not modeled, the traffic speed is overestimated (i.e., vehicle delay is underestimated). During 7:15~7:30, the traffic demand usually reaches its peak values and vehicles begin to be stored and spill-back to the upstream of the bottleneck. Therefore, the travel times between 7:30 AM to 8:00 AM are underestimated by the queuing theory compared with the Inrix observation, although it is less underestimated than the BPR function.

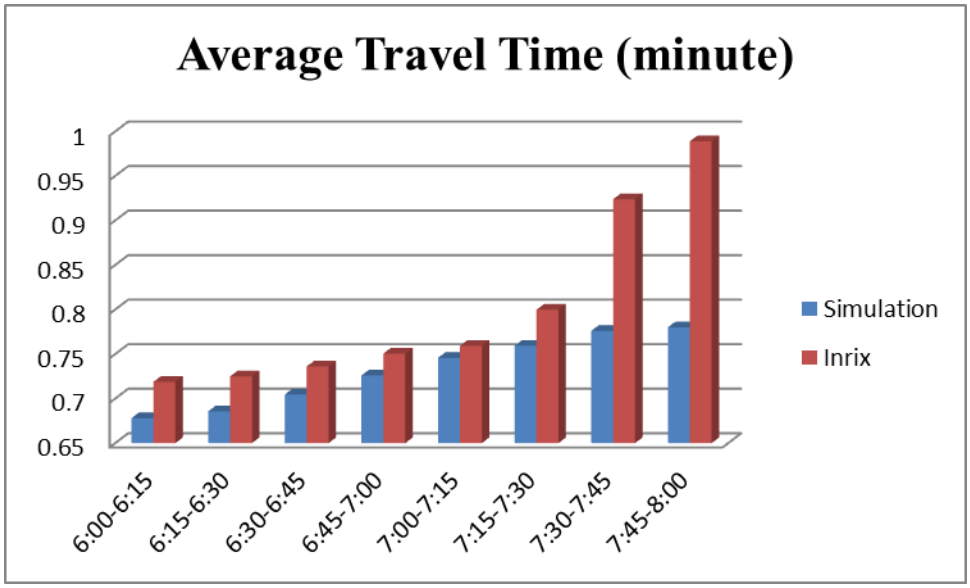

Figure 5.15 Average Travel Time: Queuing Simulation vs. Inrix (Stochastic Capacity)

Comparing Figure 5.14 and Figure 5.16, after introducing the stochastic capacity into the queuing theory function, the general trend of variability of link travel time is consistent with the field observation; while the values of travel time standard deviation is systematically higher than the Inrix observations, especially when the demand level is relatively high. The overestimation of travel time standard deviation could be the combined actions of the limitation of the queuing theory, i.e., the queue spill-back phenomenon is not modeled and there is no constraint applied on the number of vehicles which can be stored at the bottleneck.

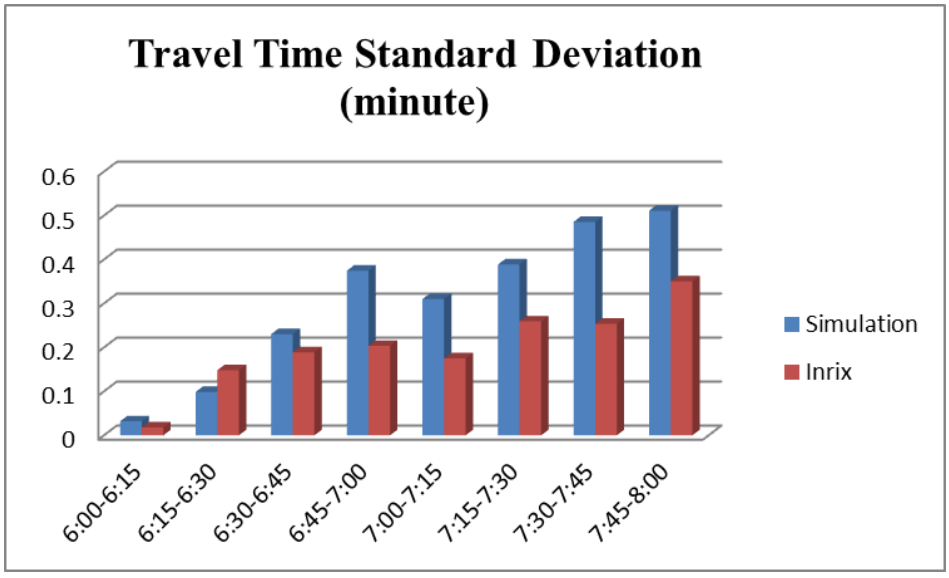

Figure 5.16 Travel Time Standard Deviation: Queuing Simulation vs. Inrix (Stochastic Capacity)

5.3.3 Shock Wave Theory

A shock wave is a boundary established at the time-space domain when one flow state changes to another. In macroscopic traffic analysis, a shock wave model is widely used to model the vehicle queue propagation. Based on the shock wave theory, the location of queue and the traffic states along the roadway at the time-space domain can be estimated, which enables a more accurate travel time or delay calculation compared with the BPR function and queuing theory discussed above. Within deterministic demand and capacity environment, the implementation of shock wave theory is relatively simple. However, when the demand and capacity become stochastic, the implementation of shock wave theory may need further investigation. In this section, two primary tasks need be addressed:

(1) Compute the shock wave functions on time-space plane based on stochastic demands and capacities;

(2) Compute the vehicle delay based on wave functions

Let's start from an illustrative example to investigate how the shock wave will propagate along the time-space plane within the stochastic demand and capacity environment and then derive the general case of wave propagation. It should be noted that all the analysis conducted below are based on the simplified triangular flow-density model. Figure 5.17 demonstrates several demand-capacity combinations for different time period (15 minute is used in this study).

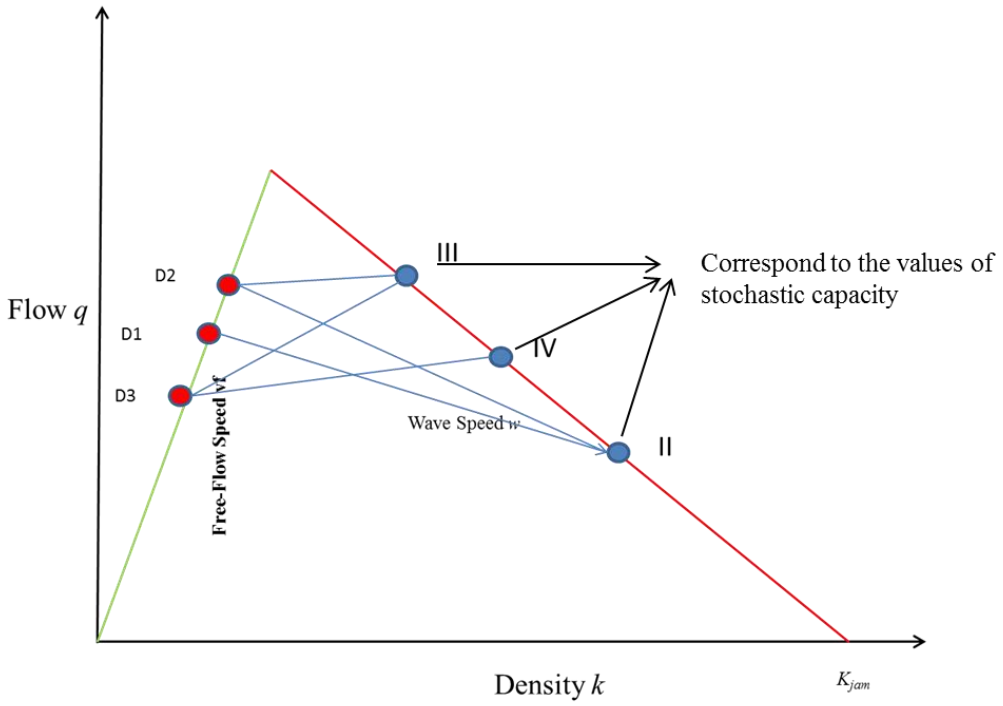

Figure 5.17 Illustrative Example of Wave Propagation with Stochastic Demand and Capacity

As shown in Figure 5.17, assume the demands of the upstream of the freeway bottleneck over three consecutive time intervals are *D1, D2,* and *D3,* respectively; assume the stochastic capacities of the freeway bottleneck are corresponding to the traffic state *II, III,* and *IV* on the *q-k* curve, respectively. It should be noted that the stochastic demand and stochastic capacity are randomly generated for every 15 minute interval. In order to model the impacts of stochastic demand and capacity, the first critical step is to determine the shock waves between different traffic states (i.e., II, III, and IV) due to the downstream stochastic capacities and the shock wave between stochastic demands and different traffic states due to the downstream stochastic capacities. For this specific example as shown in Figure 5.17, the corresponding shock wave propagation in the time-space plane is shown in Figure 5.18. The possible vehicle trajectories in respond to such shock wave propagation are also illustrated in Figure 5.18 based on the travelling speed in different traffic states calculated from Figure 5.17.

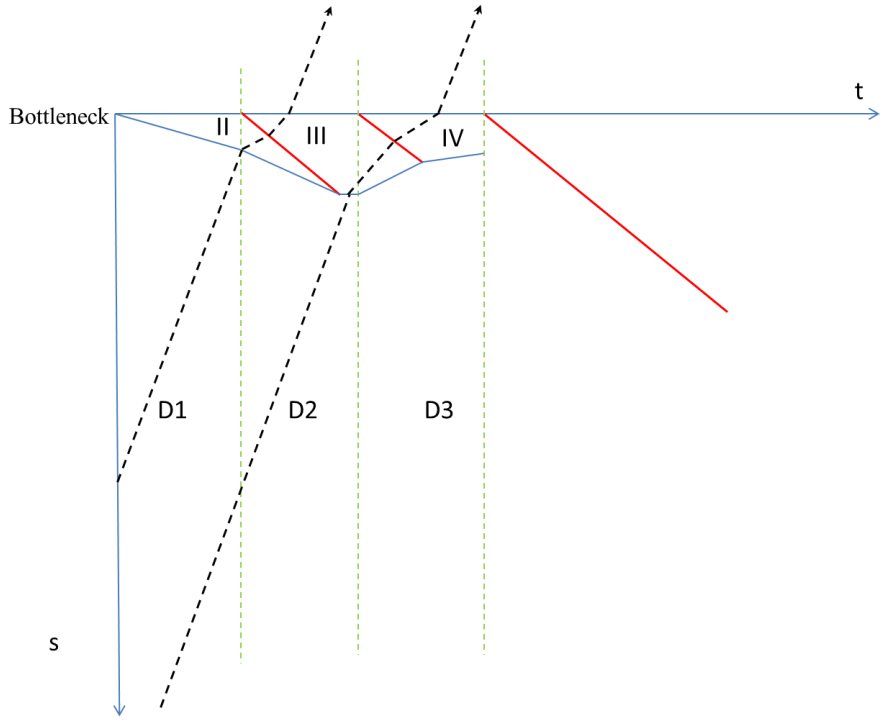

Figure 5.18 Demonstration of Wave Propagation for the Illustrative Example

As shown in Figure 5.18, the dash green line represents the boundary between each time interval, in which the stochastic demand and capacity are generated; the red line represents the shock wave between different traffic states (i.e., II, III, and IV) due to the downstream stochastic capacities; and the blue line represents the boundary between stochastic demands and traffic states due to the downstream stochastic capacities. It should be noted that under the assumption of triangular flow-density model, only the shock waves between stochastic demand and capacities are useful for the travel time or vehicle delay estimation. Therefore, by investigating the above illustrative example, all the possible shock wave propagations are summarized and demonstrated in Figure 5.19.

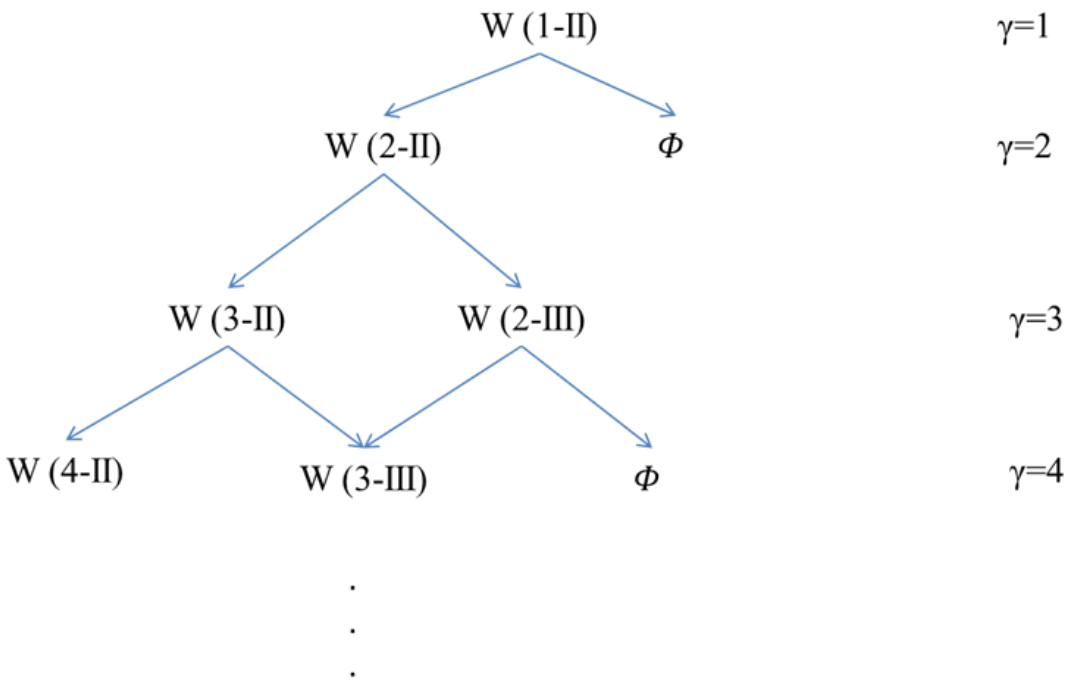

Figure 5.19 Summary of Shock Wave Propagation

Let's define a new variable, γ, which is the index of the γ^{th} shock wave between possible demand and capacity combination and we can find that:

$$\gamma = i + j - 2 \tag{5-12}$$

Where,

i = index of demand state (i=1, 2, 3…)

j = index of capacity state (j=II, III, IV…)

When $\gamma = 1$, it is clear that

$$W_{1-II}(t) = w_{1-II} * t \tag{5-13}$$

Where,

$W_{i-II}(t)$ = function of shock wave between traffic state *1* and *II* in term of time *t*

w_{1-II} = shock wave speed between traffic state *1* and *II*

When γ =*2*, it is clear that $W_{2-II}(t)$ is a function which passes the point (Δt, Δt* w_{1-II}) with slope w_{2-II}, where Δt is the time interval to generate stochastic demand and capacity (in this study, Δt=0.25 hour).

When γ=*2*, we need identify which wave state, W_{3-II} or W_{2-III}, will be applied for next. In order to doing this, we need calculate the intersection between $W_{2-II}(t)$ and the function of the red line shown in Figure 5.16, which is:

$$S(t) = w_c(t - \Delta t) \tag{5-14}$$

Where,

S(t) = the function of shock wave generated from the bottleneck

w_c = the wave speed

If the intersection point has a time value greater than 2Δt, the next wave state is W_{3-II}; otherwise it is W_{2-III}. If the next wave state is W_{3-II}, the corresponding wave function will pass the point (2Δt, $W_{2-II}(2\Delta t)$) with slope w_{3-II}; otherwise, the wave function will pass the intersection point with slope w_{2-III}.

Based on above discussion, the shock wave propagation within stochastic demand and capacity environment can be further generalized as follows:

For $\gamma = i + j - 2$

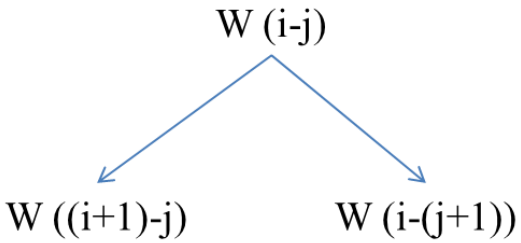

Where,

i = index of demand state (i=1, 2, 3…)

j = index of capacity state (j=II, III, IV…)

Since the time period of interest in this study is from 6:00 AM to 8:00 AM, the maximum of i is 8. Therefore, the termination condition of above shock wave propagation can be defined as:

(1) If $i > 8$, then stop.

(2) If $i+2 = j+1$, $W_{(i-(j+1))} = \Phi$

It is obvious that the maximum of $\gamma = i+j-2=8+9-2=15$.

From γ to $\gamma+1$, we need identify which wave state, $W_{((i+1)-j)}$ or $W_{(i-(j+1))}$, will be applied for next state. In order to doing this, we need calculate the intersection between $W_{(i-j)}(t)$ and the function of shock wave generated from the bottleneck, $S(t) = w_c(t - \Delta t(i-1))$. If the intersection point has a time value greater than $\Delta t * i$, the next shock wave state is $W_{((i+1)-j)}$; otherwise, it is $W_{(i-(j+1))}$. If the next shock wave state is

$W_{((i+1)-j)}$, the shock function will pass the point $(\Delta t*i, W_{(i-j)}(\Delta t*i))$ with slope $w_{((i+1)-j)}$; otherwise, the function will pass the intersection point with slope $w_{(i-(j+1))}$.

Conduct the above process until $i>8$, and the piecewise function of shock waves, $W(t)$, are obtained on the space-time plane based on stochastic demand and capacity. The number of pieces is equal to γ. Based on the function of shock waves, the vehicle delay can be calculated, which is discussed below.

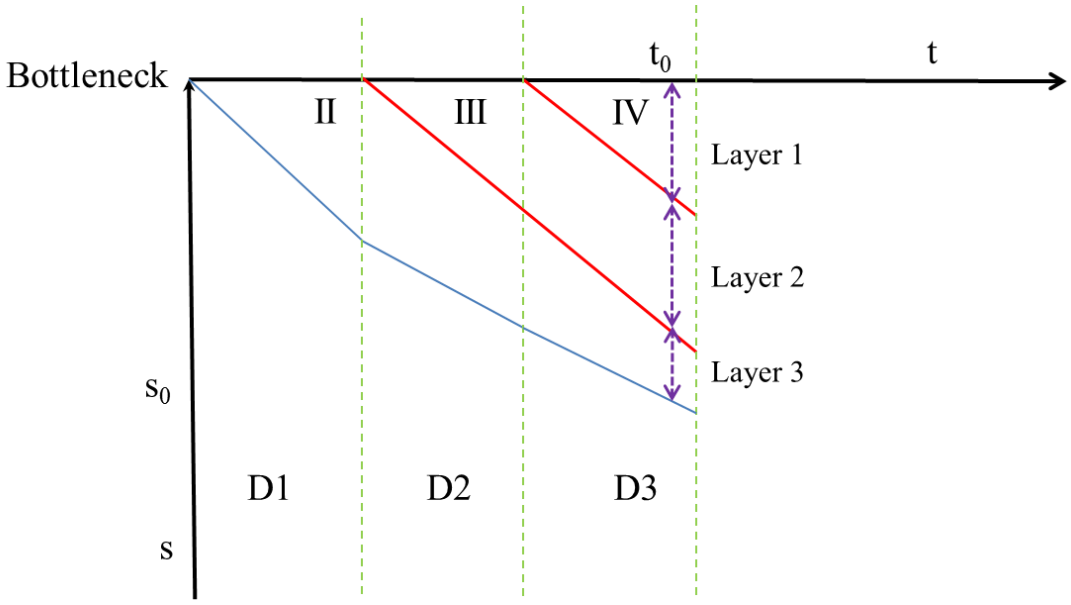

Figure 5.20 Illustrative Example of Vehicle Delay Calculation

Let's also start from an illustrative example to investigate how to calculate the vehicle delay based on a specific example. Assume the shock wave propagation in the time-space plane is shown in Figure 5.20.

Since we are already able to determine the shock wave function, at any time t_0, the state and the location (s_0) of shock wave are known. In order to calculate the average vehicle delay, it is necessary to identify how many traffic states (layers, in following discussion) are covered from the location s_0 to the point of bottleneck. As shown in Figure 5.20, there are three layers are covered at time t_0 and it is clear the shock wave function is $W_{(3-II)}$ (where, $i=3$ and $j=II$). It is also clear that at the third demand interval (i.e, $i=3$), the maximum number of layers is equal to 3. Therefore, it is easy to derive that if the shock wave function is $W_{(i-j)}$ at time t_0, the number of layer from s_0 to the point of bottleneck is equal to $i+2-j$.

Based on Figure 5.16, the height of the first layer (closest to the bottleneck, whose state is $i+1$), H_1, can be calculated as:

$$H_1 = w_c * (t - \Delta t(i-1)) \tag{5-15}$$

Where,

w_c = the wave speed of shock wave generated from the bottleneck

Similarly, the height of the second layer (whose state is i), H_2, can be calculated as:

$$H_2 = w_c * \Delta t \tag{5-16}$$

We also can derive that for the $(i+2-j)^{th}$ layer (whose sate is $(i+1)-(i+2-j)+1=j$), its height, H_s, can be calculated as:

$$H_s = |W(t)| - \sum_{s=1}^{i+1-j} H_s \tag{5-17}$$

Where,

s = index for the layers

As soon as the height of each layer is calculated at any time t_0, it can be proved that the total vehicle delay in the *dt* time is:

$$D(t) = \sum_s (H_s * K_s) * (\frac{1}{V_s} - \frac{1}{V_f}) \quad (5\text{-}18)$$

Where,

D(t) = total vehicle delay

K_s = density in the corresponding layer

V_s = vehicle speed in the corresponding layer

V_f = free flow vehicle speed (V_f =75 mph in this study*)*

In above equation, the density, K_s, and the vehicle speed, V_s, in different layers are fully determined by the values of stochastic capacities, since each layer corresponds to one traffic state (i.e., II, III or IV shown in Figure 5.18). The height of the layer at time *t* is determined by the speed of the shock waves between different layers. Especially for the last layer (i.e., layer 3 shown in Figure 5.18), the height of the layer at time *t* is determined by the speed of the shock wave between the stochastic demands and different traffic states due to the downstream stochastic capacities. Therefore, the total vehicle delay is fully determined by the stochastic demand and stochastic capacity, if freeway flow vehicle speed is assumed constant.

The total vehicle delay over certain time interval can be calculated as:

$$D = \int D(t)dt \quad (5\text{-}19)$$

Similarly, constant capacity value combined with the demand distribution will be applied first to demonstrate the travel time variability due to the traffic demand variance. The combination of stochastic capacity and demand will be evaluated subsequently. Again, a Monte Carlo simulation is performed to generate the stochastic capacity and demand based on the capacity/demand distributions calibrated above. Within the deterministic capacity environment, Figure 5.21 demonstrates the comparison between the simulated average link travel time and real-world average link travel time measured by Inrix for different time interval. Figure 5.22 shows the corresponding travel time standard deviation comparison.

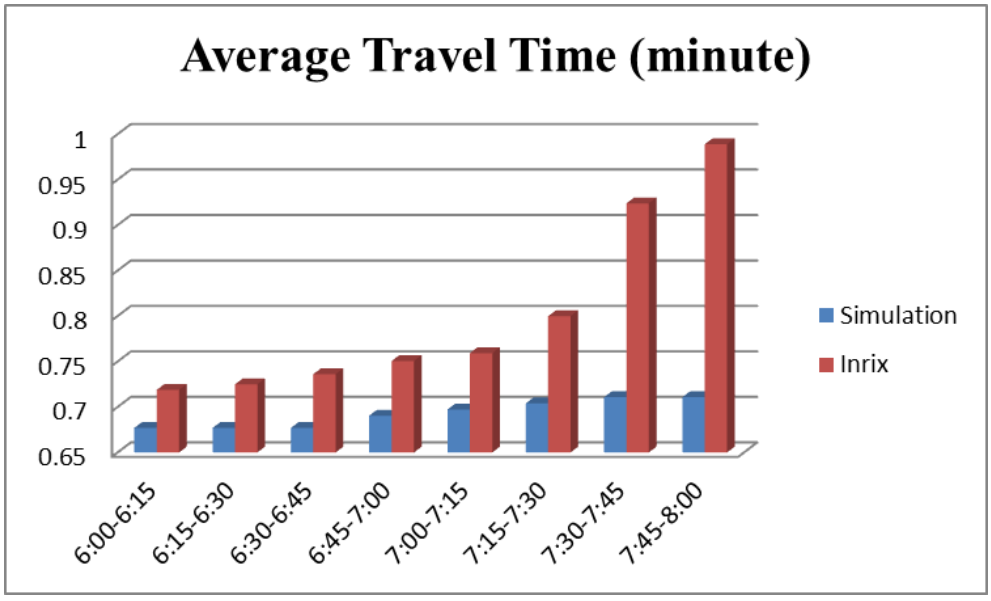

Figure 5.21 Average Travel Time: Shockwave Simulation vs. Inrix (Deterministic Capacity)

As shown in Figure 5.21, within the deterministic capacity environment, the simulated link travel time is systematically and significantly lower than the Inrix observations. Although the trend of travel time over different time periods is consistent with

the Inrix observation, the model in general significantly underestimate the delays for all time period. More importantly, as demonstrated in Figure 5.22, the simulated link travel time standard deviation is much lower than the real-world observations, although its performance is slightly better than the BPR function and queuing model during the peak period. In general, consistent with the results of BPR function and queuing model, it suggests that the demand variability does not explain the travel time variability observed in the field.

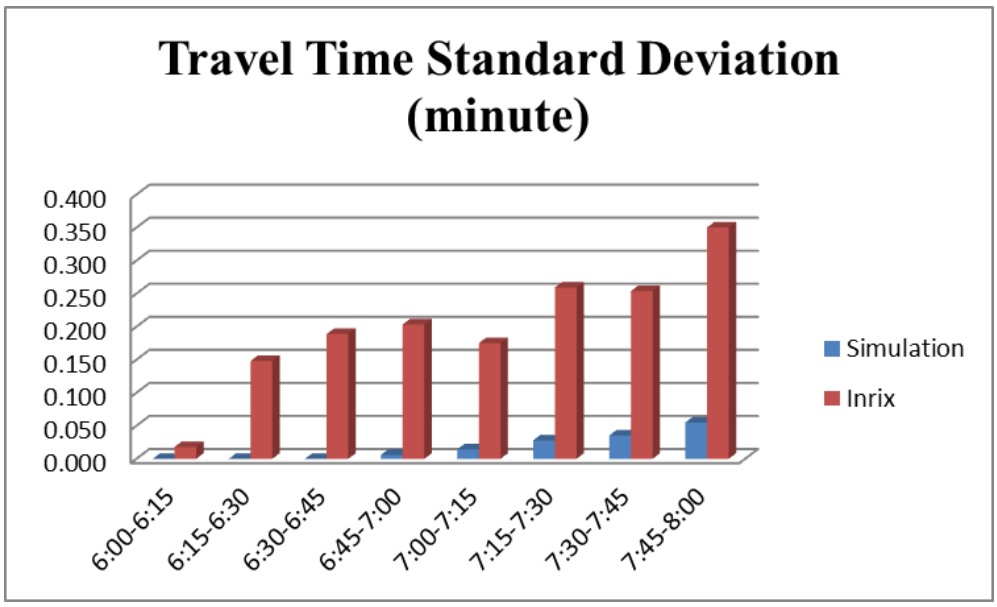

Figure 5.22 Travel Time Standard Deviation: Shockwave Simulation vs. Inrix (Deterministic Capacity)

Within stochastic capacity environment, Figure 5.23 demonstrates the comparison between the simulated average link travel time and real-world average link travel time measured by Inrix for different time intervals. Figure 5.24 shows the corresponding travel time standard deviation comparison.

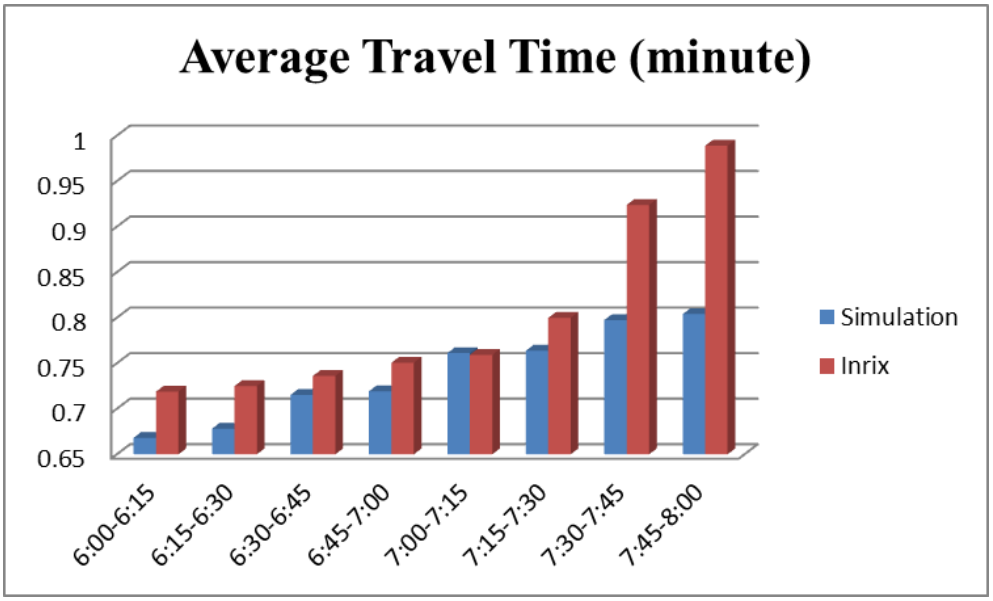

Figure 5.23 Average Travel Time: Shockwave Simulation vs. Inrix (Stochastic Capacity)

As shown in Figure 5.23, after introducing the stochastic capacity into the shockwave model, the simulated link travel time begins to get closer to the field travel time observations during the time period from 6:00 AM to 7:30 AM. During the time period 7:30 AM to 8:00 AM, the simulated link travel time is still lower than the Inrix observation; while its performance is better than both BPR function and queuing model. The underlying reason is that both vehicle queuing phenomenon and the queue spill-back phenomenon are modeled.

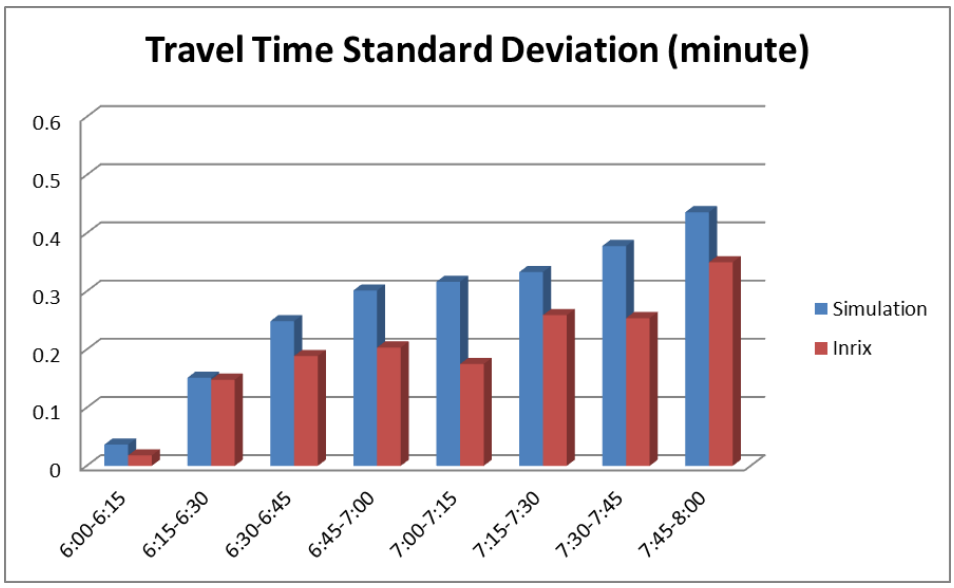

Figure 5.24 Travel Time Standard Deviation: Shockwave Simulation vs. Inrix (Stochastic Capacity)

In Figure 5.24, after introducing the stochastic capacity into the shock wave theory, variability of link travel time becomes closer to the field observation. Although the values of travel time standard deviation are still systematically higher than the Inrix observations, the performance is much better than the queuing model.

It is also of interest to compare the systemic performance measure of the differences between values predicted by above three models and the values actually observed. Table 5.2 summarizes the root-mean-square deviation (RMSD) of average travel time estimation of different models within both deterministic and stochastic capacity environment, and Table 5.3 summarizes the root-mean-square deviation (RMSD) of travel time standard deviation estimation of different models. The RMSD can be calculated as:

$$RMSD = \sqrt{\frac{1}{n}\sum_{i=1}^{n}(TT_i - TT_s)^2} \quad (5\text{-}20)$$

Where,

n= number of time interval

TT_i = travel time estimated by Inrix

TT_s = travel time estimated by different models

Table 5.2 The RMSD of Average Travel Time

RMSD	Deterministic Capacity			Stochastic Capacity		
	Overall	6:00-7:00	7:00-8:00	Overall	6:00-7:00	7:00-8:00
BPR Function	0.1346	0.0397	0.1862	0.1229	0.0297	0.1713
Queuing Model	0.1554	0.0569	0.2122	0.0910	0.0345	0.1240
Shock-Wave Model	0.1355	0.0528	0.1842	0.0849	0.0393	0.1134

As shown in Table 5.2, the models incorporated with stochastic capacity have better average travel time in general than their counterpart with deterministic capacity. Within the stochastic capacity environment, shock wave model provides the best estimation in terms of overall average travel time estimation. However, between 6:00 AM and 7:00AM, which represents the non-peak period, the BPR function provide the best estimation among three models; between 7:00 AM and 8:00 AM, which represents the peak period, the shock wave model provide the best estimation in terms of average travel time.

Table 5.3 The RMSD of Travel Time Standard Deviation

RMSD	Deterministic Capacity			Stochastic Capacity		
	Overall	6:00-7:00	7:00-8:00	Overall	6:00-7:00	7:00-8:00
BPR Function	0.2218	0.1525	0.2578	0.1545	0.0970	0.1957
Queuing Model	0.2098	0.1596	0.2406	0.1362	0.0916	0.1694
Shock-Wave Model	0.1972	0.1556	0.2315	0.0893	0.0583	0.1120

The results in Table 5.3 suggest that the stochastic capacity models will explain the travel time variability more accurately than the deterministic capacity models. Among the three different models, shock-wave model in general provides the best estimation in terms of travel time standard deviation.

5.4 Summary

In this chapter, the impact of the stochastic capacity on the roadway travel time prediction is evaluated on different analytical models and compared with the field observations. A 0.85-mile freeway link in Raleigh, North Carolina, is selected for the empirical study to evaluate the effectiveness of the travel time prediction functions derived from several different theories. Based on the sensor data downloaded from traffic.com, both stochastic demand and stochastic capacity were calibrated for the study site. It is found that the demand is a random variable with a generalized logistic distribution and strongly time-correlated between consecutive time intervals. The stochastic demand and stochastic capacity are applied on three different analytical models, namely BPR function, queuing theory and kinematic wave theory, to evaluate their impacts on travel time prediction. The

applications on the BPR function and queuing theory are really straightforward. The approach to apply the stochastic demand and stochastic capacity on the kinematic wave theory is developed in this chapter.

The prediction results were compared with the travel time observations from Inrix. With same demand level, the models incorporated with stochastic capacity result in better estimation of average travel time in general than their counterpart with deterministic capacity. Within the stochastic capacity environment, shock wave model provides the best estimation in terms of overall average travel time estimation. However, during the non-peak period, the BPR function provides the best estimation of average travel time among three models; during the peak period, the shock wave model provides the best estimation in terms of average travel time. Regarding the travel time variability, the models incorporated with stochastic capacity will explain the travel time variability more accurately than the one with deterministic capacity. Among the three different models, shock-wave model in general provides the best estimation in terms of travel time standard deviation.

6. SUMMARY, CONCLUSIONNS AND RECOMMENDATIONS

6.1 Summary

Many previous models, both travel demand and operational models, have tended to use deterministic capacity values for the formation and discharge of queues that are essentially equivalent to the *HCM* capacity levels. However, the current HCM freeway capacity definition does not adequately represent the true nature of flow breakdown and queue discharge capacity at freeway bottlenecks. Based on the empirical traffic data, the freeway breakdown phenomenon is stochastic, not deterministic. In other words, breakdown is a probabilistic event and can occur over a range of flow values.

While this study was focused on greater understanding of the stochastic nature of freeway onramp bottlenecks with a view toward providing a valid basis for stochastic modeling, the research yields an important finding for deterministic models as well. The statistical analysis and modeling for this research show that the *HCM* capacity levels are more representative of the upper tail of the breakdown and queue discharge observations (or conversely the lower limit of the pre-breakdown and queue discharge distributions). The expected or mean value of pre-breakdown flow and queue discharge at the freeway onramp bottleneck appears to be approximately 400 pc/h/ln lower than the *HCM*-based values. It should be acknowledged that the actual number could vary due to the assumption of the impacts of heavy vehicles. However, the implication of this finding is that many currently used network flow modeling platforms are likely to be under representing the frequency, duration, and therefore the traffic operational impact of freeway system bottlenecks. In

practice, the pre-breakdown and queue discharge models described herein can be integrated into macroscopic or mesoscopic simulation models to better characterize freeway stochastic properties, and to assist in identifying facilities that are vulnerable to breakdown.

Despite the limitations and simplifying assumptions contained within this study, all primary objectives of the research were satisfied. At the macro-level, most of the possible outliers of the pre-breakdown flow rate are screened out from the dataset used for the development of stochastic capacity and queue discharge model. At the micro-level, the underlying reason of stochastic capacity and queue discharge rate is investigated by studying the vehicle trajectory data. The shift between individual vehicle in terms of jam density and wave speed are also shown as stochastic instead of deterministic. Finally, the study demonstrates to what extent the stochastic capacity concept will impact the traditional traffic operational analysis. By incorporating the stochastic demand and capacity into several widely used travel time estimation models, their performance in terms of comparisons with field observations are evaluated.

In sum, the specific contributions of this study are listed as follows:

- A new method was developed to identify the bottleneck breakdown. Rather than using a single speed threshold, a combination of speed and density thresholds was proposed to identify the freeway breakdown conditions.
- A framework was developed to model stochastic bottleneck breakdown using an empirically fitted average pre-breakdown flow rate probability distribution.

- A recursive queue discharge model, which represents the stochastic, time-correlated nature of freeway bottleneck queue discharge, was developed.
- A connection was built between the stochastic capacity at macro-level and the heterogeneity of individual driving behaviors at micro-level.
- A theoretical approach was developed to account for the travel time variance introduced by stochastic capacity. This could be used in travel time reliability studies and route choice models for real-world application or DTA simulation in the future.

6.2 Conclusion

The following list provides the primary conclusion/contributions from the research:

- A combination of locally calibrated speed and density thresholds was found to more effectively identify the freeway breakdown conditions across all study sites than a single speed threshold;
- Breakdown at freeway onramp bottleneck is a probabilistic event and can occur over a range of flow values. The probability distributions of pre-breakdown flow rates at seven freeway onramp study sites were found to be well-modeled by a generalized logistic probability distribution;
- The queue discharge rate at freeway onramp bottleneck is a stochastic variable as well. Moreover, the queue discharge rate series are strongly time correlated and converge to the mean discharge rate for breakdowns that are initiated with stochastic pre-breakdown flow rate. The proposed recursive queue discharge model was found to be robust and effective based on the empirical validation results;

- At micro-level, the shift between individual vehicle in terms of jam density and wave speed was also found to be well-modeled by a random variable rather than deterministic value;
- It is reasonable to conclude that the heterogeneity of k_{jam} and w at the micro-level results from individual driving behavior. Since capacity is fully determined by the wave speed and jam density, the stochastic capacity and queue discharge rate observed in the field data (marco-level) are also generated by the heterogeneity between individual driving behaviors;
- Demand variability fails to explain the travel time variability observed in the field. After introducing the stochastic capacity into the traditional models, the variability of link travel time is modeled more accurately.

6.3 Recommendations

The research documented in this paper provides a solid foundation for continued refinement of the proposed methodology and extension to other types of bottlenecks. Future research will be dependent on the identification and assembly of extensive freeway bottleneck data sets. Recommendations for follow-on research include:

- Identification and analysis of additional factors that may influence the pre-breakdown headway distribution such as the number of travel lanes, heavy vehicle percentage, and driver population characteristics;

- The assumption of drivers' heterogeneity having no impact on the free-flow traffic condition should be released in future study. Further research should be conducted to study free-flow conations and nearly congested conditions;
- The assumption of simplified triangular traffic flow model should be released in future study. More realistic traffic flow model should be investigated in future.

Moreover, there are a couple of recommendations for practical application:

- When practitioners try to incorporate stochastic capacity and queue discharge into their traffic analysis, site-specific calibration is recommended to calibrate the parameters of the models;
- Shock-wave traffic model is strongly recommended for the roadway travel time study when the stochastic capacity and queue discharge are incorporated into the analysis.

7. REFERENCES

1. Cambridge Systematics. *Traffic Congestion and Reliability: Trends and Advanced Strategies for Congestion Mitigation.* Federal Highway Administration, 2005.
2. Ni D.H. Multiscale Modeling of Traffic Flow, Mathematica Aeterna, Vlo.1, 2011, no. 01, pp. 27-54
3. Peeta, S. and A. Ziliaskopoulos. Foundations of Dynamic Traffic Assignment: The Past, the Present, and the Future. *Networks and Spatial Economics*, Vol.1, 2001, pp. 233-265.
4. Mahmassani, H. S. Dynamic Network Traffic Assignment and Simulation Methodology for Advanced System Management Application. *Networks and Spatial Economics*, Vol. 1, 2001, pp. 267-292.
5. HCM, *Highway Capacity Manual*. Transportation Research Board, Washington D.C, 2000.
6. ELEFTERIADOU, L., ROESS, R.P. and MCSHANE, W.R. Probabilistic Nature of Breakdown at Freeway Merge Junctions. In *Transportation Research Record: Journal of the Transportation Research Board*, No. 1484, Transportation Research Board of the National Academies, Washington D.C., 1995.
7. MINDERHOUD, M.M., BOTMA, H. and BOVY, P.H.L. Roadway Capacity Estimation Methods Explained and Assessed. In *Transportation Research Record: Journal of the Transportation Research Board*, No. 1572, Transportation Research Board of the National Academies, Washington D.C., 1997.

8. PERSAUD, B., YAGAR, S. and BROWNLEE, R. Exploration of the Breakdown Phenomenon in Freeway Traffic. In *Transportation Research Record: Journal of the Transportation Research Board*, No. 1634, Transportation Research Board of the National Academies, Washington D.C., 1998.
9. KUEHNE, R.D. and ANSTETT, N. Stochastic Methods for Analysis of Traffic Pattern Formation. *Proceedings of the 14th International Symposium on Transportation and Traffic Theory*. Jerusalem, 1999.
10. LORENZ, M. and ELEFTERIADOU, L. A Probabilistic Approach to Defining Freeway Capacity and Breakdown. *Proceedings of the 4th International Symposium on Highway Capacity*, pp. 84-95. TRB-Circular E-C018, Transportation Research Board, Washington D.C, 2000.
11. OKAMURA, H., WATANABE, S. and WATANABE, T. An Empirical Study on the Capacity of Bottlenecks on the Basic Suburban Expressway Sections in Japan. *Proceedings of the 4th International Symposium on Highway Capacity*, pp. 120-129. TRB Circular E-C018, Transportation Research Board, Washington D.C, 2000.
12. CHEN, C.A., A. SKABARDONIS, P. VARAIYA. Systematic Identification of Freeway Bottlenecks," In *Transportation Research Record: Journal of the Transportation Research Board*, No. 1867, Transportation Research Board of the National Academies, Washington D.C., 2004.
13. ELEFTERIADOU, L. R.P. ROESS, W.R. MCSHANE "The Probabilistic Nature of Breakdown at Freeway Merge Junctions," In *Transportation Research Record: Journal*

of the Transportation Research Board, No. 1484, Transportation Research Board of the National Academies, Washington D.C., 1995.

14. Jia A., B.M. Williams and N.M. Rouphail. Identification and Calibration of Site Specific Stochastic Freeway Breakdown and Queue Discharge. In *Transportation Research Record: Journal of the Transportation Research Board*, in press, Transportation Research Board of the National Academies, Washington D.C., 2010.
15. Zurlinden, H. Ganzjahresanalyse des Verkehrsflusses auf Straben (Whole-Year-Analysis of Highway Traffic). Doctoral Thesis, Institute for Transportation and Traffic Engineering, Ruhr-University Bochum, No. 26. Bochum, 2003.
16. Brilon W., Geistefeldt, J. and Regler, M. Reliability of Freeway Traffic Flow: A Stochastic Concept of Capacity. *Proceedings of the 16th International Symposium on Transportation and Traffic Theory*. College Park, Maryland, 2005.
17. Brilon, W., Geistefeldt, J. AND Zurlinden, H. Implementing the Concept of Reliability for Highway Capacity Analysis, In *Transportation Research Record: Journal of the Transportation Research Board*, No. 2027, Transportation Research Board of the National Academies, Washington D.C., 2007.
18. Dong, J. and Mahmassani, H.S. Flow Breakdown and Travel Time Reliability. Forthcoming in *Transportation Research Record: Journal of the Transportation Research Board*, 2009.

19. DONG, J. and MAHMASSANI, H.S. Flow Breakdown, Travel Reliability and Real-time Information in Route Choice Behavior. Forthcoming in *the proceedings of the 18th International Symposium on Transportation and Traffic Theory*, 2009.
20. Yang, H., H.J. Huang. The multi-class, multi-criteria traffic network equilibrium and system optimum problem. Transportation Research, Part B, Vol. 38, 2004, pp. 1-15.
21. Hu,T. and Mahmassani, H. S. Day-to-Day Evolution of Network Flows under Real-time Information and Reactive Signal Control, *Transportation Research, Part C*, Vol. 5, No. 1, 1997, pp. 51-69.
22. Shrinivasan K.K., and Guo Z. Day-to-Day Evolution of Network Flows Under Route Choice Dynamics In Commuter Decisions. In *Transportation Research Record: Journal of the Transportation Research Board*, No. 1894, Transportation Research Board of the National Academies, Washington D.C., 2004, pp. 198-208.
23. Jha, M., Madanat S., and Peeta, S. Perception Updating and Day-to-Day Travel Choice Dynamics in Traffic Networks with Information Provision. *Transportation Research, Part C*, Vol. 6, No. 3, 1998, pp. 189-212.
24. Chen, R. B., and H. S. Mahmassani. Travel Time Perception and Learning Mechanisms in Traffic Networks. In *Transportation Research Record: Journal of the Transportation Research Board*, No. 1894, Transportation Research Board of the National Academies, Washington D.C., 2004, pp. 209-221.

25. Brownstone, D., and Small, K.A. Valuing Time and Reliability: Assessing the Evidence from Road Pricing Demonstrations. *Transportation Research, Part A*, Vol. 39, 2004, pp. 279–293.
26. Lam, T., and Small, K.A. The Value of Time and Reliability: Measurement from A Value Pricing Experiment. *Transportation Research Part E*, Vol. 37, 2001, pp. 231–251.
27. Mahmassani, H.S. and Herman, R. Interactive Experiments for the Study of Trip maker Behaviour Dynamics in Congested Commuting Systems. in Jones, P. (ed.) *Developments in Dynamic and Activity-Based Approaches to Travel Analysis*, Gower, Aldershot, England, 1990, pp. 272-298.
28. Simon, H. A. A Behavioral Model of Rational Choice. *Quarterly Journal of Economics,* Vol. 69, 1955, pp. 99–118.
29. Daganzo, C., and Sheffi, Y., 1977. On stochastic models of traffic assignment. Transportation Science, 253-274
30. Horowitz, J., 1984. The stability of stochastic equilibrium in a two-link transportation network. Transportation Research B 18(1), 13-28.
31. Mahmassani, H., Chang, G., 1986. Experiments with departure time choice dynamics of urban commuters. Transportation Research B 20(4), 297-320.
32. Lo, H.K. and Tung, Y.K., Network with degradable links: capacity analysis and design, Transportation Research Part B 37 (4), 2003, pp. 345–363.
33. Clark, S.D., Watling, D.P., Modelling network travel time reliability under stochastic demand. Transportation Research Part B 39 (2), 2005, 119–140.

34. Ng, M.W., Waler, S.T., A computationally efficient methodology to characterize travel time reliability using the fast Fourier transform, Transportation Research Part B: Methodological. 2010.
35. Zhou, X., Rouphail, N.M., and Li, M., Analytical Models for Quantifying Travel Time Variability Based on Stochastic Capacity and Demand Distribution, TRB 90th Annual Meeting, Compendium of Papers CD-ROM, January 2011.
36. TRANSGUIDE, http://www.transguide.dot.state.tx.us/ Accessed January 6, 2009
37. PeMS, https://pems.eecs.berkeley.edu/?redirect=%2F%2F%3Fdnode%3DState Accessed January 18, 2009
38. Snedecor, George W. and Cochran, William G. Statistical Methods, Eighth Edition, Iowa State University Press, 1989.
39. NIST/SEMATECH, "e-Handbook of Statistical Methods," 2005.
40. CHAKRAVARTI, LAHA, and ROY. Handbook of Methods of Applied Statistics, Volume I, John Wiley and Sons, 1967, pp. 392-394.
41. Next Generation Simulation (NGSIM), http://ngsim-community.org, Accessed June 2012.
42. US Department of Transportation, FHWA, 2008b. Interstate 80 Freeway Dataset. <http://www.tfhrc.gov/about/06137.htm> .
43. Newell, G.F., A simplified car-following theory: a lower order model, Transportation Research Part B 36(3), 195-205, 2002.

44. Brockfeld, E., Kuhne, R., Wagner, P., Calibration and validation of microscopic models of traffic flow. Transportation Research Record: Journal of the Transportation Research Board 1934, 179-187, 2005.
45. Ossen, S., and Hoogendoorn, S.P., Validity of trajectory-based calibration approach of car-following models in the presence of measurement errors, Transportation Research Record: Journal of the Transportation Research Board 2088, 2008, pp.117–125.
46. Coifman, b.A., Wang, Y., Average velocity of waves propagating through congested freeway traffic, 16th international Symposium on Transportation and Traffic Theory, Elsevier, MD, USA, pp. 165-179, 2005.
47. Windover, J.R., and Cassidy, M.J., Some observed details of freeway traffic evolution, Transportation Research Part A 35(10), pp 881-894, 2001.
48. Chiabaut, N., Buisson, C., and Leclercq, L., Fundamental diagram estimation through passing rate measurements in congestion, IEEE Transactions on Intelligent Transportation Systems 10(2), pp.355-359, 2009.
49. Chiabaut, N., Leclercq, L., and Buisson, C., Form heterogeneous drivers to macroscopic patterns in congestion, Transpiration Research Part B 44, pp. 299-308, 2010.
50. Traffic.com, http://stakeholder.traffic.com/mainmenu/stakeholder/index.html, accessed May, 2012.
51. Inrix, https://www.ritis.org/ accessed May, 2012
52. Adolf D. May, Traffic Flow Fundamentals, Prentice Hall, Englewood Cliffs, New Jersey 07632, ISBN 0-13-926072-2

53. Bureau of Public Roads (1964). Traffic Assignment Manual. U.S. Dept. of Commerce, Urban Planning Division, Washington D.C.

54. Singh, R., and R. Dowling, Improved Speed-Flow Relationships: Application to Transportation Planning Models. Proc., 7th TRB Conference on the Application of Transportation Planning Methods, TRB, National Research Council, Washington, D.C., 2002, pp. 340-349.

55. Huntsinger L. F., and N.M. Rouphail, Bottleneck and Queuing Analysis: Calibrating Volume-Delay Functions of Travel Demand Models, Transportation Research Record: Journal of the Transportation Research Board 2255, 117-124, 2011.

APPENDICES

APPENDIX A: CANDIDATE STUDY SITES

Candidate Study Sites in Bay Area (Count: 37)

Roadway	Type	Name	Direction	# Lane	Distance to Downstream (KM)
I880	On-Ramp	Fremont Blvd.	S	4	9.1
	On-Ramp	Thornton Ave.	S	4	4.4
	On-Ramp	Alvarado-Fremont Blvd.	S	4	0.9
	On-Ramp	Alvarado-Niles Rd	S	4	0.9
	On-Ramp	2400' S of Alvarado niles Rd	S	4	2.7
	On-Ramp	Industrial Parkway	S	4	6.4
	Weaving	West A St.	S	5	N.A
	Weaving	SB 101 To NB 880	N	4	35.4
	On-Ramp	Tennyson Rd.	N	4	12.1
	Weaving	Marina Blvd /Davis St.-1	N	4	7.6
	On-Ramp	42nd / High St.	N	4	0.9
	Weaving	29th Ave.	N	4	0.7
	Weaving	23rd Ave	N	4	N.A
I80	On-Ramp	University Ave	W	5	2.4
	On-Ramp	West of Gilman St rm-w-diag	W	5	3.1
	On-Ramp	Carlson Blvd	W	4	5.7
	Weaving	San Pablo Dam Rd	W	4	0.8
	Weaving	800' E of San Pablo Dam Rd	W	4	1.6
	Weaving	El Portal Dr	W	4	4.8
	Weaving	Pinole Valley Rd	W	4	N.A
	On-Ramp	Ashby Ave	E	5	1.6

	On-Ramp	University Ave	E	5	N.A
I780	Weaving	780 on ramp from 5th street	E	2	N.A
I680	On-Ramp	Livorna Rd	S	4	6.6
	Lane Drop	Geary Rd/Treat Blvd	S	6 to 5	N.A
	Weaving	Sycamore Valley Rd	N	4	1.8
	On-Ramp	El Cerro Blvd	N	4	0.7
	On-Ramp	El Cerro Blvd	N	4	6.1
	Weaving	Rudgear Rd	N	4	N.A
I580	On-Ramp	Airway Blvd	W	4	6.0
	On-Ramp	Hacienda Dr. rm-w-diag	W	5	34.4
	Weaving	NB Macarthur Blv	W	4	4.0
	On-Ramp	Beaumont Ave/Park Blvd-1	W	4	N.A
	Lane Drop	Lane Drop	E	5 to 4	N.A
I280	On-Ramp	N of Mclaughlin ave	N	5	8.9
	Weaving	Bascom & Leland	N	5	1.2
	On-Ramp	400 ft S of 280/17/880 IC	N	4	N.A

Candidate Sites in San Antonio Area (Count: 53)

Roadway	Type	Location	Direction	# Lane	Distance to Downstream (KM)
US90	On-Ramp	Junction 1604	E	2	3.8
	On-Ramp	Junction 410	E	2	3.7
	On-Ramp	New Life Circle	E	3	2.1
	On-Ramp	Junction to S Callaghan Rd	E	3	2.4

	On-Ramp	Junction to SW 36th St	E	5	2.7
	On-Ramp	Brady Blvd	E	5	>5
	On-Ramp	S General McMullen Dr	W	5	3.1
	Weaving	Junction to S Acme Rd	W	4	2.3
	On-Ramp	New life Circle	W	3	3.9
	On-Ramp	Junction 410	W	2	1
IH10	On-Ramp	Not available	E	2	1
	On-Ramp	Not available	E	2	6.6
	On-Ramp	La Cantera Pkwy	E	2	0.8
	On-Ramp	Nina Louise Dr	E	2	1.9
	On-Ramp	Junction 1604	E	2	2.2
	On-Ramp	De Zavala Rd	E	2	2.5
	On-Ramp	Huebner Rd	E	2	0.7
	On-Ramp	Expo Blvd	E	2	1.5
	On-Ramp	Wurzbach Rd	E	2	1.8
	On-Ramp	Fountain Circle	E	2	0.7
	On-Ramp	Colonies North Mall	W	2	2.3
	On-Ramp	Junction (Huebner Rd)	W	2	0.9
	On-Ramp	Not available	W	2	1.4
	On-Ramp	Junction (De Zavala Rd)	W	2	1.5
	On-Ramp	Junction (Utsa Blvd)	W	2	0.9
IH37	On-Ramp	Donop Rd	N	2	6
	On-Ramp	Junction (410)	N	2	2.8
	On-Ramp	SE Military Dr	N	2	1.7
	On-Ramp	Not available	S	2	1.2

	On-Ramp	Pecan Valley Dr	S	2	2
	On-Ramp	SE Military Dr	S	2	2.8
	On-Ramp	Junction 410	S	2	2.7
	On-Ramp	Not available	S	2	7.7
IH35	On-Ramp	Junction US281	N	4	1.9
	On-Ramp	N Walters St	N	3	0.7
	On-Ramp	Exit 159B	N	3	2
	On-Ramp	Shipman Dr	N	3	3.2
	On-Ramp	Not available	N	3	2
	On-Ramp	Exit 164 A	N	3	1.6
IH35	On-Ramp	N Panam Expy	N	3	1.5
	On-Ramp	Walzem Rd	N	3	2.8
	Weaving	Exit 158	N	4	1.3
	Weaving	Tech Com Rd	N	4	1.2
	Weaving	Exit 170A	N	4	2.3
	On-Ramp	Toeppenwein Rd	S	3	1.7
	On-Ramp	Judson Rd	S	3	1.6
	Weaving	Exit 168	S	4	1.2
	Weaving	Exit 167B	S	4	3.5
	On-Ramp	Walzem Rd	S	3	0.5
	On-Ramp	Not available	S	3	1.4
	On-Ramp	164B	S	3	1.4
	On-Ramp	164A	S	3	2.5
	On-Ramp	Brooke Army Medical Center	S	3	0.8

APPENDIX B: FLOW-SPEED CURVES OF STUDY SITES

Site 1

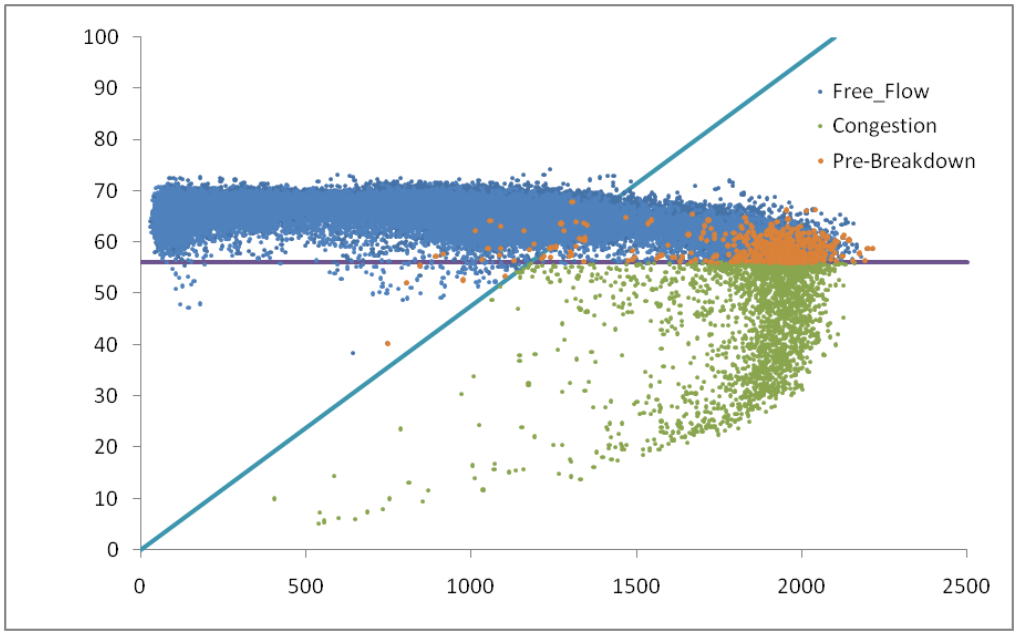

Site 2

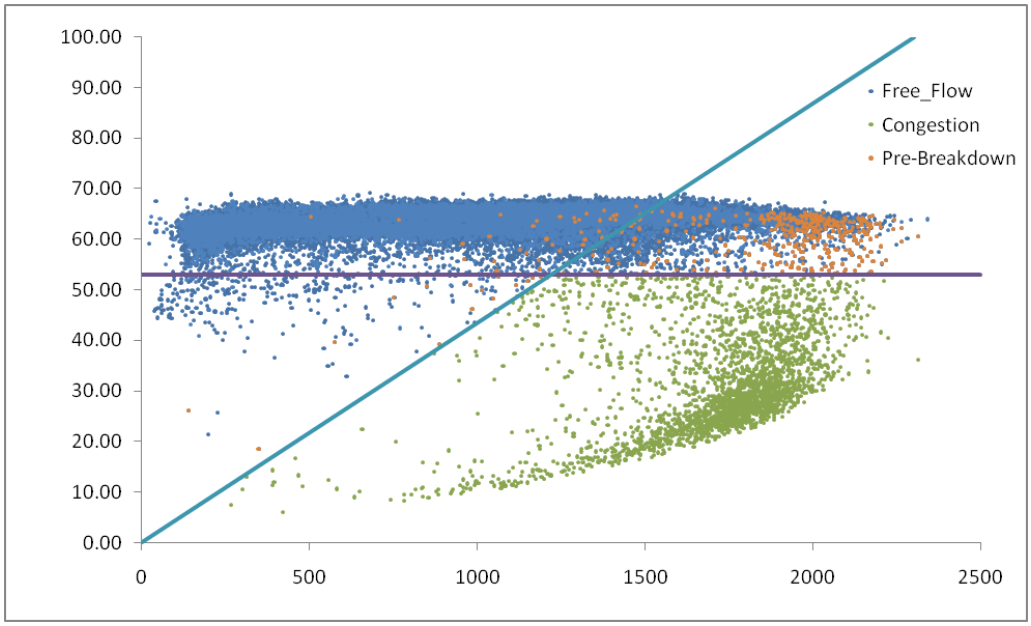

Site 4

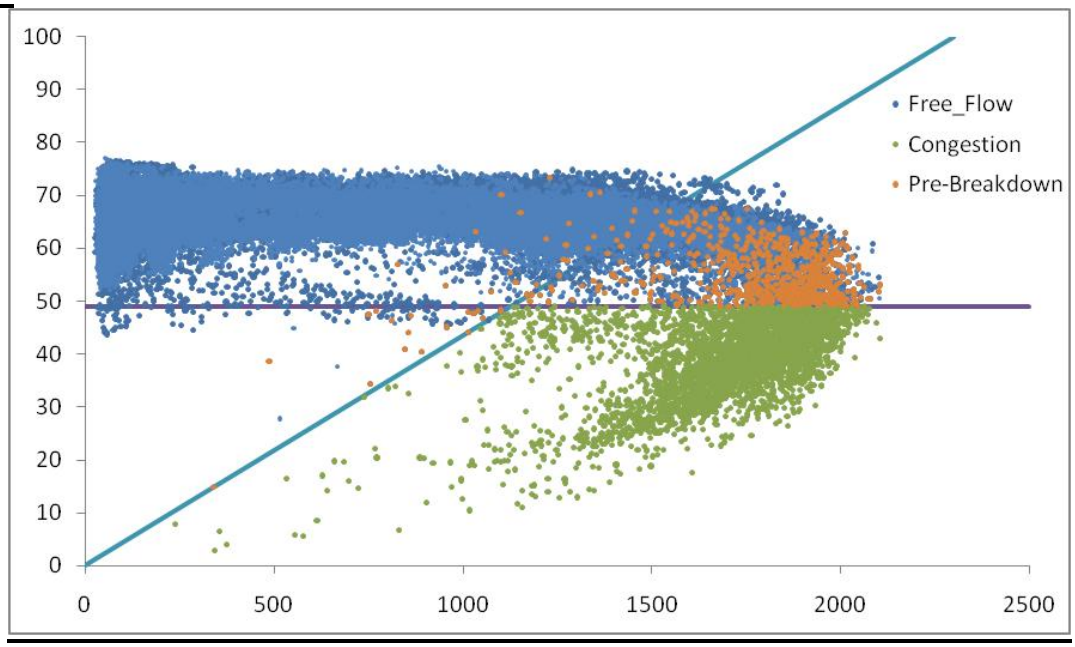
100
90
80
70
60
50
40
30
20
10
0
0
500
1000
1500
2000
2500
Free_Flow
Congestion
Pre-Breakdown

Site 5

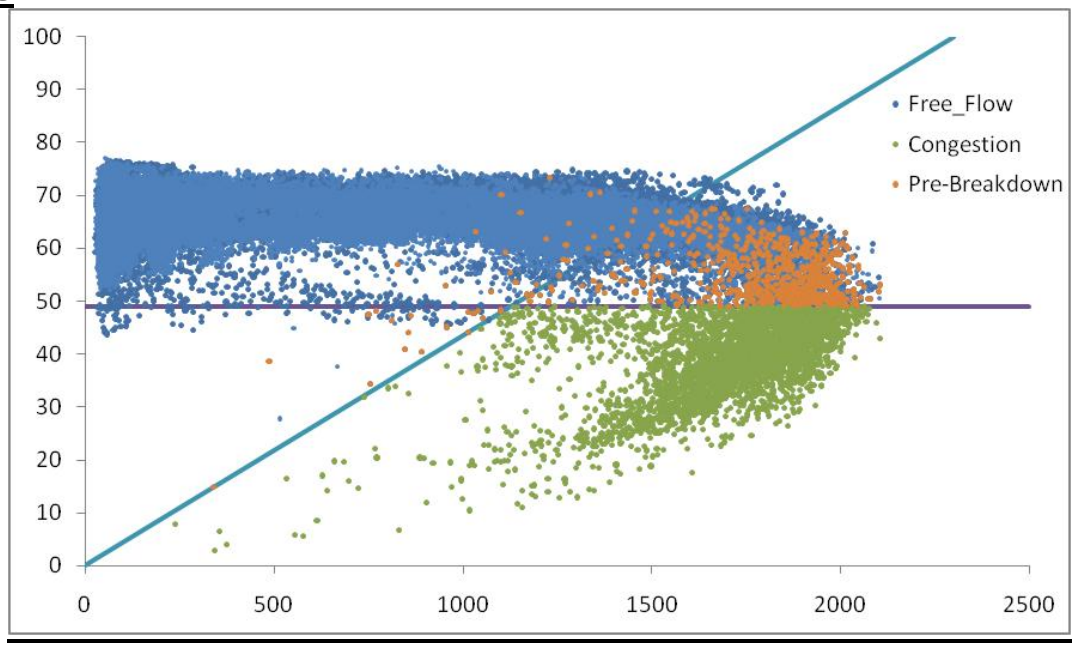
100
90
80
70
60
50
40
30
20
10
0
0
500
1000
1500
2000
2500
Free_Flow
Congestion
Pre-Breakdown

Site 6

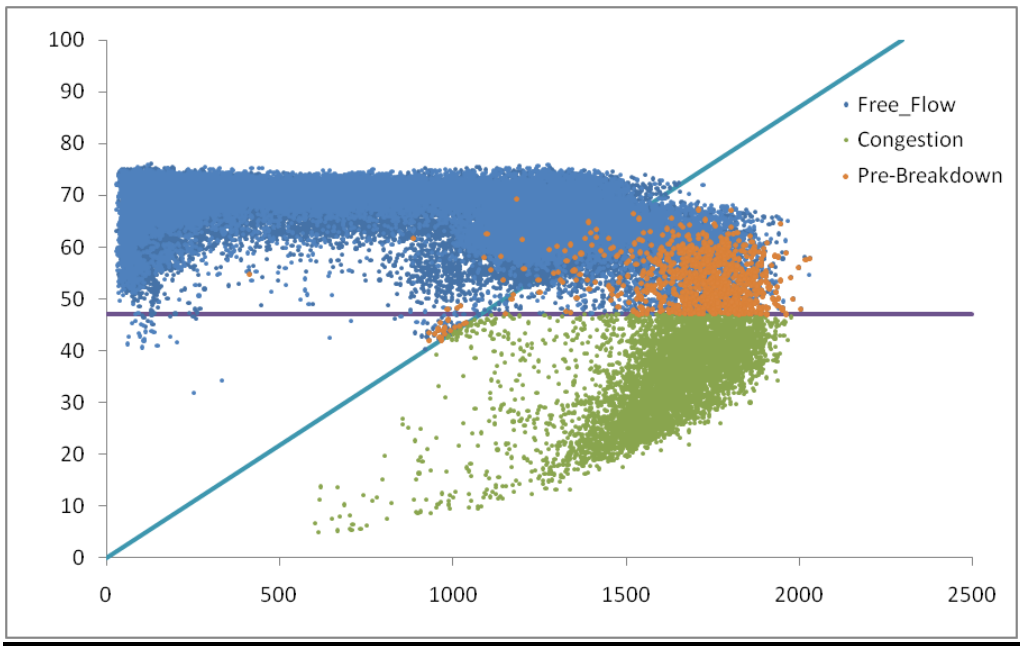
100
90
80
70
60
50
40
30
20
10
0
0
500
1000
1500
2000
2500
Free_Flow
Congestion
Pre-Breakdown

Site 7

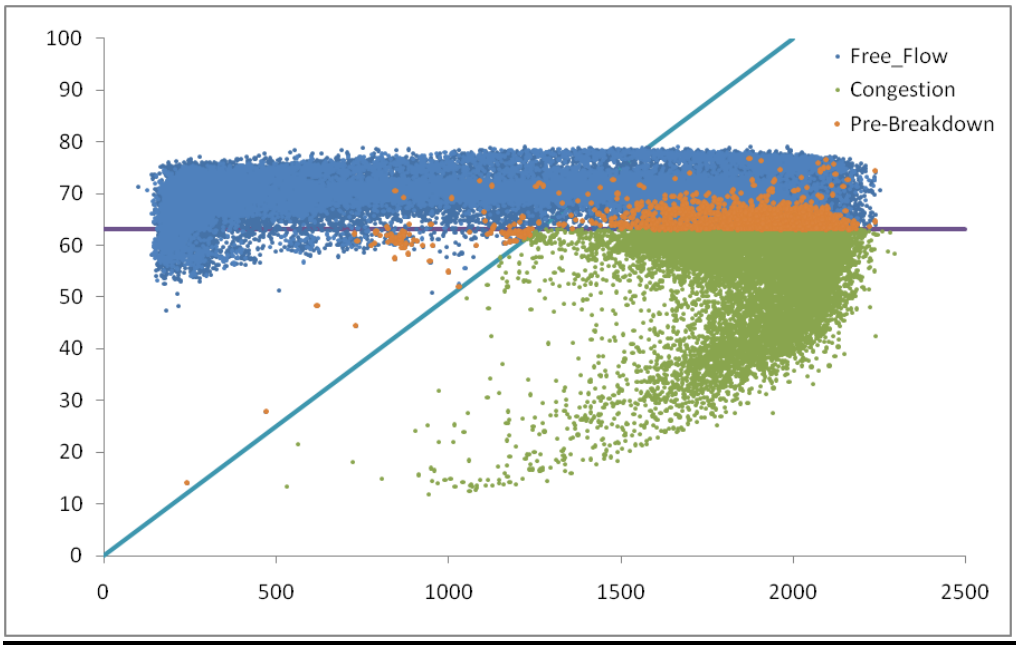
100
90
80
70
60
50
40
30
20
10
0
0
500
1000
1500
2000
2500
Free_Flow
Congestion
Pre-Breakdown

APPENDIX C: GOODNESS OF FIT OF THE CAPACITIES

Goodness of Fit – Summary for Site 1

#	Distribution	Kolmogorov Smirnov		Anderson Darling		Chi-Squared	
		Statistic	Rank	Statistic	Rank	Statistic	Rank
24	Gen. Logistic	0.03136	3	0.45835	1	6.4828	1
2	Burr	0.03443	4	0.55651	2	7.605	2
11	Error	0.04001	7	1.0072	5	8.4697	3
31	Johnson SU	0.03786	5	0.73189	3	8.4721	4
38	Log-Logistic (3P)	0.03036	2	0.82577	4	9.3159	5
28	Hypersecant	0.03947	6	1.1814	7	9.4168	6
4	Cauchy	0.07096	35	4.7215	34	11.04	7
40	Logistic	0.04263	8	1.0809	6	11.513	8
33	Laplace	0.05616	17	2.4848	22	15.152	9
43	Nakagami	0.05802	20	2.1107	15	15.861	10
30	Inv. Gaussian (3P)	0.05806	21	2.0792	14	16.979	11
19	Gamma	0.06158	24	2.4126	19	17.303	12
37	Log-Logistic	0.05699	19	1.9109	10	17.961	13
16	Fatigue Life (3P)	0.05532	15	1.959	12	18.069	14
6	Chi-Squared (2P)	0.06015	22	2.2811	17	18.123	15
44	Normal	0.05632	18	1.9992	13	19.069	16
42	Lognormal (3P)	0.05233	10	2.1889	16	19.244	17
39	Log-Pearson 3	0.05302	12	1.4378	8	19.556	18
22	Gen. Gamma	0.06215	25	2.4726	20	20.136	19
29	Inv. Gaussian	0.05569	16	2.3936	18	20.961	20
10	Erlang (3P)	0.05528	14	2.4797	21	21.912	21
15	Fatigue Life	0.06529	28	2.7709	27	22.788	22
41	Lognormal	0.0652	27	2.7633	26	22.789	23
63	Weibull	0.0731	36	3.3795	32	23.434	24
36	Log-Gamma	0.066	29	2.8443	28	23.726	25
64	Weibull (3P)	0.05287	11	1.8801	9	24.089	26
20	Gamma (3P)	0.06603	30	2.8738	29	24.774	27
9	Erlang	0.0669	31	2.6732	23	25.175	28
32	Kumaraswamy	0.05164	9	1.9447	11	26.131	29
23	Gen. Gamma (4P)	0.06701	32	2.7267	24	26.37	30

27	Gumbel Min	0.08161	38	5.2237	35	27.477	31
49	Pearson 6	0.06811	33	3.0161	30	28.311	32
47	Pearson 5	0.06829	34	3.083	31	29.396	33
1	Beta	0.06488	26	5.3767	36	29.511	34
48	Pearson 5 (3P)	0.07551	37	3.6576	33	32.918	35
50	Pearson 6 (4P)	0.06067	23	2.7441	25	33.949	36
26	Gumbel Max	0.11473	45	17.135	42	48.576	37
5	Chi-Squared	0.08298	39	14.012	38	55.63	38
17	Frechet	0.13403	47	17.871	43	71.178	39
51	Pert	0.10393	42	14.859	39	95.452	40
60	Triangular	0.10424	43	16.373	41	108.45	41
18	Frechet (3P)	0.11392	44	15.796	40	126.85	42
56	Rayleigh (2P)	0.24167	48	50.178	46	268.69	43
54	Power Function	0.27105	50	64.1	47	417.61	44
57	Reciprocal	0.25851	49	68.467	48	498.25	45
14	Exponential (2P)	0.36341	51	119.58	51	926.33	46
45	Pareto	0.37424	52	126.12	52	998.77	47
35	Levy (2P)	0.51123	54	160.5	53	1786.0	48
55	Rayleigh	0.45259	53	167.34	54	4237.1	49
7	Dagum	0.61517	59	246.8	58	7717.2	50
46	Pareto 2	0.54382	56	199.62	55	8944.3	51
13	Exponential	0.5755	57	215.07	57	8947.8	52
34	Levy	0.65119	60	256.74	60	13886.0	53
59	Student's t	1.0	62	7557.5	61	1.3192E+10	54
3	Burr (4P)	0.52987	55	201.26	56	N/A	
8	Dagum (4P)	0.61044	58	255.66	59	N/A	
12	Error Function	1	63	N/A		N/A	
21	Gen. Extreme Value	0.05343	13	21.429	45	N/A	
25	Gen. Pareto	0.09482	40	108.58	49	N/A	
52	Phased Bi-Exponential	1	64	N/A		N/A	
53	Phased Bi-Weibull	0.11676	46	13.313	37	N/A	
58	Rice	0.99614	61	13184.0	62	N/A	
61	Uniform	0.10373	41	110.28	50	N/A	
62	Wakeby	0.02308	1	20.02	44	N/A	
65	Johnson SB	No fit					

Goodness of Fit – Summary for Site 2

#	Distribution	Kolmogorov Smirnov		Anderson Darling		Chi-Squared	
		Statistic	Rank	Statistic	Rank	Statistic	Rank
64	Weibull (3P)	0.01958	1	1.4799	2	16.848	3
24	Gen. Logistic	0.02205	2	0.48162	1	10.028	1
62	Wakeby	0.02546	3	71.966	38	N/A	
32	Kumaraswamy	0.02792	4	1.8544	3	15.786	2
31	Johnson SB	0.0344	5	44.063	23	N/A	
27	Gumbel Min	0.03867	6	4.99	5	33.428	4
2	Burr	0.03938	7	4.8212	4	35.05	5
21	Gen. Extreme Value	0.04369	8	176.65	44	N/A	
1	Beta	0.05129	9	6.6871	6	45.269	6
38	Log-Logistic (3P)	0.06372	10	16.364	7	137.69	8
63	Weibull	0.07121	11	18.804	8	129.04	7
39	Log-Pearson 3	0.08567	12	466.16	52	N/A	
28	Hypersecant	0.09777	13	28.753	9	177.21	9
40	Logistic	0.10082	14	28.91	10	196.89	11
30	Inv. Gaussian (3P)	0.10493	15	34.701	14	233.76	15
43	Nakagami	0.10651	16	35.096	17	199.88	12
29	Inv. Gaussian	0.10667	17	40.615	20	277.17	22
44	Normal	0.10688	18	34.856	15	228.39	14
16	Fatigue Life (3P)	0.10715	19	34.858	16	226.17	13
4	Cauchy	0.11002	20	29.859	11	192.43	10
6	Chi-Squared (2P)	0.11126	21	37.274	18	241.98	18
42	Lognormal (3P)	0.1133	22	39.4	19	268.02	21
25	Gen. Pareto	0.11346	23	553.5	56	N/A	
53	Phased Bi-Weibull	0.11387	24	82.429	39	N/A	
50	Pearson 6 (4P)	0.11512	25	48.579	28	369.82	33
19	Gamma	0.11774	26	42.072	21	262.88	19
10	Erlang (3P)	0.12041	27	44.351	24	310.21	25
9	Erlang	0.12073	28	43.264	22	267.06	20
11	Error	0.12075	29	34.509	12	238.84	16
33	Laplace	0.12075	30	34.509	13	238.84	17
22	Gen. Gamma	0.12208	31	45.627	25	308.91	24

23	Gen. Gamma (4P)	0.12567	32	45.831	26	301.44	23
48	Pearson 5 (3P)	0.12662	33	47.013	27	319.6	27
51	Pert	0.12718	34	53.561	35	344.38	29
37	Log-Logistic	0.12783	35	49.425	31	368.96	32
41	Lognormal	0.12958	36	51.943	32	367.36	30
15	Fatigue Life	0.13089	37	52.687	33	368.36	31
36	Log-Gamma	0.13114	38	53.043	34	375.92	34
20	Gamma (3P)	0.13248	39	48.867	29	310.69	26
61	Uniform	0.1339	40	377.54	47	N/A	
49	Pearson 6	0.13621	41	57.283	36	399.18	35
58	Rice	0.13654	42	49.095	30	323.36	28
47	Pearson 5	0.13755	43	59.012	37	414.25	36
26	Gumbel Max	0.17443	44	133.77	41	456.19	37
17	Frechet	0.20827	45	136.85	42	813.0	40
54	Power Function	0.21279	46	118.4	40	778.13	39
60	Triangular	0.25193	47	156.11	43	527.15	38
5	Chi-Squared	0.25321	48	523.48	55	1517.5	41
18	Frechet (3P)	0.26436	49	270.97	46	N/A	
56	Rayleigh (2P)	0.32334	50	264.28	45	1907.0	42
55	Rayleigh	0.38133	51	405.51	48	7011.1	48
3	Burr (4P)	0.41652	52	411.85	49	4380.7	46
14	Exponential (2P)	0.41909	53	418.13	50	4353.2	45
45	Pareto	0.44276	54	454.32	51	3843.2	44
46	Pareto 2	0.48738	55	517.51	54	15335.0	52
57	Reciprocal	0.49503	56	624.34	58	2383.5	43
13	Exponential	0.52272	57	563.55	57	15175.0	51
35	Levy (2P)	0.56329	58	509.31	53	8192.6	49
34	Levy	0.6472	59	688.99	59	23772.0	53
8	Dagum (4P)	0.69085	60	1435.8	60	4865.4	47
7	Dagum	0.78118	61	1784.2	61	9187.1	50
52	Phased Bi-Exponential	1.0	62	50884.0	63	1.2819E+9	54
59	Student's t	1.0	63	21139.0	62	1.6453E+10	55
12	Error Function	1	64	N/A		N/A	
65	Johnson SU	No fit					

Goodness of Fit – Summary for Site 3

#	Distribution	Kolmogorov Smirnov		Anderson Darling		Chi-Squared	
		Statistic	Rank	Statistic	Rank	Statistic	Rank
64	Weibull (3P)	0.02829	1	0.55699	2	8.6482	1
24	Gen. Logistic	0.03067	2	0.46321	1	12.76	3
32	Kumaraswamy	0.03514	3	0.65163	3	9.4379	2
2	Burr	0.03556	4	1.491	5	15.864	4
31	Johnson SB	0.04082	5	9.5875	9	N/A	
62	Wakeby	0.04549	6	28.417	36	N/A	
27	Gumbel Min	0.04568	7	1.2533	4	16.511	5
21	Gen. Extreme Value	0.04866	8	85.216	44	N/A	
39	Log-Pearson 3	0.05583	9	132.7	46	N/A	
38	Log-Logistic (3P)	0.05879	10	6.2419	7	48.352	8
63	Weibull	0.06603	11	4.915	6	36.365	6
1	Beta	0.0859	12	9.2815	8	41.63	7
42	Lognormal (3P)	0.08596	13	12.469	13	82.54	15
40	Logistic	0.09363	14	10.663	10	83.3	16
16	Fatigue Life (3P)	0.09364	15	12.418	12	77.505	9
30	Inv. Gaussian (3P)	0.09529	16	12.704	14	82.055	13
29	Inv. Gaussian	0.09689	17	14.846	21	95.516	22
44	Normal	0.09702	18	12.829	15	78.902	10
43	Nakagami	0.09796	19	13.137	16	80.407	11
6	Chi-Squared (2P)	0.0999	20	13.675	18	82.395	14
28	Hypersecant	0.10189	21	10.854	11	81.307	12
10	Erlang (3P)	0.10648	22	15.407	23	95.26	21
19	Gamma	0.10652	23	15.375	22	96.616	23
9	Erlang	0.10832	24	15.657	24	93.88	20
22	Gen. Gamma	0.10842	25	16.314	25	100.55	25
25	Gen. Pareto	0.10858	26	223.04	52	N/A	
41	Lognormal	0.11386	27	18.32	29	125.05	30
37	Log-Logistic	0.114	28	17.152	27	119.38	29
4	Cauchy	0.11453	29	13.349	17	88.592	19
15	Fatigue Life	0.11461	30	18.496	31	125.98	31
20	Gamma (3P)	0.1152	31	17.157	28	110.26	27

36	Log-Gamma	0.11524	32	18.721	33	126.04	32
51	Pert	0.1155	33	16.398	26	101.24	26
48	Pearson 5 (3P)	0.11907	34	18.572	32	117.11	28
49	Pearson 6	0.11936	35	20.346	34	133.98	33
47	Pearson 5	0.11959	36	20.517	35	136.84	34
23	Gen. Gamma (4P)	0.12483	37	18.449	30	99.651	24
11	Error	0.12695	38	13.69	19	86.315	17
33	Laplace	0.12786	39	13.826	20	88.388	18
53	Phased Bi-Weibull	0.13674	40	42.946	37	N/A	
61	Uniform	0.13689	41	165.23	48	N/A	
26	Gumbel Max	0.16521	42	51.151	40	180.36	35
17	Frechet	0.18693	43	51.299	41	297.3	37
18	Frechet (3P)	0.1885	44	44.894	38	355.21	39
60	Triangular	0.22077	45	52.408	42	339.85	38
5	Chi-Squared	0.22411	46	147.91	47	416.35	40
54	Power Function	0.22622	47	49.834	39	260.01	36
50	Pearson 6 (4P)	0.26879	48	77.498	43	620.76	41
56	Rayleigh (2P)	0.34856	49	118.33	45	857.66	43
55	Rayleigh	0.39269	50	181.89	49	3320.1	49
14	Exponential (2P)	0.4297	51	186.56	50	1382.6	47
45	Pareto	0.45063	52	200.94	51	1381.1	46
57	Reciprocal	0.52305	53	292.31	57	988.11	45
13	Exponential	0.53154	54	247.58	54	7057.8	51
46	Pareto 2	0.53234	55	248.05	55	7088.3	52
3	Burr (4P)	0.57557	56	273.41	56	842.38	42
35	Levy (2P)	0.57955	57	232.61	53	2963.8	48
8	Dagum (4P)	0.6007	58	295.93	58	943.21	44
58	Rice	0.61103	59	1699.5	61	N/A	
34	Levy	0.65026	60	300.85	59	11088.0	53
7	Dagum	0.86056	61	1118.1	60	6078.4	50
52	Phased Bi-Exponential	1.0	62	18932.0	63	N/A	
59	Student's t	1.0	63	9071.8	62	6.1852E+9	54
12	Error Function	1	64	N/A		N/A	
65	Johnson SU	No fit					

Goodness of Fit – Summary for Site 4

#	Distribution	Kolmogorov Smirnov		Anderson Darling		Chi-Squared	
		Statistic	Rank	Statistic	Rank	Statistic	Rank
62	Wakeby	0.02308	1	20.02	44	N/A	
38	Log-Logistic (3P)	0.03036	2	0.82577	4	9.3159	5
24	Gen. Logistic	0.03144	3	0.45836	1	6.4829	1
2	Burr	0.03443	4	0.55651	2	7.605	2
31	Johnson SU	0.03786	5	0.73189	3	8.4721	4
28	Hypersecant	0.03947	6	1.1814	7	9.4168	6
11	Error	0.04001	7	1.0072	5	8.4697	3
40	Logistic	0.04263	8	1.0809	6	11.513	8
32	Kumaraswamy	0.05164	9	1.9447	11	26.131	29
42	Lognormal (3P)	0.05233	10	2.1889	16	19.244	17
64	Weibull (3P)	0.05287	11	1.8801	9	24.089	26
39	Log-Pearson 3	0.05302	12	1.4378	8	19.556	18
21	Gen. Extreme Value	0.05343	13	21.429	45	N/A	
10	Erlang (3P)	0.05528	14	2.4797	21	21.912	21
16	Fatigue Life (3P)	0.05532	15	1.959	12	18.069	14
29	Inv. Gaussian	0.05569	16	2.3936	18	20.961	20
33	Laplace	0.05616	17	2.4848	22	15.152	9
44	Normal	0.05632	18	1.9992	13	19.069	16
37	Log-Logistic	0.05699	19	1.9109	10	17.961	13
43	Nakagami	0.05802	20	2.1107	15	15.861	10
30	Inv. Gaussian (3P)	0.05806	21	2.0792	14	16.979	11
6	Chi-Squared (2P)	0.06015	22	2.2811	17	18.123	15
50	Pearson 6 (4P)	0.06067	23	2.7441	25	33.949	36
19	Gamma	0.06158	24	2.4126	19	17.303	12
22	Gen. Gamma	0.06215	25	2.4726	20	20.136	19
1	Beta	0.06488	26	5.3767	36	29.511	34
41	Lognormal	0.0652	27	2.7633	26	22.789	23
15	Fatigue Life	0.06529	28	2.7709	27	22.788	22
36	Log-Gamma	0.066	29	2.8443	28	23.726	25
20	Gamma (3P)	0.06603	30	2.8738	29	24.774	27
9	Erlang	0.0669	31	2.6732	23	25.175	28

23	Gen. Gamma (4P)	0.06701	32	2.7267	24	26.37	30
49	Pearson 6	0.06811	33	3.0161	30	28.311	32
47	Pearson 5	0.06829	34	3.083	31	29.396	33
4	Cauchy	0.07096	35	4.7215	34	11.04	7
63	Weibull	0.0731	36	3.3795	32	23.434	24
48	Pearson 5 (3P)	0.07551	37	3.6576	33	32.918	35
27	Gumbel Min	0.08161	38	5.2237	35	27.477	31
5	Chi-Squared	0.08298	39	14.012	38	55.63	38
25	Gen. Pareto	0.09482	40	108.58	49	N/A	
61	Uniform	0.10373	41	110.28	50	N/A	
51	Pert	0.10393	42	14.859	39	95.452	40
60	Triangular	0.10424	43	16.373	41	108.45	41
18	Frechet (3P)	0.11392	44	15.796	40	126.85	42
26	Gumbel Max	0.11473	45	17.135	42	48.576	37
53	Phased Bi-Weibull	0.11676	46	13.313	37	N/A	
17	Frechet	0.13403	47	17.871	43	71.178	39
56	Rayleigh (2P)	0.24167	48	50.178	46	268.69	43
57	Reciprocal	0.25851	49	68.467	48	498.25	45
54	Power Function	0.27105	50	64.1	47	417.61	44
14	Exponential (2P)	0.36341	51	119.58	51	926.33	46
45	Pareto	0.37424	52	126.12	52	998.77	47
55	Rayleigh	0.45259	53	167.34	54	4237.1	49
35	Levy (2P)	0.51123	54	160.5	53	1786.0	48
3	Burr (4P)	0.52987	55	201.26	56	N/A	
46	Pareto 2	0.54382	56	199.62	55	8944.3	51
13	Exponential	0.5755	57	215.07	57	8947.8	52
8	Dagum (4P)	0.61044	58	255.66	59	N/A	
7	Dagum	0.61517	59	246.8	58	7717.2	50
34	Levy	0.65119	60	256.74	60	13886.0	53
58	Rice	0.99614	61	13184.0	62	N/A	
59	Student's t	1.0	62	7557.5	61	1.3192E+10	54
12	Error Function	1	63	N/A		N/A	
52	Phased Bi-Exponential	1	64	N/A		N/A	
65	Johnson SB	No fit					

Goodness of Fit – Summary for Site 5

#	Distribution	Kolmogorov Smirnov		Anderson Darling		Chi-Squared	
		Statistic	Rank	Statistic	Rank	Statistic	Rank
62	Wakeby	0.0323	1	24.014	34	N/A	
24	Gen. Logistic	0.05012	2	1.1767	1	23.376	2
27	Gumbel Min	0.06344	3	3.4789	3	32.337	6
21	Gen. Extreme Value	0.06974	4	78.018	45	N/A	
31	Johnson SB	0.07049	5	10.367	13	N/A	
38	Log-Logistic (3P)	0.07196	6	5.0335	6	35.614	7
2	Burr	0.07438	7	2.7523	2	21.493	1
32	Kumaraswamy	0.0756	8	3.5979	5	27.773	4
64	Weibull (3P)	0.07561	9	3.5961	4	27.773	3
4	Cauchy	0.07741	10	5.8689	7	31.173	5
63	Weibull	0.08224	11	6.0145	8	44.666	10
39	Log-Pearson 3	0.10065	12	121.59	47	N/A	
11	Error	0.10178	13	8.3858	10	36.437	8
33	Laplace	0.10178	14	8.3858	11	36.437	9
28	Hypersecant	0.11081	15	8.1028	9	52.61	11
40	Logistic	0.12009	16	9.129	12	75.049	12
25	Gen. Pareto	0.12139	17	214.88	54	N/A	
5	Chi-Squared	0.12254	18	60.352	42	161.92	34
1	Beta	0.12292	19	13.355	19	87.623	15
30	Inv. Gaussian (3P)	0.1278	20	12.528	15	96.984	19
43	Nakagami	0.13033	21	12.396	14	85.381	13
29	Inv. Gaussian	0.13074	22	14.209	22	102.01	22
44	Normal	0.1313	23	12.618	16	92.149	17
23	Gen. Gamma (4P)	0.13182	24	13.265	18	97.736	20
51	Pert	0.13258	25	28.759	36	228.68	35
42	Lognormal (3P)	0.13419	26	13.769	20	105.43	24
16	Fatigue Life (3P)	0.13533	27	13.122	17	91.85	16
6	Chi-Squared (2P)	0.13678	28	13.892	21	102.98	23
53	Phased Bi-Weibull	0.13858	29	28.529	35	N/A	
19	Gamma	0.13892	30	14.572	23	96.167	18
22	Gen. Gamma	0.14173	31	15.542	25	106.16	25

20	Gamma (3P)	0.14335	32	16.339	27	116.5	30
37	Log-Logistic	0.14445	33	15.436	24	99.84	21
10	Erlang (3P)	0.14552	34	16.156	26	107.45	26
41	Lognormal	0.14704	35	17.244	28	113.54	28
15	Fatigue Life	0.14759	36	17.362	29	114.15	29
36	Log-Gamma	0.14819	37	17.569	30	112.47	27
47	Pearson 5	0.15252	38	19.064	33	127.25	32
61	Uniform	0.15447	39	168.15	48	N/A	
48	Pearson 5 (3P)	0.15628	40	18.541	32	121.28	31
9	Erlang	0.15975	41	18.223	31	86.384	14
18	Frechet (3P)	0.18919	42	45.477	37	359.88	38
26	Gumbel Max	0.19358	43	49.326	38	143.69	33
49	Pearson 6	0.19514	44	53.911	40	458.65	40
17	Frechet	0.2242	45	50.453	39	259.15	36
50	Pearson 6 (4P)	0.23712	46	55.567	41	431.46	39
60	Triangular	0.2532	47	60.488	43	283.86	37
54	Power Function	0.27664	48	74.8	44	476.03	41
56	Rayleigh (2P)	0.33787	49	110.96	46	789.41	42
55	Rayleigh	0.40949	50	186.54	50	3985.9	48
7	Dagum	0.43312	51	192.57	52	5887.8	49
14	Exponential (2P)	0.43662	52	178.27	49	1977.9	45
45	Pareto	0.45124	53	189.49	51	2132.2	46
57	Reciprocal	0.4655	54	201.15	53	960.44	43
13	Exponential	0.54224	55	247.21	56	8573.8	50
46	Pareto 2	0.54353	56	248.0	57	8606.1	51
3	Burr (4P)	0.54796	57	254.33	58	N/A	
35	Levy (2P)	0.55766	58	220.06	55	3354.2	47
34	Levy	0.64907	59	297.95	59	13400.0	52
8	Dagum (4P)	0.6494	60	347.22	60	1161.7	44
58	Rice	0.86046	61	14751.0	62	N/A	
59	Student's t	1.0	62	8810.1	61	1.0475E+10	53
52	Phased Bi-Exponential	1.0	63	36397.0	63	N/A	
12	Error Function	1	64	N/A		N/A	
65	Johnson SU	No fit					

Goodness of Fit – Summary for Site 6

#	Distribution	Kolmogorov Smirnov		Anderson Darling		Chi-Squared	
		Statistic	Rank	Statistic	Rank	Statistic	Rank
24	Gen. Logistic	0.02753	1	0.41367	1	5.8574	1
62	Wakeby	0.03968	2	16.628	35	N/A	
31	Johnson SB	0.04122	3	17.314	36	N/A	
21	Gen. Extreme Value	0.053	4	50.84	44	N/A	
2	Burr	0.0556	5	1.5886	4	11.463	2
32	Kumaraswamy	0.05759	6	1.3962	2	16.679	4
64	Weibull (3P)	0.05777	7	1.4065	3	16.676	3
27	Gumbel Min	0.05961	8	1.9268	5	16.684	5
39	Log-Pearson 3	0.06419	9	66.464	46	N/A	
38	Log-Logistic (3P)	0.07533	10	4.2976	6	43.734	7
63	Weibull	0.08115	11	4.5193	7	38.362	6
40	Logistic	0.10019	12	7.6268	10	51.895	8
28	Hypersecant	0.10085	13	7.3536	8	60.533	10
4	Cauchy	0.11213	14	7.5128	9	64.408	13
43	Nakagami	0.11365	15	9.4314	13	65.967	14
42	Lognormal (3P)	0.11558	16	9.6342	17	67.694	15
1	Beta	0.1163	17	9.9319	18	59.178	9
25	Gen. Pareto	0.11675	18	124.35	52	N/A	
29	Inv. Gaussian	0.1169	19	10.494	21	73.288	21
16	Fatigue Life (3P)	0.11785	20	9.4569	14	68.463	16
30	Inv. Gaussian (3P)	0.11859	21	9.5822	16	69.878	18
44	Normal	0.11863	22	9.5306	15	69.735	17
19	Gamma	0.12457	23	10.788	22	75.029	22
23	Gen. Gamma (4P)	0.12471	24	10.354	19	70.748	19
9	Erlang	0.12561	25	10.894	23	75.959	24
6	Chi-Squared (2P)	0.12572	26	10.492	20	73.052	20
49	Pearson 6	0.12629	27	10.996	24	75.952	23
11	Error	0.12926	28	8.4141	11	62.59	11
33	Laplace	0.12926	29	8.4141	12	62.59	12
22	Gen. Gamma	0.12944	30	11.376	25	78.769	25
20	Gamma (3P)	0.13189	31	11.622	26	79.288	26

37	Log-Logistic	0.13307	32	11.912	28	95.502	35
48	Pearson 5 (3P)	0.1338	33	12.064	29	82.171	27
10	Erlang (3P)	0.13423	34	11.759	27	82.486	28
41	Lognormal	0.1353	35	12.433	31	84.483	30
50	Pearson 6 (4P)	0.13553	36	12.234	30	83.124	29
15	Fatigue Life	0.13589	37	12.507	32	84.485	31
36	Log-Gamma	0.13636	38	12.645	33	84.716	32
47	Pearson 5	0.14129	39	13.555	34	88.027	33
61	Uniform	0.15869	40	100.72	48	N/A	
5	Chi-Squared	0.16339	41	34.355	40	93.16	34
51	Pert	0.16921	42	18.822	37	129.7	37
26	Gumbel Max	0.17377	43	34.56	41	129.23	36
53	Phased Bi-Weibull	0.20269	44	55.123	45	N/A	
18	Frechet (3P)	0.21003	45	31.225	38	261.98	40
17	Frechet	0.21752	46	33.579	39	212.88	39
60	Triangular	0.26743	47	42.674	42	184.27	38
54	Power Function	0.30814	48	48.328	43	292.4	41
56	Rayleigh (2P)	0.33161	49	73.486	47	560.16	42
55	Rayleigh	0.41389	50	118.55	50	2739.4	47
14	Exponential (2P)	0.43951	51	114.82	49	1240.8	45
45	Pareto	0.45559	52	121.35	51	1041.4	44
57	Reciprocal	0.47239	53	136.18	53	629.63	43
13	Exponential	0.54632	54	155.56	55	5768.6	48
46	Pareto 2	0.55119	55	157.59	56	5785.7	49
3	Burr (4P)	0.55466	56	161.77	57	N/A	
35	Levy (2P)	0.56778	57	139.8	54	2304.1	46
8	Dagum (4P)	0.6207	58	195.88	59	N/A	
34	Levy	0.65219	59	186.9	58	9003.6	51
7	Dagum	0.76656	60	367.18	60	7829.1	50
58	Rice	0.819	61	2225.7	61	N/A	
59	Student's t	1.0	62	5508.5	62	7.1714E+9	52
52	Phased Bi-Exponential	1.0	63	23584.0	63	N/A	
12	Error Function	1	64	N/A		N/A	
65	Johnson SU	No fit					

Goodness of Fit – Summary for Site 7

#	Distribution	Kolmogorov Smirnov		Anderson Darling		Chi-Squared	
		Statistic	Rank	Statistic	Rank	Statistic	Rank
62	Wakeby	0.04493	1	12.4	13	N/A	
24	Gen. Logistic	0.05739	2	1.2584	1	20.358	4
38	Log-Logistic (3P)	0.05799	3	2.9544	4	7.5245	1
64	Weibull (3P)	0.05969	4	2.2015	2	25.836	8
2	Burr	0.06718	5	2.7498	3	17.396	2
21	Gen. Extreme Value	0.0767	6	42.334	37	N/A	
27	Gumbel Min	0.08434	7	5.4015	6	36.857	10
4	Cauchy	0.09117	8	3.9364	5	19.775	3
11	Error	0.09356	9	6.1946	8	22.72	5
33	Laplace	0.09356	10	6.1946	7	22.72	6
28	Hypersecant	0.09474	11	7.3662	9	25.406	7
43	Nakagami	0.10612	12	9.8442	11	34.953	9
40	Logistic	0.1068	13	8.9662	10	37.151	11
1	Beta	0.11115	14	10.502	12	57.581	12
30	Inv. Gaussian (3P)	0.11258	15	15.531	21	78.61	19
29	Inv. Gaussian	0.12398	16	14.306	17	73.321	18
31	Johnson SB	0.12623	17	60.743	42	N/A	
25	Gen. Pareto	0.12679	18	171.86	55	N/A	
42	Lognormal (3P)	0.12784	19	12.868	15	62.041	13
44	Normal	0.12826	20	12.759	14	66.708	15
16	Fatigue Life (3P)	0.12972	21	12.94	16	65.002	14
23	Gen. Gamma (4P)	0.1344	22	14.713	19	88.35	22
19	Gamma	0.1353	23	14.624	18	71.945	16
20	Gamma (3P)	0.13696	24	15.535	22	94.83	23
48	Pearson 5 (3P)	0.1373	25	18.61	25	82.892	20
10	Erlang (3P)	0.14083	26	15.232	20	86.311	21
50	Pearson 6 (4P)	0.14342	27	17.331	23	109.75	24
9	Erlang	0.1606	28	18.394	24	73.227	17
22	Gen. Gamma	0.16178	29	20.104	27	123.64	26
58	Rice	0.16843	30	18.931	26	115.02	25
26	Gumbel Max	0.17799	31	37.859	36	N/A	

61	Uniform	0.17914	32	86.263	43	N/A	
41	Lognormal	0.1819	33	25.652	28	163.94	27
36	Log-Gamma	0.18339	34	26.017	29	171.8	28
63	Weibull	0.18967	35	28.56	31	196.8	32
15	Fatigue Life	0.19254	36	27.825	30	179.6	29
6	Chi-Squared (2P)	0.19729	37	97.083	45	195.92	31
5	Chi-Squared	0.20103	38	92.582	44	187.16	30
18	Frechet (3P)	0.20501	39	37.699	35	N/A	
37	Log-Logistic	0.20692	40	33.108	33	248.21	35
47	Pearson 5	0.211	41	35.399	34	241.77	34
49	Pearson 6	0.21259	42	30.548	32	203.06	33
51	Pert	0.24491	43	42.907	38	263.71	36
32	Kumaraswamy	0.25469	44	53.826	40	445.2	38
54	Power Function	0.27369	45	51.515	39	322.92	37
17	Frechet	0.29769	46	59.709	41	N/A	
39	Log-Pearson 3	0.33397	47	539.36	60	N/A	
55	Rayleigh	0.41929	48	108.13	47	1598.0	50
60	Triangular	0.45031	49	106.93	46	563.6	41
56	Rayleigh (2P)	0.46931	50	115.57	48	1118.1	47
14	Exponential (2P)	0.52925	51	142.29	49	500.6	40
13	Exponential	0.54463	52	147.55	50	739.45	43
46	Pareto 2	0.54809	53	148.97	51	706.87	42
45	Pareto	0.55574	54	154.68	52	475.89	39
35	Levy (2P)	0.61881	55	164.62	53	818.7	44
8	Dagum (4P)	0.62557	56	179.26	57	N/A	
53	Phased Bi-Weibull	0.63068	57	165.05	54	N/A	
34	Levy	0.64503	58	178.88	56	1015.2	46
7	Dagum	0.6827	59	244.02	58	830.28	45
57	Reciprocal	0.77801	60	447.29	59	1399.3	49
52	Phased Bi-Exponential	0.94643	61	2112.7	61	1187.6	48
12	Error Function	0.99868	62	4922.9	62	N/A	
59	Student's t	1.0	63	5499.0	63	N/A	
3	Burr (4P)	N/A		N/A		N/A	
65	Johnson SU	No fit					

APPENDIX D: THE DISTRIBUTIONS OF CAPACITIES

Site 1

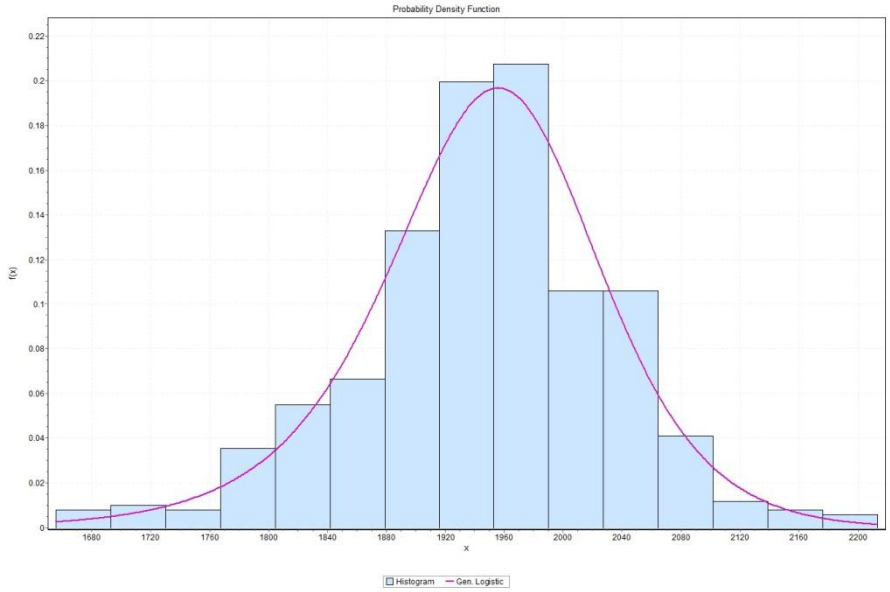

Site 2

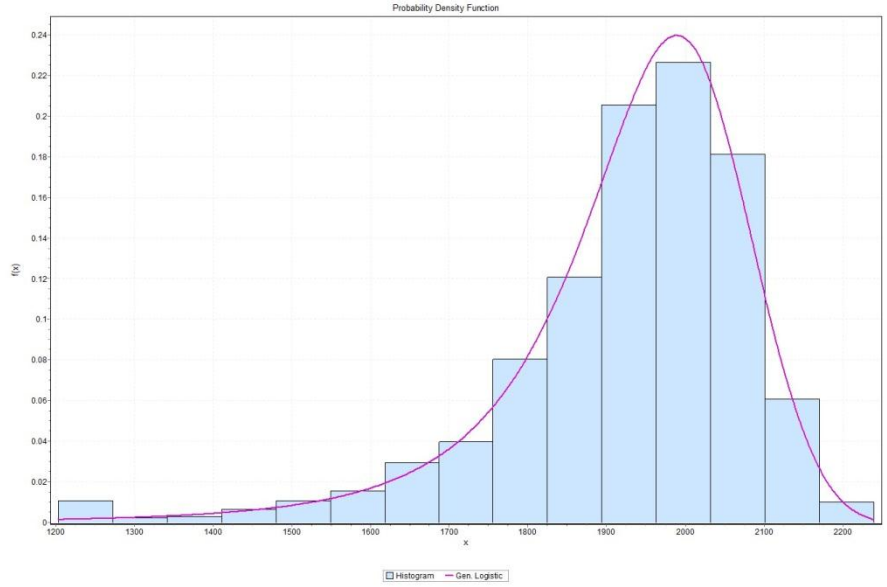

Site 3

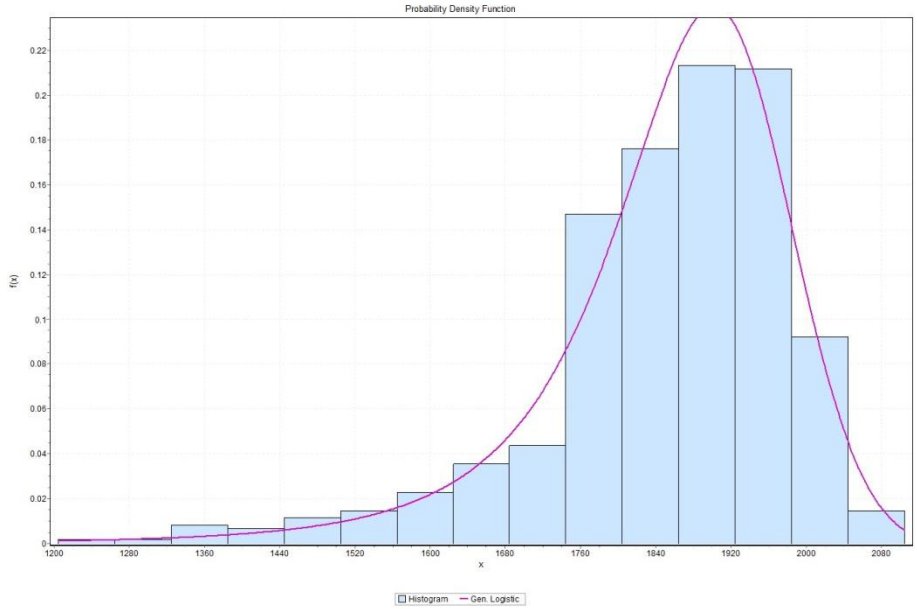
Probability Density Function
f(x)
x
Histogram
Gen. Logistic

Site 4

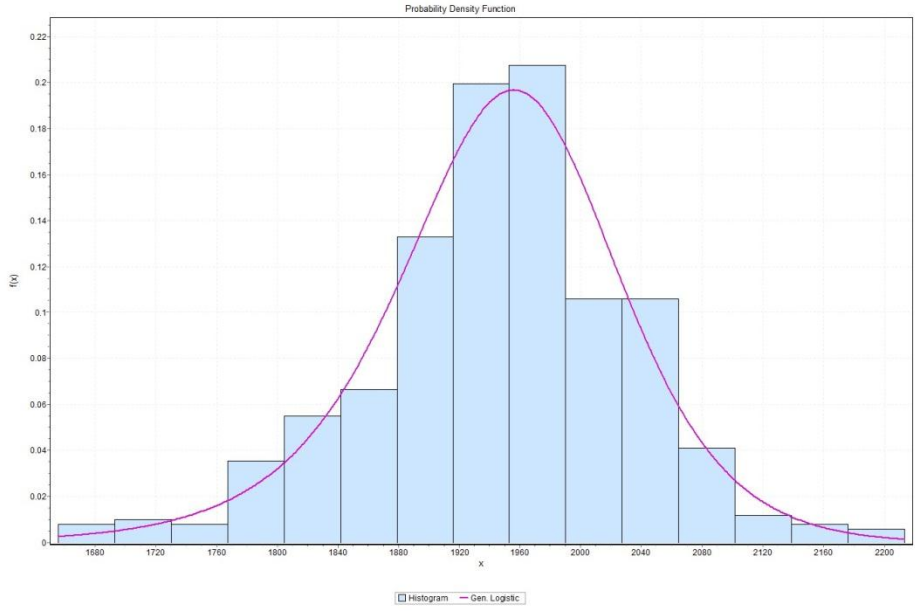
Probability Density Function
f(x)
x
Histogram
Gen. Logistic

Site 5

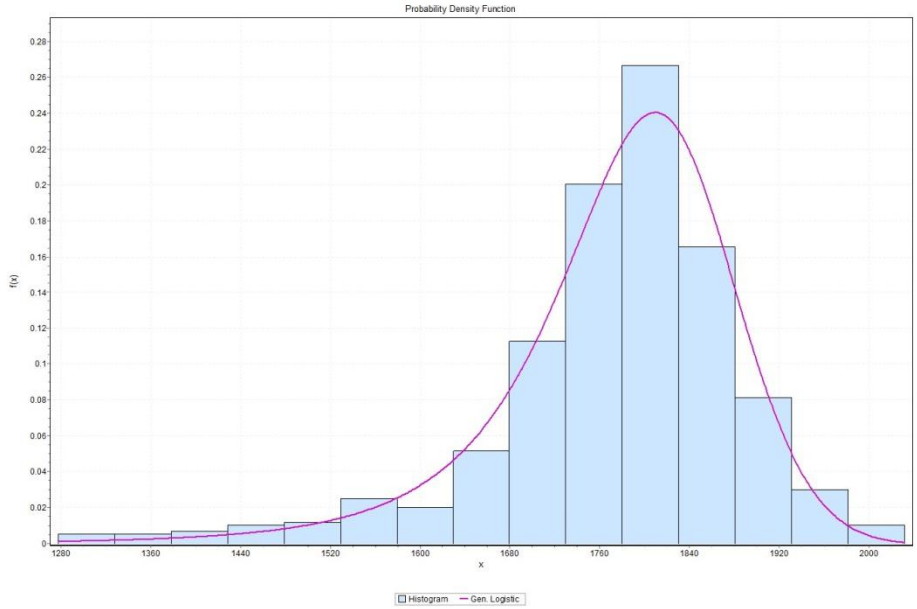
Probability Density Function
f(x)
x
Histogram
Gen. Logistic

Site 6

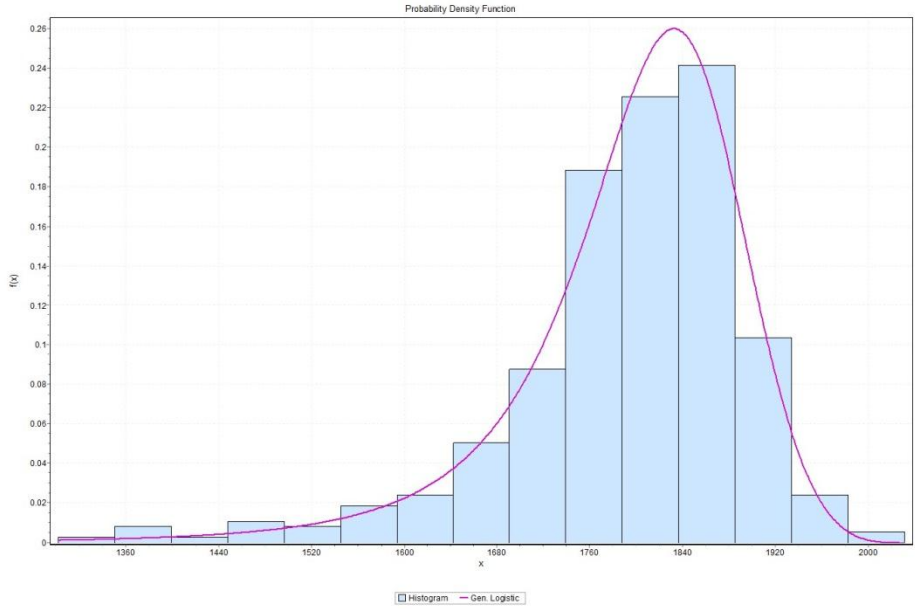
Probability Density Function
f(x)
x
Histogram
Gen. Logistic

Site 7

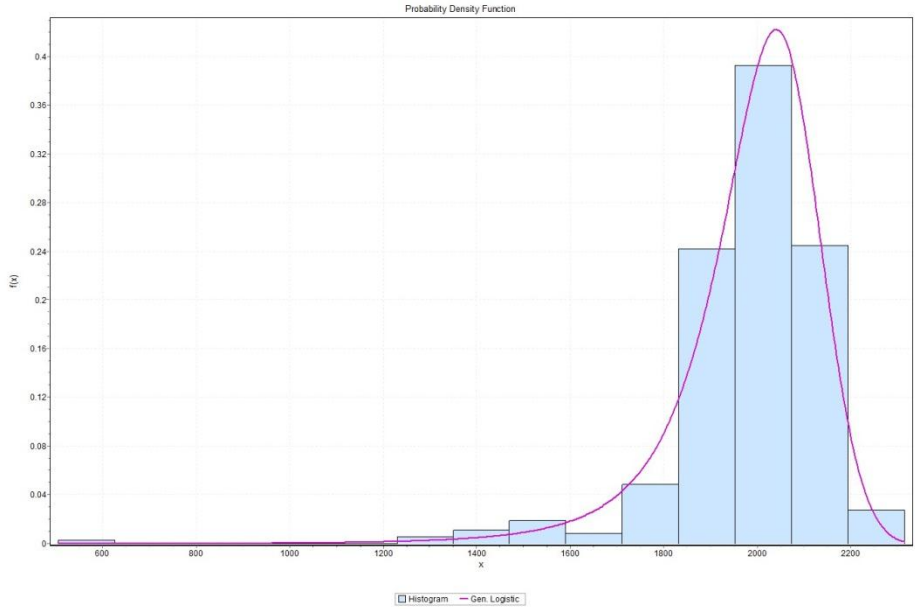
Probability Density Function
f(x)
0.4
0.36
0.32
0.28
0.24
0.2
0.16
0.12
0.08
0.04
0
600
800
1000
1200
1400
1600
1800
2000
2200
x
Histogram
Gen. Logistic

APPENDIX E: THE DISTRIBUTIONS OF DEMAND

Demand Distribution (6:15-6:30)

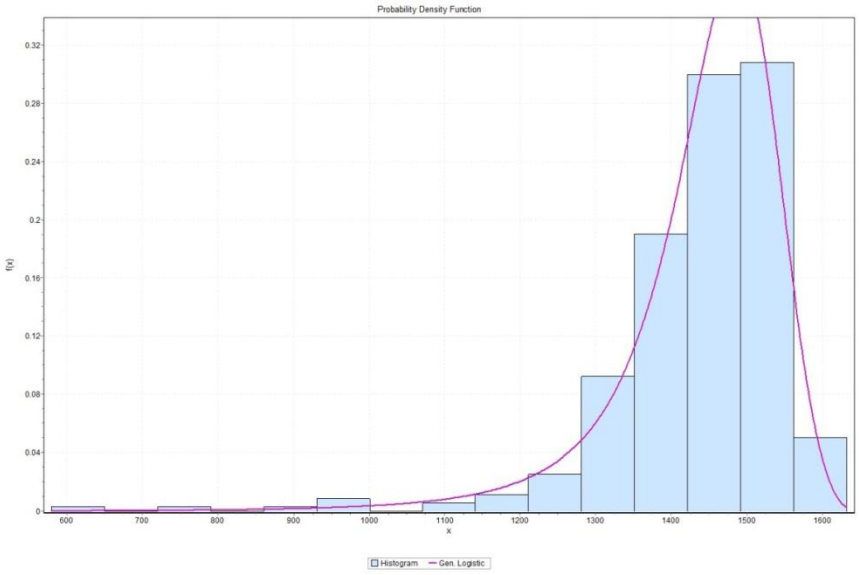

Demand Distribution (6:30-6:45)

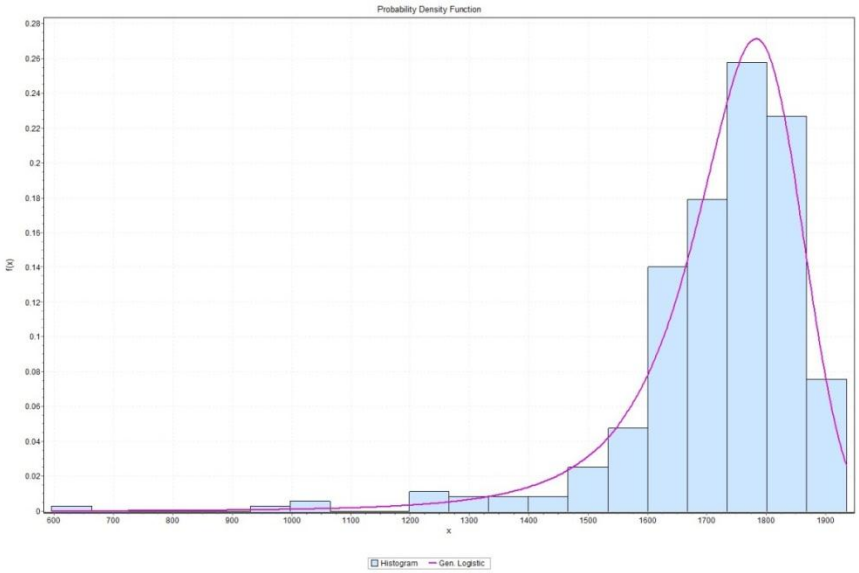

Demand Distribution (6:45-7:00)

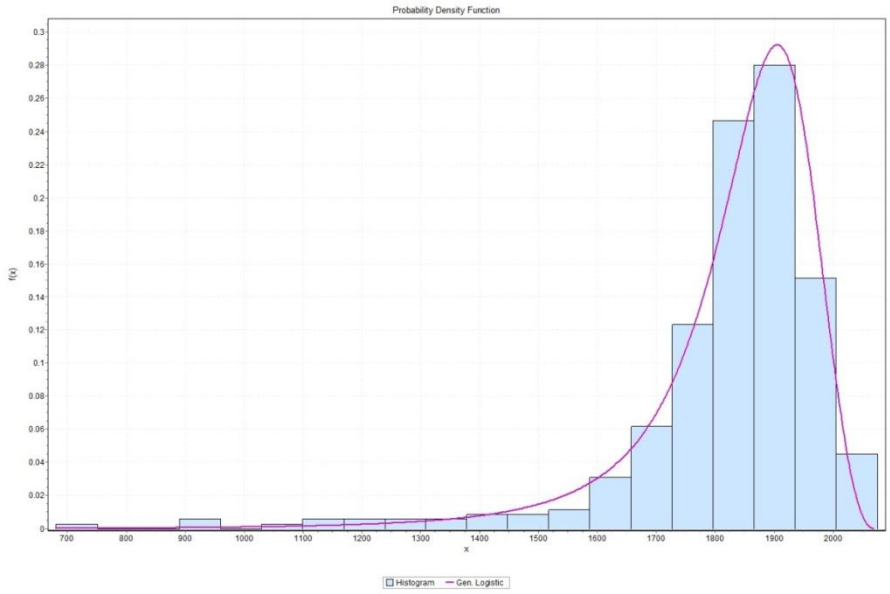

Demand Distribution (7:00-7:15)

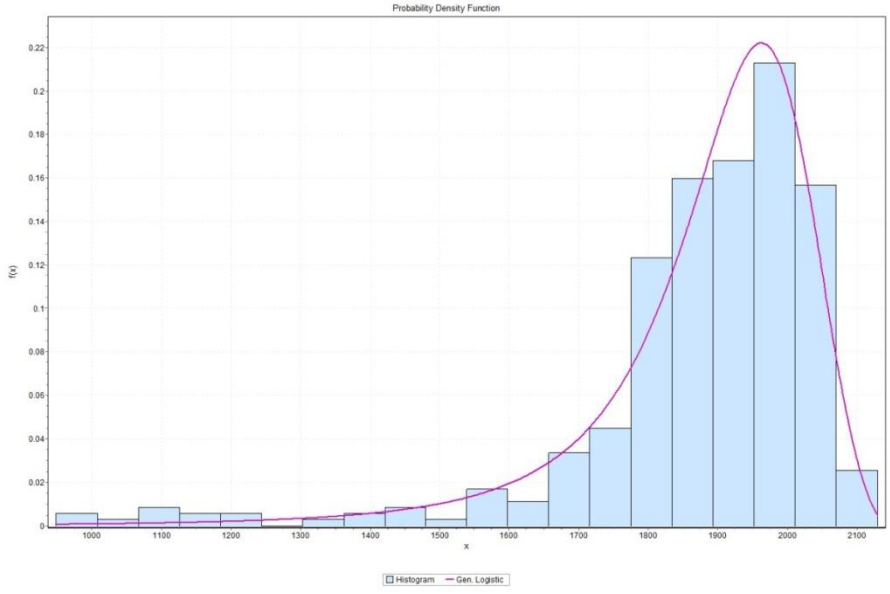

Demand Distribution (7:15-7:30)

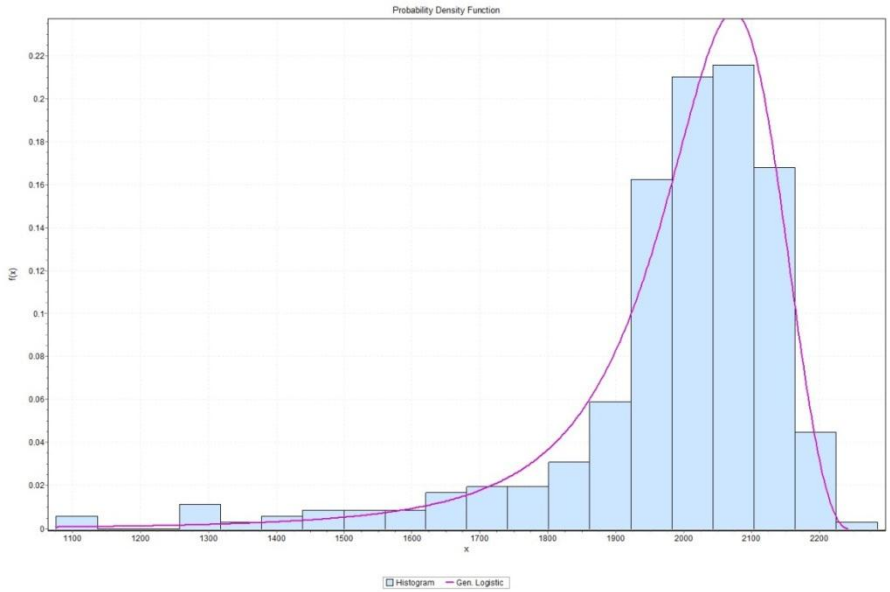

Demand Distribution (7:30-7:45)

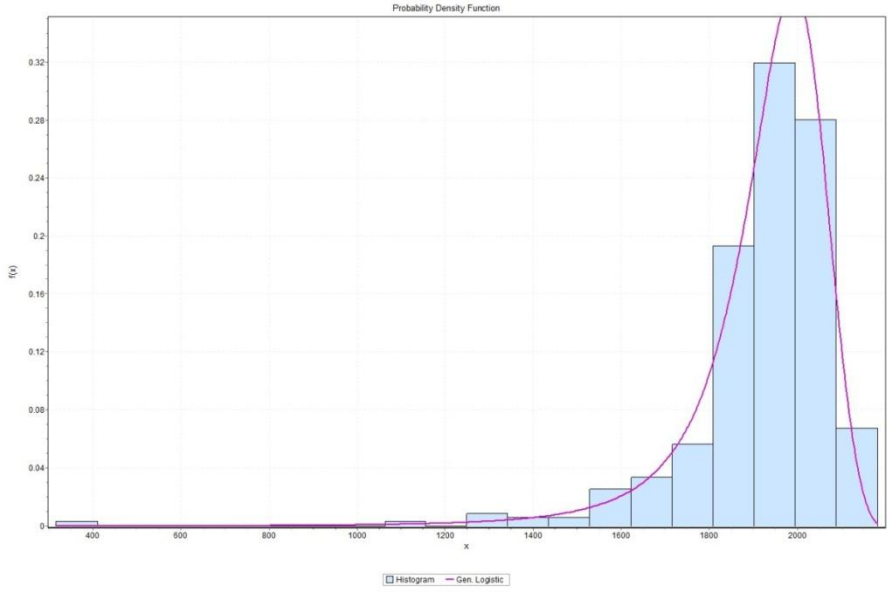

Demand Distribution (7:45-8:00)

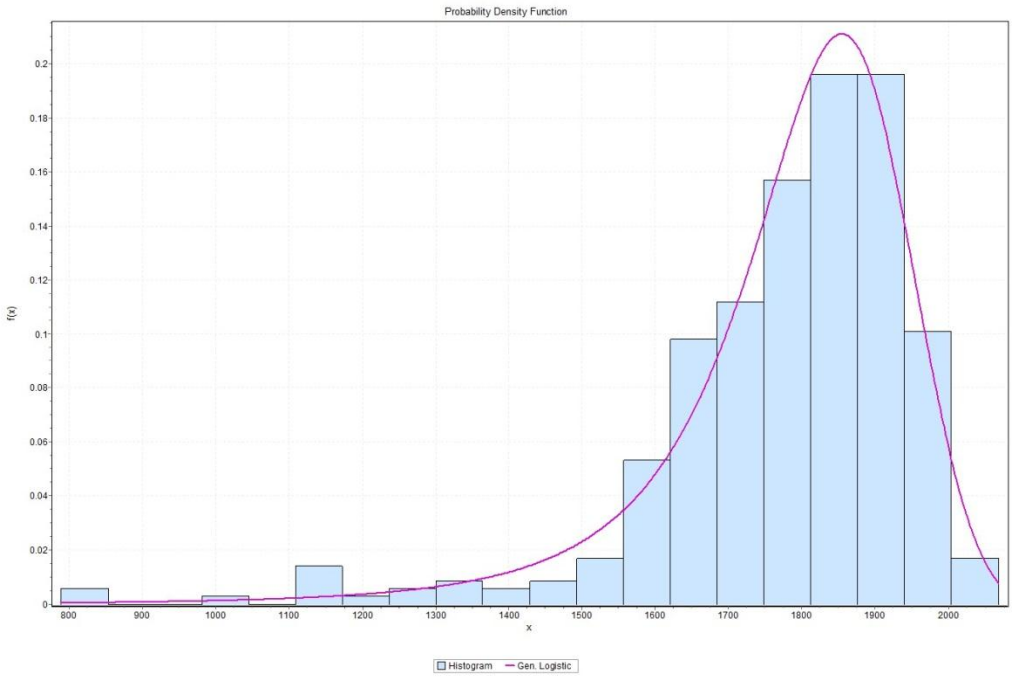

APPENDIX F: SIMULATION FRAMEWORK AND SYSTEM IMPLEMENTATION

The system evolution-modeling simulation framework for the enhanced version of DYNASMART-P is illustrated in Figure F-1. In the proposed modeling framework, static demand (i.e. the same number of vehicles with fixed departure times) is simulated over different days.

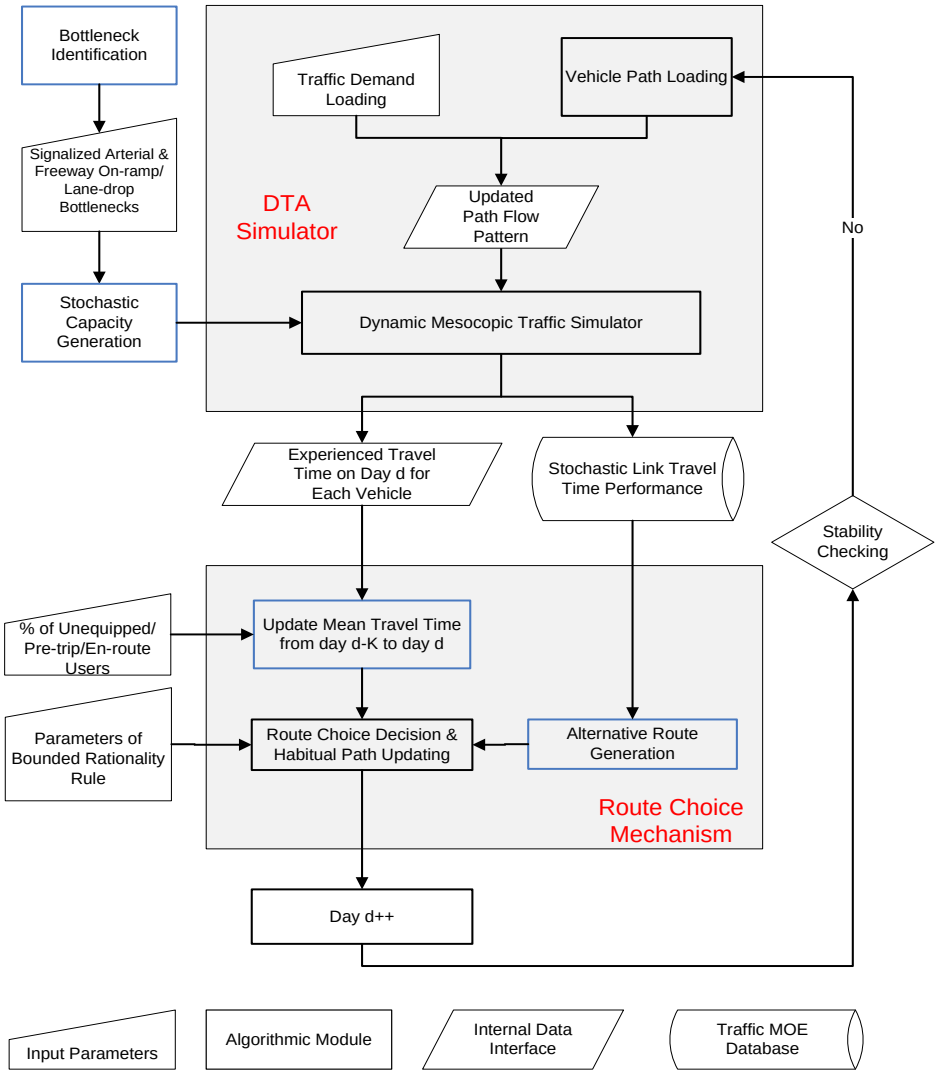

Figure F-1 Comprehensive Conceptual Simulation Framework

In the above conceptual simulation framework, four critical inputs (illustrated in the input boxes in Figure F-1) should be pre-specified by users, which are listed as follows:

- Time-dependent traffic demand,
- Bottleneck locations,
- Percentage of unequipped, pre-trip and en-route users,
- Parameters of the bounded rationality rule.

Figure F-1 demonstrates the entire conceptual simulation framework currently implemented in DYNASMART-P. However, the two key components, stochastic capacity generation on freeway bottlenecks and signalized arterial and route choice mechanism are not illustrated in detail. Due to their significance, the implementation frameworks of the capacity generation and route choice models are demonstrated in Figure F-2 and Figure F-3, respectively.

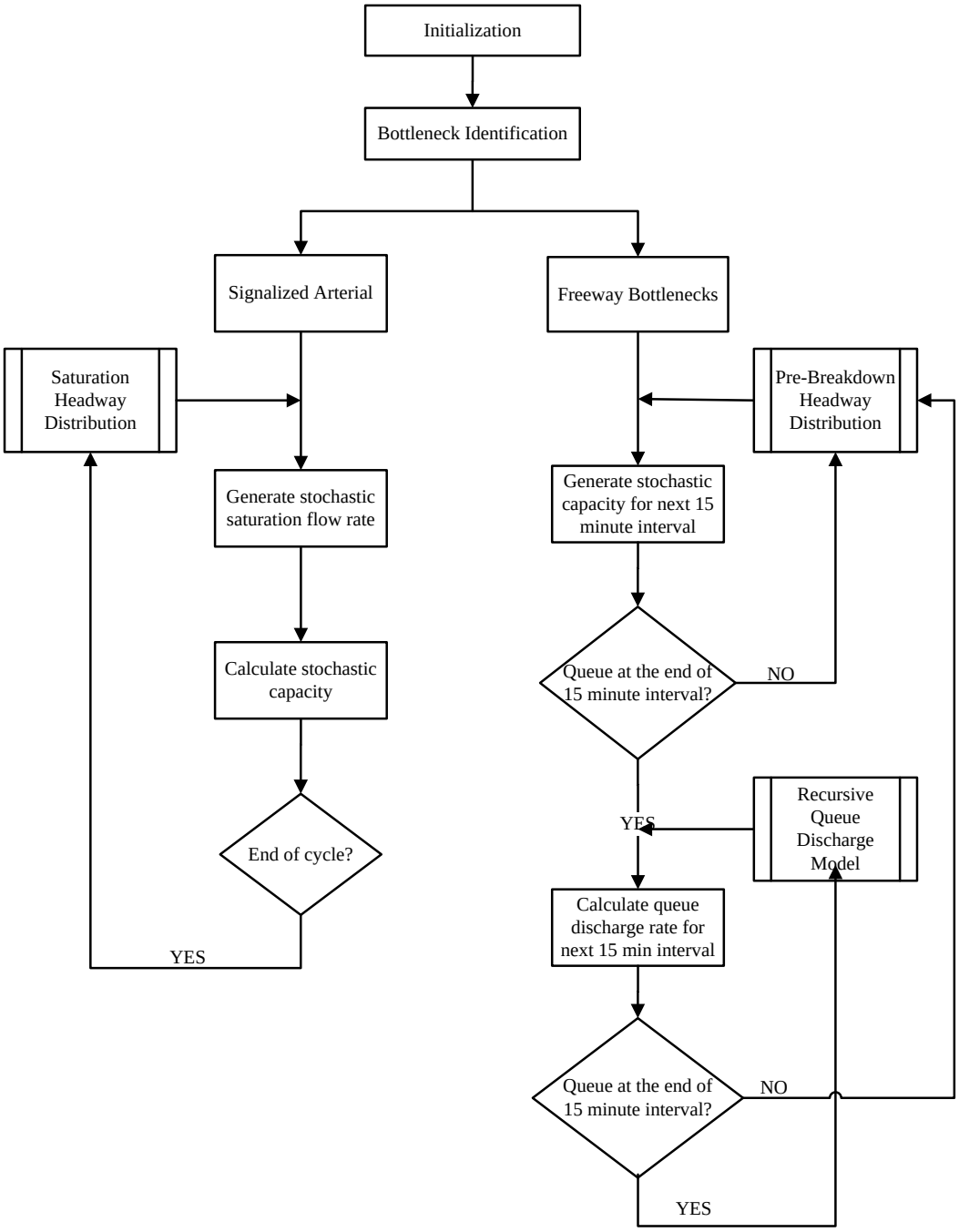

Figure F-2 Implementation Framework of Stochastic Capacity Generation

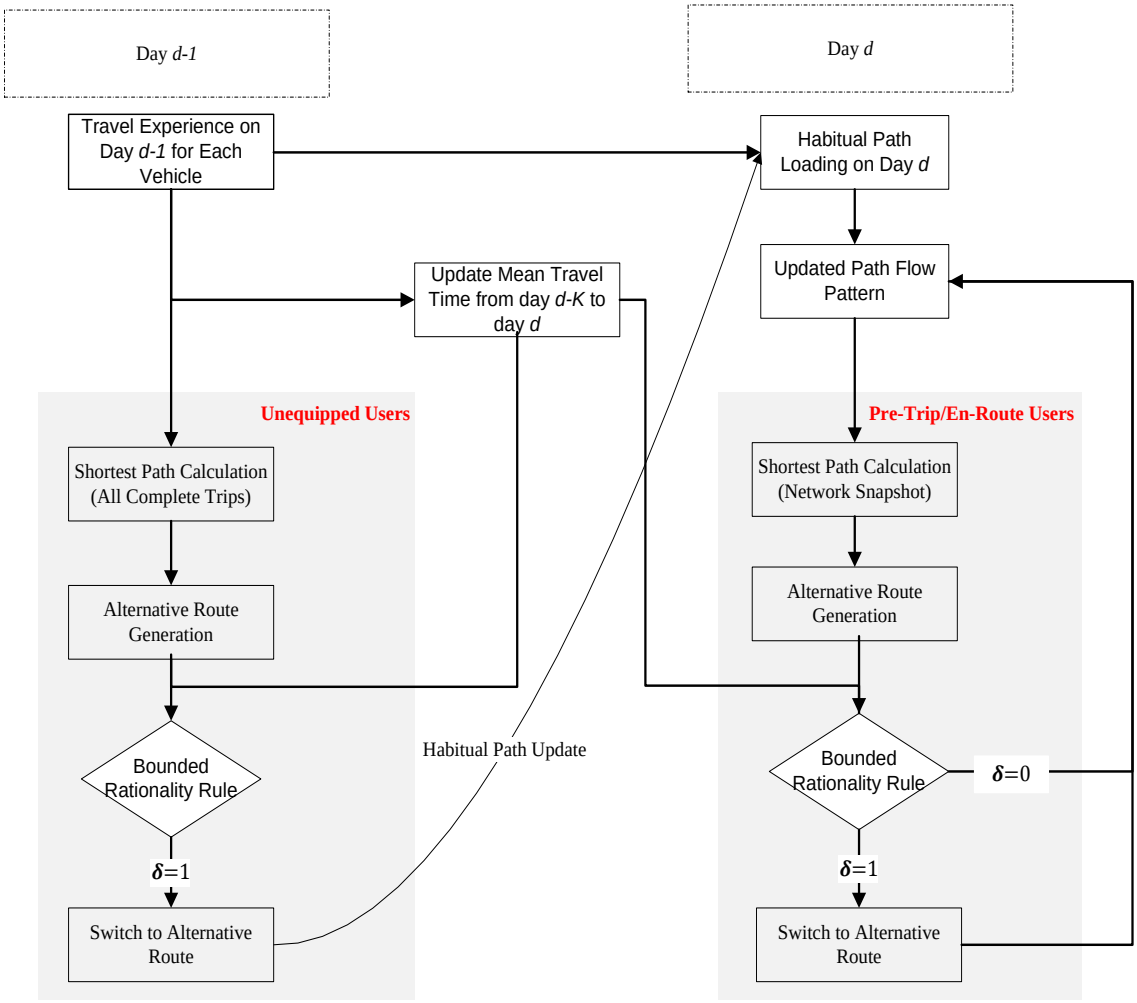

Figure F-3 Implementation Framework of Route Choice Mechanism

Multiple User Classes

Three types of user classes are considered in this study: pre-trip information users, en-route information users, and unequipped users. The different user classes have access to different types of travel information to help them make their route choice decisions. Pre-trip information is acquired by pre-trip users before departure, through the internet, TV, radio, and cell phones. En-route information that describes the estimated time of arrival is provided

to en-route users during the trip by GPS navigation devices, radio channels, and Variable Message Signs. The personal post-trip information acquired by unequipped users is typically based on a commuter's experienced travel time, in addition to potential external information sources from television and newspaper reports.

In this heterogeneous information environment, each user class has different ways to estimate travel time on the alternative path, T_v^a, and different decision–making locations and times. The pre-trip users estimate T_v^a based on the network real-time snapshot conditions just prior their departure and make the route choice decision at the departure time. The en-route users make route choice decisions each time they reach a node where alternative routes are available and estimate T_v^a based on the network real-time snapshot conditions. The unequipped users determine whether to change their habitual path on day *d* at the end of day *d-1*, when all trips complete and estimate the travel time on the shortest path based on average path travel times on day *d-1*.

It should be noted that in reality, many people are creatures of habit and unlikely to make route changes right away, if ever. Moreover, the information quality could vary for different user classes. Thus, following assumptions are made about how different user classes receive information and how this information triggers route switching considerations.

a) Pre-trip and en-route users are always willing to switch their routes;

b) Only a certain percent (*p*) of unequipped users have the access to post-trip information and are willing to switch their routes;

c) Pre-trip/en-route users receive the information with higher quality than unequipped users.

The value of *p* also requires a site-specific calibration effort. For example, Haselkom et al. found that 20.06% of drivers are willing to switch their routes in the study area in Washington State; while Abdel et al indicated that 15.50% of drivers are willing to switch routes in Los Angeles.